2005

Modeling and simulation to investigate effects of static mixer, carrier gas, temperature and pressure on the mixing ratio of carbon nanotubes growth reactors

David Addie Noye
University of Northern Iowa

MODELING AND SIMULATION TO INVESTIGATE EFFECTS OF STATIC MIXER, CARRIER GAS, TEMPERATURE AND PRESSURE ON THE MIXING RATIO OF CARBON NANOTUBES GROWTH REACTORS

An Abstract of a Dissertation

Submitted

in Partial Fulfillment

of the Requirements for the Degree

Doctor of Industrial Technology

Approved:

Dr. John T. Fecik, Professor, Chair

Dr. Susan J. Koch, Dean of the Graduate College

David Addie Noye

University of Northern Iowa

July 2005

ABSTRACT

The problem of this study was to investigate the effects of static mixer, carrier gas, carrier gas inlet pressures, and reactor operating temperatures on the mixing ratio of carbon nanotube synthesizing reactor. The methodology included design of static mixers, mathematical modeling, and computer modeling and simulation experiments.

The simulation experiment was performed based on single phase carrier gas modeling due to difficulty and time for three phase fluid modeling. First only nitrogen carrier gas in addition to the other three factors under constant inlet flow velocity and inlet temperature was simulated. Secondly, the same procedure was applied to argon carrier gas.

Three temperature values were extracted at exit of model reactors with internal configuration varied with types of static mixers. The bulk temperature and temperature deviations were calculated. The deviations were then divided by the bulk temperature to obtain the mixing ratios from which the mixing indices were determined. In addition, the stream lines for each treatment were obtained to validate the quantitative mixing indices.

A 4-way analysis of variance (ANOVA) was completed, and the diagnostics check on the transformed data showed that the statistical assumptions were met. Thus, the inferential statistics and conclusions confirming or disconfirming the original research questions and research hypotheses were then determined at significant level of .05.

In conclusion, the baffle static mixer showed significant improvement over the existing reactor in the mixing ratio using single phase buffer gas flow. Also the reactor

temperature showed significant effect on the mixing ratio. On the other hand, the type of carrier gas and pressure did not show significant effect on the mixing ratio.

This indicated that the appropriate reactor temperatures in addition to improving the inner configuration of the carbon nanotube growth reactors with static mixers can improve achieving uniform atomic distances between carrier gases, carbon and metal catalyst vapors. In the case of laser and solar methods this can then lead to uniform plume formation, cooling, nucleation, growth, diameter and length of carbon nanotubes. The purity of carbon nanotubes can improve and consequently lead to higher yield and improved productivity of the laser vapor method and other methods of growing carbon nanotubes such as the solar, arc, flame and chemical vapor deposition. This will further contribute to cheaper purification cost and hence the overall price of carbon nanotubes.

MODELING AND SIMULATION TO INVESTIGATE EFFECTS OF STATIC MIXER, CARRIER GAS, TEMPERATURE AND PRESSURE ON THE MIXING RATIO OF CARBON NANOTUBES GROWTH REACTORS

A Dissertation

Submitted

in Partial Fulfillment

of the Requirements for the Degree

Doctor of Industrial Technology

Approved:

Dr. John T. Fecik, Chair

Dr. Ronald E. O'Meara, Co-Chair

Dr. Scott R. Giese, Committee Member

Dr. Andrew R. Gilpin, Committee Member

Dr. Paul M. Shand, Committee Member

David Addie Noye

University of Northern Iowa

July 2005

Dedicated to
My wife Addie-Noye, Florence
and to
My children Addie-Noye, Eugenia Naa Shormeh; Addie-Noye, Eugene Nii Noye; and
Addie-Noye, Eugenie Naa-Afieye.

ACKNOWLEDGEMENTS

The author would like to acknowledge the guidance and encouragement of the advisory committee members: Dr. John Fecik, advisor, Dr. Ronald O'Meara, co-advisor, Dr. Scott Giese, Dr. Andrew R. Gilpin, and Dr. Paul M. Shand. Without their continuous advice and assistance, this research would have been impossible.

Special thanks would be given to Dr. John Fecik, advisor who provided steady leadership, spent a lot of time and gave unflinching support for this research. The author also expresses his gratitude to the Department of Industrial Technology, College of Natural Sciences, and Graduate College of the University of Northern Iowa for providing funding including purchase of FEMLAB software that made this study possible.

Additionally, debt of gratitude is owed to Dr. Mohammed Fahmy and Dr. Clifton Chancey who gave me occasional but significant guidance that contributed to the completion of this study. Similarly, to the entire administrative staff of the Department of Industrial Technology and International Services Office of the University of Northern Iowa, particularly, Ross Schupbach for their ever readiness to address my needs.

The greatest debt is owed to Dr. Ronald Bro, who the author worked with in Ghana and made it possible to complete his doctoral program with the Department of Industrial Technology of the University of Northern Iowa. Further, special debt of gratitude is owed to my wife Mrs. Florence Addie-Noye for whom without sacrificing the completion of her undergraduate studies in Ghana to assist me through challenging times this study could never have been completed. I extend similar gratitude to my entire family and reliable friends for their steady and timely support.

TABLE OF CONTENTS

PAGE

PAGE

PAGE

PAGE

PAGE

PAGE

PAGE

PAGE

PAGE

PAGE

LIST OF TABLES

TABLE PAGE

LIST OF FIGURES

FIGURE PAGE

PAGE

PAGE

PAGE

CHAPTER 1

INTRODUCTION

Research Problem

The discovery of fullerene led to a new era in carbon material science in 1985. Following this discovery, in 1991, Iijima discovered carbon nanotubes (CNT) with a diameter range between 3-10 nm. The carbon nanotube is a novel nanostructured material with excellent material properties and exhibits interesting behavior. It can be either single walled (SWNT) or multi-walled (MWNT) (Lai, Li, Lin & Yang, 2001; Nicolini, 1996; Popov, 2003; Ratner, D & Ratner, M., 2003).

The SWNT version can be either metallic or semiconductor. Nanotubes are very stiff, very stable and can be built with their length exceeding their thickness thousands of times. With regards to mechanical properties, the Young's modulus of single-walled carbon nanotube exceeds that of steel by over five (5) times, and the tensile strength is more than 375 times. They are stable in high temperatures as well as in an argon environment. In addition, they exhibit strong resistance against strong acid (Kannangara, Raguse, Simmons, Smith, & Wilson, 2002; Nicolini, 1996; Popov, 2003; Ratner & Ratner, 2003).

Chou, Thostenson, Erik and Zhifeng (2001), Lai et al. (2001), Kannangara et al. (2002) and Ratner and Ratner (2003) have reported on several potential applications of carbon nanotubes. They indicated that nanotubes based field-emission flat panel displays have been demonstrated. They also reported that nanotubes can be used to produce flat television and artificial organs. In addition, carbon nanotubes will enable automakers to

replace steel bodies with stronger and lighter plastic composites (Mitsui Co., 2001). In addition, Mitsui (2001) has reported that the global demand for carbon nanotubes is expected to be about 4 trillion Japanese Yen by the year 2020.

Since the discovery of carbon nanotubes, there have been rapid advancements in the technologies for synthesizing carbon nanotubes employed at the laboratory level. The first of these techniques is pulsed arc discharge (PAD). Other methods of recent developments and refinements include continuous arc production, pulsed laser ablation, chemical vapor deposition (CVD), high pressure carbon monoxide conversion (HiPCO), solar, and flame combustion methods among others. Most of these methods use a gaseous form of carbon either directly or indirectly and sometimes associated with or without metal catalyst material as initial or intermediate raw material. If SWNTs are to be produced, metal catalysts are used. On the other hand if MWNTs are to be produced no metal catalyst is used. In addition, buffer or carrier gases (which are usually chemically inert gases such as argon, nitrogen, and helium) are employed for the production of carbon nanotubes. These carrier gases must be in the appropriate atomic distances for carbon nanotubes to be formed (Allard Jr. et al., 2002; Botton, Braidy & El Khakani, 2002; Chen et al., 2002; Chiashi, Kohno, Kojima, Maruyama & Miyauchi, 2002; Fabian, 2001; Flamant et al., 2001; Papadopoulos, 2000; Smith, 2001; Zhang, 1995).

Recent studies have concluded that results from the laboratory scale experiments have indicated the suitability of these techniques for bulk production of carbon nanotubes. In addition, several investigators have reported increases in productivity (defined as the percentage yield times the production rate), simple and safe processing

methods, and indicated the readiness for scale up or industrial or large scale production of the carbon nanotubes (Chiashi et al., 2002; Fabian, 2001; Flamant et al., 2001; Lai et al., 2001; Li, Xu, Wu & Zhu, 2002).

Following these advances, commercial production has begun in Japan, and Mitsui (2001) was said to be planning to build a carbon nanotubes mass-plant. Mitsui (2001), however, claims that the high cost of the carbon nanotubes is preventing its commercialization. Other researchers have also indicated that there are serious constraints limiting large scale production of carbon nanotubes. These limitations include the need to understand the growth process in order to be able to control the carbon nanotubes being synthesized (Chiashi et al., 2002; Flamant et al., 2001; Lai et al., 2001; Li et al., 2002).

Some of the conditions that need to be better understood in order to benefit from successful scaling up of the methods of producing nanotubes have been reported either as recommendations or issues raised by some of the investigators. For instance Fan, Geohegan, Guillorn, Puretzky and Schittenhelm (2002) reported that the majority of single wall carbon nanotubes (SWNT) growth occurred from condensed clusters and nanoparticles of carbon and metal catalyst in contact with one another. Despite this observation, besides using a mixture of graphite and catalyst powders, only one study has been cited that experimented with jets to bring carbon nanoparticles and metal catalyst closer together to improve both yield and volume of carbon nanotubes (Povitsky, 2002).

Furthermore, Achiba et al. (2003) indicated that a higher abundance of carbon nanotubes with controlled diameter distribution can be achieved by laser vaporization

procedure in a mixed gas phase where the effect of molecular mass can be optimized. Further, in spite of this awareness, only one study by Povitsky (2002) was found with the purpose of mixing carbon and metal catalyst vapors using turbulent multiple impinging jets. No other studies were located with the purpose of either mixing carbon and metal catalyst vapors and carrier gases or mixing the different carrier gases at the gas phase during the growth of carbon nanotubes in order to achieve controlled diameter distribution and higher yield of carbon nanotubes.

In addition, Flamant et al. (2001) reported that the yield or selectivity of SWNT depends on the ratio of carbon vapor flow rate to the buffer/carrier gas flow rate in the presence of an annealing zone in the reactor. Yet no research was found with the sole purpose of increasing yield by improving the ratio between the carbon-metal catalyst vapors and carrier gas flow rates. Also, despite the fact that Flamant et al. have reported that improving reactor design (configuration) increased the carbon vaporization rate beyond expectation or prediction in one of their solar methods of synthesizing carbon nanotubes, no studies appeared to have had the sole purpose of improving the design of reactors (configuration) for producing carbon nanotubes.

From the foregoing and in agreement with the present research, it was inferred that there were still several issues related to understanding the growth of carbon nanotubes that need to be addressed. In this study, therefore, one of these problems was explored further to understand the conditions that impact on the control (uniform distribution of atoms and molecules, uniform plume formation, uniform cooling and uniform nucleation) and growth of carbon nanotubes. Specifically, this study was

intended to investigate the combined effects of improving reactor design and operating conditions on the mixing of carrier gases and carbon-metal catalyst vapors to improve the concentration/mixing ratio between carbon-metal catalyst vapors and carrier gases with the view of improving the growth control (diameter, length and purity), yield (volume) and consequently productivity of carbon nanotubes.

This reactor design improvement was done by integrating a static or passive or in-line mixer in the carbon and metal catalyst vapor phase zone into an existing reactor specifically used for producing carbon nanotubes in order to mix the gases and vapors. In order for this study to be applicable in practice to most methods of producing carbon nanotubes, the static mixer was introduced in the single wall carbon nanotubes laser type synthesizing reactor at the region or regime where the carbon and metal catalysts vapors are still in the gaseous phase as reported by Fan, Geohegan, Guillorn et al. (2002) and Fan, Geohegan, Pennycook et al. (2002). Figure 1 indicates the proposed mixing zone in which the static mixer was introduced. However, during computer modeling and simulation only single phase carrier gas flow was used to test the proposed reactor design improvement due to time limitations associated with difficulty in modeling and simulating a multi-phase fluid flow.

This internal re-configuration of the reactor was expected to result in improvement in the carrier gas and carbon-metal catalyst vapor concentration or mixing ratio, thus improving the yield and productivity in the methods employed for synthesizing carbon nanotubes. Further, in order to minimize development cost and to explore several options, computer modeling and simulation experiments were the main experimental

methods employed for collecting data. In addition, for this study to be useful, input data used in the simulation experiments were based on available experimental data.

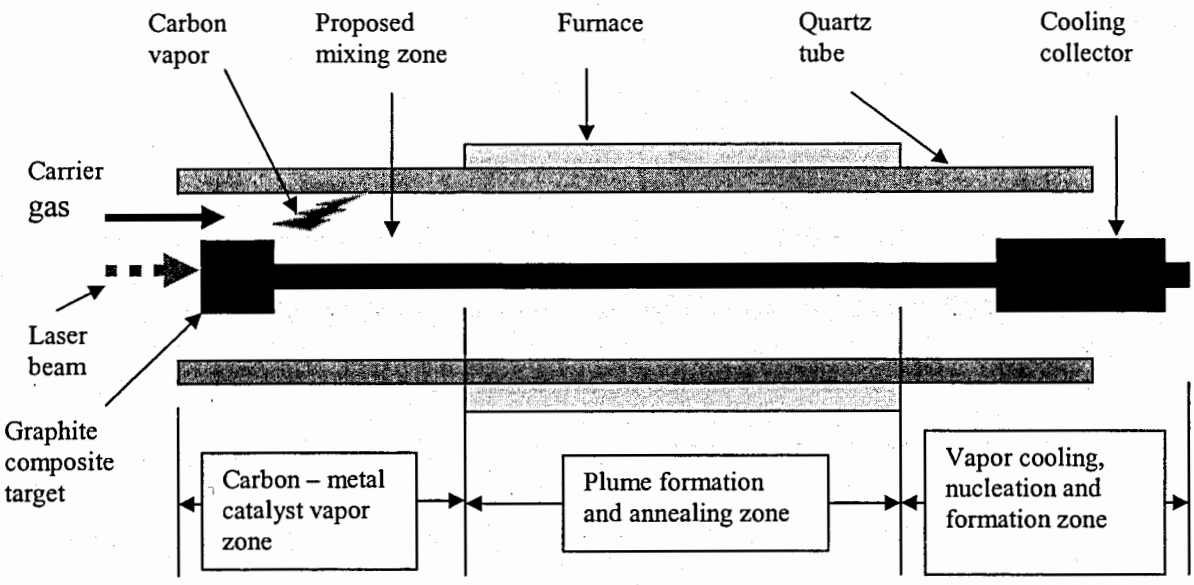

Figure 1. Schematic diagram of an existing laser vaporization reactor without static mixer. The diagram shows the mixing zone where the proposed static mixer was introduced into the reactor. The diagram also shows three sequential zones. The carbon vapor zone shows vaporization of carbon and metal catalyst. These vapors remain in vapor phase for a short period before changing to plume and consequentially cool and nucleate to form carbon nanotubes. It is during the vapor phase that the carrier gas was mixed with the vaporized carbon and metal catalyst to achieve effective mixing as a precondition to contribute to approximate uniform distribution of atoms/molecules and hence consistent plume formation, steady cooling, and therefore homogeneous nucleation leading to the expected boost in yield and consequently to an increase in productivity.

Statement of the Problem

The problem of this study was to investigate the effects of type of static mixer, type of carrier gas (argon and nitrogen gases), carrier gas inlet pressures, and reactor operating temperatures on the mixing ratio of carbon nanotube synthesizing reactors.

Statement of Purpose

The purpose of this study was to improve the design and performance of reactors used for growing carbon nanotubes in order to improve carbon-metal catalyst vapors and carrier gas mixing/concentration ratio to create preliminary conditions for controlled growth (through obtaining uniform distribution of atoms/molecules, and hence uniform plume, thereby achieving uniform cooling and uniform nucleation) to increase percentage purity and achieve uniform size and consequently to maximize yield and increase productivity of formed carbon nanotubes.

Statement of Need/Justification

There were five main factors that comprised the need for this study. The first factor was that for several years, static mixers have been used as a low cost and efficient mixing device employed in reactors to enhance mixing or concentration ratios between fluids including gases for other technological applications. One significant fact noted was that studies on these mixers have shown that different substances, characteristics of the substances, operating conditions and the geometry of the mixers all have different mixing effects. Consequently, the vaporized carbon and various metal catalyst materials and the different carrier gases employed in carbon nanotubes production may all have different mixing effects and as a result have different concentration or mixing ratios for optimal

production of carbon nanotubes (Achiba et al., 2003; Devahastin & Mujumdar, 2001; Devahastin, Mujumdar & Wang, 2004; Fang & Lee, 2001; Gong, Luo & Wu, 2004).

In spite of this awareness, relevant confirmatory studies were yet to be located that described the merits and demerits of the static or in-line or passive mixers under known carbon nanotubes growth and operating conditions specifically for improving mixing of carrier gases or mixing carrier gases together with carbon-metal catalyst vapors needed for successful growth control (diameter, length, and purity), maximizing yield and consequently increasing productivity of carbon nanotubes. Reports from several studies have indicated effectiveness of a laser vaporization method for synthesizing single wall carbon nanotubes employ carbon and metal catalyst vapors and various types of carrier gases. This method is said to have the highest yield but lowest productivity, and the productivity was defined by Flamant et al. (2001) as percentage yield times the production rate (Akos, Bogaerts, Chen & Gijbels, 2003; Devahastin & Mujumdar, 2001; Devahastin et al., 2004; Fang & Lee, 2001; Flamant et al., 2001; Gong et al., 2004).

On the other hand, other known methods such as solar that also use similar raw materials were said to have higher productivity but lower yields. Hence, understanding the role of static mixers together with operating conditions associated with mixing of different carrier gases will help understand and hopefully help improve carbon-metal catalyst vapors and carrier gas concentration/mixing ratios and consequently improve growth control, yield and productivity of most of the various methods employed in carbon nanotubes production (Akos et al., 2003; Devahastin & Mujumdar, 2001; Devahastin et al., 2004; Fang & Lee, 2001; Flamant et al; Gong et al., 2004).

Secondly, there is also the need or justification to contribute to a data base for a national repository of manufacturing processes, assembly planning, and modeling (Gaines & Regli, 1997). Gaines and Regli (1997) have reported on the introduction of design, planning and assembly repository at the National Institute of Standards and Technology (NIST) with the goal of providing a publicly accessible collection of 2-D and 3-D CAD, solid models, assemblies and process planning from industry problems. Gaines and Regli (1997) are of the view that the repository to be developed in collaboration with government agencies, industry, and academia will provide a library of example data that can be available to the research community.

In addition, the third reason for this study is that, on the future of simulation, Bowden, Ghosh and Harrell (2000) reported that Fishwick (1997) had proposed that technologies such as the internet or world wide web, Common Object Request Broker (CORBA) and Distributed Component Object Model (DCOM) promise to enable parallel and distributed model execution and provide mechanism for maintaining distributed model repositories. According to Bowden et al. (2000), when these models are available, they can be shared by many modelers.

Further, the fourth reason for conducting this simulation modeling of static mixers was to explore theoretically based methodology. There are two known types of data gathering methods for analysis, the theoretical and empirical. The empirical techniques gather data from concrete, repeatable, and verifiable observations by the researcher. Empirical data are normally gathered by a measurement device accurately calibrated. On the other hand, theoretical techniques gather data based on speculation of future course of

action. These data gathering techniques can be derived from computer simulation, intuition or speculation for future course of action for building models and for analysis (Bogaerts, Chen, Gijbels & Vertes, 2003; Council on Technology Education [CTE], 1987).

In this study, the theoretical data gathering technique, using intuition, speculation and most importantly computer simulation regarding introduction of static mixers for mixing gases for growing carbon nanotubes was adopted as a means of collecting data. This dramatically reduced time and cost for actual physical experimentation which if conducted might not have yielded the results expected (Bogaerts et al., 2003; CTE, 1987).

Finally, the fifth reason for the study was that, in support of the use of theoretical models to speculate about the role of static mixers in improving growth of carbon nanotubes, the National Science Foundation [NSF], (n.d.) has provided an adequate framework for such studies. The following quote from NSF on nanomanufacturing program summarized the need for this study:

> "The program covers interdisciplinary research and promotes multi-functionality across all energetic domains, including mechanical, thermal, fluidic, chemical, biochemical, electromagnetic, optical etc. The focus of NanoManufacturing is in a systems approach, encompassing nanoscale materials and structures, fabrication and integration processes, production equipment and characterization instrumentation, theory/modeling/simulation and control tools, biomimetic design and integration of multiscale functional systems, and industrial application" (NSF).

From the foregoing, the additional benefits of employing simulation modeling of static mixers with carrier gases to improve design of nanotubes synthesizing reactors and hence growth of carbon nanotubes cannot therefore be overemphasized. Further, the

benefits to be derived from this study have been amplified by Conway and Maxwell in their quote "We no longer have the luxury of time to tune and debug new manufacturing systems on the floor, since the expected economic life of a new system, before revision will be required, has become frighteningly short" (Bowden et al., 2000, p. 275).

Research Questions and Statement of Hypotheses

Research Questions

The following research questions were designed to be explored in this study:

Research question one. Will a static mixer in a carbon and metal catalyst vapor zone of a laser vaporization reactor for synthesizing carbon nanotubes improve the mixing or concentration ratio between carbon-metal catalyst vapors and carrier gases?

Research question two. Will the main factors, namely type of static mixer, type of carrier gas, carrier gas inlet pressure, and reactor operating temperature have significant effects on the mixing ratio between carbon-metal catalyst vapors and carrier gas at controlled carrier gas inlet flow rate and inlet temperature?

Statement of Hypotheses

The following hypotheses were intended to be used in this study:

Hypothesis one. The null hypothesis 1, H_{01} is that there are no strong relationships between independent variables (type of static mixer, type of carrier gas-argon and nitrogen, carrier gas inlet pressures, and reactor operating temperatures) and the dependent variable (mixing ratio) at constant carrier gas inlet flow rate and inlet temperature. The alternative hypothesis 1, H_{a1} is that there are strong relationships between independent variables (type of static mixer, type of carrier gas- argon and

nitrogen, carrier gas inlet pressures, and reactor operating temperatures) and the dependent variable (mixing ratio) at constant carrier gas inlet flow rate and inlet temperature.

Hypothesis two. The null hypothesis 2, H_{02} is that there are no significant differences between type of carrier gas (Argon and Nitrogen) on the dependent variable (mixing ratio) due to the effects of type of static mixer, carrier gas inlet pressures, and reactor operating temperatures at constant carrier gas inlet flow rate and inlet temperature. The alternative hypothesis 2, H_{a2} is that there are significant differences between type of carrier gas (Argon and Nitrogen) on the dependent variable (mixing ratio) due to the effects of type of static mixer, carrier gas inlet pressures, and reactor operating temperatures at constant carrier gas inlet flow rate and inlet temperature.

Hypothesis three. The null hypothesis 3, H_{03} is that there are no significant differences between types of static mixer on the dependent variable (mixing ratio) due to the effects of type of carrier gas (Argon and Nitrogen), carrier gas inlet pressures, and reactor operating temperatures at constant carrier gas inlet flow rate and inlet temperature. The alternative hypothesis 3, H_{a3} is that there are significant differences between types of static mixer on the dependent variable (mixing ratio) due to the effects of type of carrier gas (Argon and Nitrogen), carrier gas inlet pressures, and reactor operating temperatures at constant carrier gas inlet flow rate and inlet temperature.

Hypothesis four. The null hypothesis 4, H_{04} is that there are no significant differences between levels of reactor operating temperature on the dependent variable (mixing ratio) due to the effects of type of static mixer, type of carrier gas (Argon and

Nitrogen), and carrier gas inlet pressures, at constant carrier gas inlet flow rate and inlet temperature. The alternative hypothesis 4, H_{a4} is that there are significant differences between levels of reactor operating temperatures on the dependent variable (mixing ratio) due to the effects of type of static mixer, type of carrier gas (Argon and Nitrogen), and carrier gas inlet pressures at constant carrier gas inlet flow rate and inlet temperature.

Hypothesis five. The null hypothesis 5, H_{05} is that there are no significant differences between levels of carrier gas inlet pressures on the dependent variable (mixing ratio) due to the effects of type of static mixer, type of carrier gas (Argon and Nitrogen), and reactor operating temperatures at constant carrier gas inlet flow rate and inlet temperature. The alternative hypothesis 5, H_{a5} is that there are significant differences between levels of carrier gas inlet pressures on the dependent variable (mixing ratio) due to the effects of type of static mixer, type of carrier gas (Argon and Nitrogen), and reactor operating temperatures at constant carrier gas inlet flow rate and inlet temperature.

Assumptions

The following assumptions were made in the pursuit of this study. These are:

1. The single wall carbon nanotubes processing steps and experimental data available on laser vaporization method for synthesizing carbon nanotubes will provide adequate actual experimental information on carbon-metal catalyst vapors, carrier gases, reactor specifications, and process specifications to be employed for the computer modeling and simulation experiments (Bogaerts et al., 2003; Fan, Geohegan, Pennycook, & Puretzky, 2000; Flamant et al; Hester & Louchev, 2003).

2. Integrating any type of static mixer into carbon nanotubes synthesizing reactor will improve the design and performance of reactors. Hence, the results of the mixing ratios (indices) obtained from single-phase carrier gas flow in the carbon–metal catalyst vapor zone of the laser method of synthesizing single wall carbon nanotubes can be generalized to multi-phase CNT gaseous raw material flow and other methods of growing nanotubes.

3. Neglecting the location or position of a graphite target with its holding rod in the middle of the front portion of the reactor and the static mixer will not affect the results significantly.

4. Argon and nitrogen carrier gases will provide statistically significant and important information for the study. This is because comparatively, argon is a noble, inert, monatomic and heavier carrier gas. On the other hand, nitrogen is chemically inert, diatomic and lighter carrier gas (Dubson, Taylor & Zafiratos, 2004; Parkes, 1961).

5. Using temperature as a tracer and measuring the temperature differences at the cross section of the exit of the static mixers will provide adequate representation of the mixing or concentration ratio of the carrier gases due to the effects of the static mixer, type of carrier gas, inlet pressure and inlet temperature.

6. In this preliminary study, neglecting the effects of reactor operating temperature on the carrier gas transport properties, that is viscosity and thermal conductivity, will not affect the results significantly.

7. Resultant mixing ratios (indices) obtained from modeling and simulation experiment of the static mixers using only single-phase carrier gases will generate

representative data for the mixing or concentration ratio between carbon–metal catalyst vapors and carrier gases when static mixers are integrated into carbon nanotubes synthesizing reactors.

Delimitations and Limitations

The following delimitations were inherent in the study:

1. The target population is reactors employed by production methods specifically for growing carbon nanotubes. These include reactors used in laser, solar, arc discharge, flame combustion, chemical vapor deposition, and high-pressure carbon monoxide conversion methods of synthesizing carbon nanotubes (Fan, Geohegan, Guillorn, Puretzky, & Schittenhelm, 2002; Flamant et al., 2001; Lai et al., 2001).

2. The subset of the population specifically examined was reactors used in laser vaporization methods for producing single wall carbon nanotubes (Fan, Geohegan, Guillorn et al., 2002).

This study was also conducted in view of the following limitations:

1. To simplify the simulation only single phase carrier gas flow will be modeled and the results generalized to three phase flow involving carbon vapor, metal catalyst vapors, and carrier gas.

2. The modeling and simulation experiment was limited to three types of static mixer designs. They were two proposed improved ones, namely baffle and aerodynamic types and an existing reactor without a static mixer. The static mixer served as the experimental and measuring units. In this exploratory study only configurations of the static mixer designs were considered under same characteristic dimensions. (The

effects of the variation in the characteristic dimensions of the static mixers should be considered in future studies).

3. The choice of carrier gases for this study were argon and nitrogen based on the reasons already stated in the assumption number 4.

4. As a procedure, the simulation experiment was performed systematically. First the carbon-metal catalyst vapor zone of the single wall carbon nanotubes reactor without a static mixer was modeled and simulated. Secondly, the reactors improved with integrated proposed static mixers were simulated sequentially. In each case, first nitrogen carrier gas was simulated and data collected. This was followed by Argon under the same treatment conditions.

5. Allard Jr. et al. (2002) reported that, approximately 5×10^{16} carbon and 10^{14} Ni/Co metal catalyst atoms vaporized remain in the vapor phase up to 100 μs. In spite of this short time, the static mixer will be located in the carbon-metal catalyst vapor zone of the laser type reactor in order to easily replicate the results to order methods that do not have this time flight limitations. Consequently, specifications of the reactor were based on the size of quartz tube (diameter 2") and graphite target (diameter 1") excluding the graphite holding rod (diameter 0.25") employed by Allard Jr. et al.

Definition of Terms

The following terms were defined to clarify their use in the context of the study:

1. Buffer or Carrier Gases: are background inert gases which flow gently to carry the vaporized carbon-metal catalyst nanoparticles through the reactor to the cooling subsystem and also to prevent vaporized carbon vapors from covering the transparent

construction materials (Fabian, 2001; Ichihashi et al., 1999; Kasuya, Kokai, Iijima, Takahashi & Yudsaka, 2002).

2. Bulk Temperature: the bulk temperature is also referred to as the cup mixing temperature. This bulk temperature was explained as the temperature of the fluid assuming that the fluid has been collected in a cup at the outflow and it has been properly mixed (COMSOL AB., 2004h; Devahastin, Mujumdar & Wang , 2004).

3. Carbon Nanotubes (CNT): are unique tubular structures of nanometer diameter and large length-to-diameter ratio. The nanotubes may consist of one and up to hundreds of concentric shells of carbon atoms with adjacent shells separation of about 0.34 nm (Popov, 2003; Ratner, D & Ratner, M., 2003).

4. Conduction: thermal conduction is the transfer of heat between two solid materials that are physically touching each other (Environmental Chemistry.Com [ECC], n.d.).

5. Convection: it is the movement of heat by a moving fluid such as liquid or gas. Convection results from differences in the densities of a material at different temperatures. As fluid such as a liquid or gas rises in temperature, it becomes less dense and consequently it becomes lighter thereby rising above its cooler and denser counterparts, which in turn sink.

6. Mixing effectiveness: it the same as the mixing index. It is the deviation of the temperature at the specific radial location of cross section of the exit channel divided by the bulk temperature multiplied by a hundred percent (Devahastin et al., 2004).

7. Mixing index: is the deviation of the temperature at the specific radial location of cross section of the exit channel divided by the bulk temperature multiplied by a hundred percent (Devahastin et al., 2004).

8. Mixing ratio: is the deviation of the temperature at the specific radial location of cross section of the exit channel divided by the bulk temperature (Devahastin et al., 2004).

9. Model: is an imitation of a physical structure or a concept designed to accurately describe and predict certain characteristics of the structure or concept in accordance with the purposes of the modeler, or a mathematical relationship which relates changes in a given response to changes in one or more factors (Alcorn, 2003; COMSOL AB., 2004b; COMSOL AB., 2004d; NIST/SEMATECH., 2003).

10. Multi-Walled Carbon Nanotubes (MWNTs): are concentric cylinders of nanotubes produced in the form of tight bundles. They are very straight indicating high crystallinity and have lengths of more than 10 μm and diameters range between 5-50 nm. They are usually purified by heating in an oxygen environment (Fabian, 2001; Zhang, 1995).

11. Simulation: is the imitation of a dynamic system using a computer model in order to evaluate and improve system performance (Bowden et al, 2000; Cross, Markatos, Rhodes & Tatchel, 1986). This simulation used for this study is not Monte Carlo simulation.

12. Single Wall Carbon Nanotubes (SWNTs): are produced in presence of a metal catalyst such as cobalt, nickel or iron. The diameters are usually between 1-10 nm

and they are usually assembled in a rope like fashion. They are normally purified by refluxing in a nitric acid solution for an extended period of time (Borowiak-Palen et al., 2002; Fabian, 2001).

13. Static Mixer: it is also called motionless or passive or in-line mixer. It is a mixer without moving parts and normally used in reactors to improve mixing or concentration ratio between two or more fluids. It is said to be well suited for laminar flow (Bauer, Bolz, Khinast & Panarello, 2003; COMSOL AB., 2004c).

CHAPTER 2

LITERATURE REVIEW

Carbon Nanotubes and Their Processing Methods

Extraordinary Properties of Carbon Nanotubes

Considerable interest has been shown in carbon nanotubes. Their amazing mechanical and electronic properties are due to their quasi-one-dimensional structure and the graphitic type of carbon atoms arrangement in the shells. Depending on particular combinations, carbon nanotubes could be metallic and hence conducting. Consequently great interest has been shown in the conductivity of carbon nanotubes. Further, the conductivity has been shown to be a function of the diameter of the nanotube. Single wall carbon nanotubes (SWNTs) are described in terms of diameter of the individual SWNT, and the length and diameter of the bundle. These geometrical features are determined by the growth conditions which are normally controlled. Growth of 30-70 nm long SWNT in 1 ms has been reported (Kamat & Liz-Marzan, 2003; Kanangara et al., 2002; Kasuya et al., 2002; Popov, 2003).

Kanangara et al. (2002) explained that some types of armchair carbon nanotubes appear to conduct better than other metallic nanotubes. In addition, the interwall reactions of multi-walled carbon nanotubes were found to redistribute the current over individual tubes across the carbon nanotube structure non-uniformly. Also, the electronic properties of single wall carbon nanotubes have been investigated with atomic force microscopes. Kannangara et al. (2002) argued that single wall carbon nanotubes are the most highly conductive carbon fibers known. They explained that this is supported by the measured

resistivity of single wall carbon nanotubes, which was found to be in the order of 10^{-4} ohms per cm at 27° C. According to Kannangara et al. (2002) measurements showed that the current density in nanotubes is greater than 10^7 A/cm^2. In addition, other investigators reported that individual carbon nanotubes may contain defects. However, these defects could be exploited to permit a single wall carbon nanotube to behave as a transistor. Further, joining nanotubes together formed transistor-like devices. Thus, a SWNT with a natural junction acted like a rectifying diode–a half transistor in a single molecule (Kanangara et al., 2002; Popov, 2003; Zhang, J., 1995).

Investigators also reported that suspended nanotubes deflected from an equilibrium position and hence were described as springs. SWNTs are stiffer than steel and are resistant to damage from physical forces. It was reported that when the tip of a carbon nanotube was pressed, it bent without damage to the tube. Consequently when the force was removed, the tip of the nanotube recovered to its original state (Kamat & Liz-Marzan, 2003; Kanangara et al., 2002). In spite of the aforementioned extraordinary properties, Kannangara et al. reported that there were rather great difficulties in quantifying these effects because exact numerical values could not be agreed upon. Kannangara et al. elaborated on the apparent difficulties by stating that the current Young's modulus of single wall carbon nanotubes is about 1 TPa, and yet this value was disputed and other reports claimed a value as high as 1.8 TPa.

The dispute on the exact figures of Young's modulus was supported by Kamat and Liz-Marzan (2003) account. For example Kannangara et al. (2002) reported that a (10, 10) armchair nanotube has a Young's modulus of 640.30 GPa. On the other hand, a (17,

0) zigzag carbon nanotube has a Young's modulus of 648.43 GPa, and a 673.94 GPa for a (12, 6) carbon nanotube. Kanangara et al. explained that the source of these differences could come from different experimental measurement procedures. On the other hand, the range of values reported by Kamat and Liz-Marzan were generally higher than those reported by Kannangara et al.

Kannangara et al. (2002) further indicated that other investigators have shown that theoretically, the Young's modulus of nanotube depended on the size and chirality of the SWNT. The theoretical figures range from 1.22 TPa for (10, 0) and (6, 6) SWNT to 1.26 TPa for large (20, 0) single wall nanotube. However, in general terms a nanotube has a calculated value of 1.09 TPa. Kannangara et al. reported that measurements of the strength of multi-wall carbon nanotubes (MWNT) with atomic force microscope (AFM) depended on the size. On the other hand, the modulus of MWNT depended on the amount of disorder in the walls of the nanotubes. This, according to these investigators confirmed the reason why MWNT breaks with the outermost layers breaking first (Kamat & Liz-Marzan, 2003; Kanangara et al., 2002).

Uses and Applications of Carbon Nanotubes

Carbon nanotubes are used as materials because of their high Young's Modulus. Thus, although, carbon fiber is used in composite materials, carbon nanotubes have great promise in the same market because of their exceptionally higher length-to-diameter ratio, notably in stress transmission (Kamat & Liz-Marzan, 2003; Kanangara et al., 2002; Popov, 2003).

SWNT deformed reversibly when charged electrochemically. As a result, the SWNT electrical properties can be exploited to generate mechanical motion from electrical energy. Accordingly nanotubes can be exploited for use as gas and other sensors for environmental, biological and chemical applications. This is because of the extreme sensitivity of nanotubes electronic properties to the presence of trace elements (Kamat & Liz-Marzan, 2003; Kannangara et al., 2002).

The usefulness of carbon nanotube storage for energy in the form of hydrogen, lithium, oxides, and metals, among others was reported by many authors. Hydrogen has better energy content on mass-to-mass basis than petrol. However, hydrogen is competing with fossil fuels because it is a gas. The target for hydrogen capacity that is of interest to automobile manufacturers is 6.5 percent by weight and this drives the importance of nanotubes (Kamat & Liz-Marzan, 2003; Kanangara et al., 2002; Popov, 2003).

Carbon nanotubes can be used to store helium. This can easily be exploited for fusion energy. Further, according to Kanangara et al. (2002) nanotubes can be used as materials such as metals including copper and also oxides. For this reason nanotubes can be employed as nano-test tubes and the carbon can be removed to create nano-copper wires for nano-electrical circuits (Kanangara et al., 2002).

There is reported use of nanotubes in batteries. Nanotubes could store lithium ions, which are charge carriers for some batteries. With graphite, six carbon atoms are needed for every one lithium ion, on the other hand due to the geometry inherent in

bundles of nanotubes, this may allow the nanotubes to accommodate more than one lithium ion for every six carbon atoms (Kanangara et al., 2002).

Further, the electronic industry has been looking for alternatives due to the continuing problems posed by miniaturization of silicon components and fine control of electronic properties at the smaller scale level (Kanangara et al., 2002). With the discovery of carbon nanotubes the solution to this previously intractable problem is now a possibility (Kanangara et al., 2002; Smith, 2001). Kannangara et al. (2002) illustrated that one of these successes was demonstration of a transistor by hooking up carbon nanotubes.

Additionally, Kanangara et al. (2002) explained that circuits have been built by draping a SWNT over three parallel gold electrodes, and polymer was added between the electrodes and potassium atoms were sprinkled on top. By this arrangement, in accordance with the Kanangara et al. account, the potassium atoms added electrons to the nanotubes. Additionally, according to Kanangara et al. carbon nanotubes have been used in a computer circuit to make a logic circuit.

As result of these successes, several companies in the world are attempting to exploit carbon nanotubes in flat panel displays. Field emission is the property that makes flat panel displays work. Presently, according to investigators, even mixtures of MWNTs, which are not so elegant, are good at field emission. They emit electrons under the influence of an electrical field. Based on these characteristic properties, millions of nanotubes are arranged just below the screen to provide the required pixel (Kamat & Liz-Marzan, 2003; Kanangara et al., 2002).

When nanotubes are appropriately substituted with various structures, they can act as axles in nano machines. It may be possible to gear different nanotubes together to translate different rotational motion or change the direction of that motion. This can be done by building gear teeth on the nanotubes. In addition, mechanically, combinations of carbon nanotubes and fullerenes have been conceived as molecular pumps or pistons. They can therefore be employed as electromechanical actuators. Researchers have made the first pump at the University of California, Berkeley. These researchers developed the first nano-bearings by attaching one end of MWNT to a stationary gold electrode. With the use of a scanning electron microscope, the researchers observed how the inner core was pulled back inside by intra-molecular van der Waals forces, thus making the MWNT act like a bearing (Kamat & Liz-Marzan, 2003; Kanangara et al., 2002).

One of the extremely interesting applications of the nanotube-bearing concept is in its use as nanoswitch. This was achieved by applying a voltage to the carbon nanotube bearing, whereby the inner central nanotube was rapidly forced to slide out. Thereby a piston was formed by moving the inner nanotube of a MWNT (Kanangara et al., 2002).

One of the over riding factors in the design of spacecraft and aircraft that enter the planet's atmosphere is the weight-to-power ratio. This is because smaller and lighter air or space borne crafts are cheaper to make. Using carbon nanotube structural materials can radically reduce structural mass, reduce size of electronics, and reduce power consumption. In addition, using such atomically precise materials and components would shrink many components (Kanangara et al., 2002).

Also thermal protection of spacecraft is very important for atmospheric re-entry and other situations that require high temperatures. Carbon nanotubes have the capabilities to withstand high temperatures. Further, the large value of the Young's modulus of carbon nanotubes in the order of one terapascal (pascals x 10^{12}) is of great benefit in withstanding aeronautical strains. This mechanical property will also assist strains during re-entry into the atmosphere (Kanangara et al., 2002).

Methods and Reactors Used for Growing Carbon Nanotubes

Since the use of the conventional electric arc production technique from 1996, several other competing new high or bulk production methods for growing both single and multi-wall carbon nanotubes have been developed. Some of these techniques are pulsed arc discharge; continuous arc production; pulsed laser ablation, and catalytically grown single-walled nanotubes, solar, and flame combustion among other methods (Chen et al., 2003; Smith, 2001; Popov, 2003). In the following subsequent subsections some of these methods and their reactors have been described.

Arc discharge method. The arc discharge is a method that can be used to produce both SWNTs and MWNTs. This method is shown schematically in Figure 2. The method works by controlling the growth conditions such as arcing current and pressure of inert gas in a chamber/vessel. Carbon atoms are then evaporated at temperatures above 3000 ^{o}C in plasma of inert gas that is ignited by high currents passing through opposing carbon cathode and anode. The inert gases often used are helium or argon gas. This method is currently a batch process and hence after the vaporization, the whole system must cool before the formed carbon nanotubes are collected (Fabian, 2001; Popov, 2003).

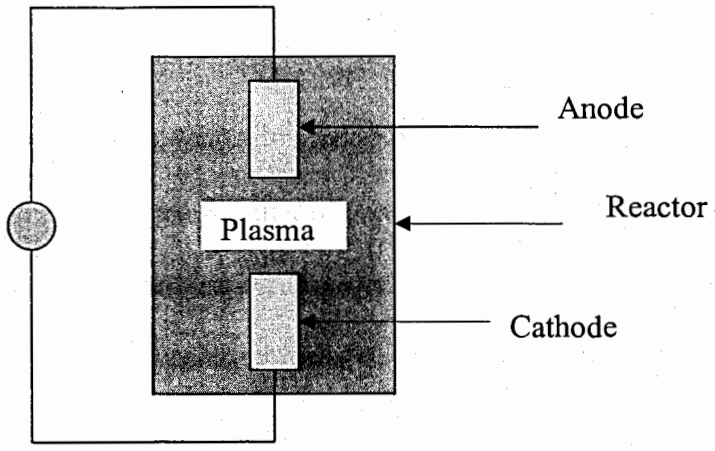

Figure 2. An arc discharge method for growing carbon nanotubes. The diagram shows two graphite electrodes (anode and cathode) in a reactor with an inert gas atmosphere. The reactor is vessel or chamber that contains the inert gas atmosphere. From "Carbon nanotubes fabrication" by C. M. Fabian, 2001.

Popov (2003) reported that there are variants of the arc discharge technique. He reported on the use of thin electrodes with voltage of approximately 18 V dc in a helium gas environment at a pressure of 500 Torr. According to him this method yielded approximately 75% carbon nanotubes and transmission electron microscope (TEM) analysis revealed MWNTs with diameters in the range of 2 to 20 nm.

He also reported that Bethune et al. (1993) used thin and bored electrodes filled with mixture of pure powdered metals of iron, nickel or cobalt at arcing current of 95-105 A dc in a helium gas environment at pressure in the range of 100-500 Torr to grow SWNT with uniform diameters of 1.2 ± 0.1 nm. Further, Popov (2003) reported that investigators had concluded that the unique growth mechanism of carbon nanotubes does

not depend on experimental conditions, but more on the kinetics of condensation of the vaporized materials.

Chemical vapor deposition method. The chemical vapor deposition (CVD) method can be used to grow either MWNTs or SWNTs. The method with a quartz tube reactor is shown schematically in Figure 3. The process involves the dissociation of hydrocarbon molecules catalyzed by a transition metal, and followed by the dissolution and saturation of carbon atoms in the metal nanoparticle. It involves heating a catalyst material to high temperatures in a tube furnace and flowing hydrocarbon gas through the tube reactor (Fabian, 2001; Popov, 2003).

The CNTs in a CVD reactor are grown over the catalyst and are collected when the system is cooled to room temperature. The key growth parameters are hydrocarbons, catalysts, and growth temperature. MWNTs use acetylene gas as the carbon source and a growth temperature between 550-1000 °C. Alternatively, SWNTs use carbon monoxide or methane as a carbon source and a much higher growth temperature ranging between 900-1200 °C (Fabian, 2001; Popov, 2003).

Similar to the arc discharge and laser methods, Popov (2003) reported that the best results for SWNT were obtained with the CVD when Fe, Ni or Co catalyst were used. He further indicated that it has been argued that nanotubes grow from the catalyst nanoparticles by tip growth or base growth depending on the contact force between the catalyst particles and the substrate. Popov (2003) also noted that Li et al (1996) synthesized MWNT with diameter of ~30 nm and length within 50 to 100 μm by using a

substrate containing iron nanoparticles embedded in mesoporous silica placed in the reactor with a flowing acetylene mixed with nitrogen at flow rate of 110 cm^3/min.

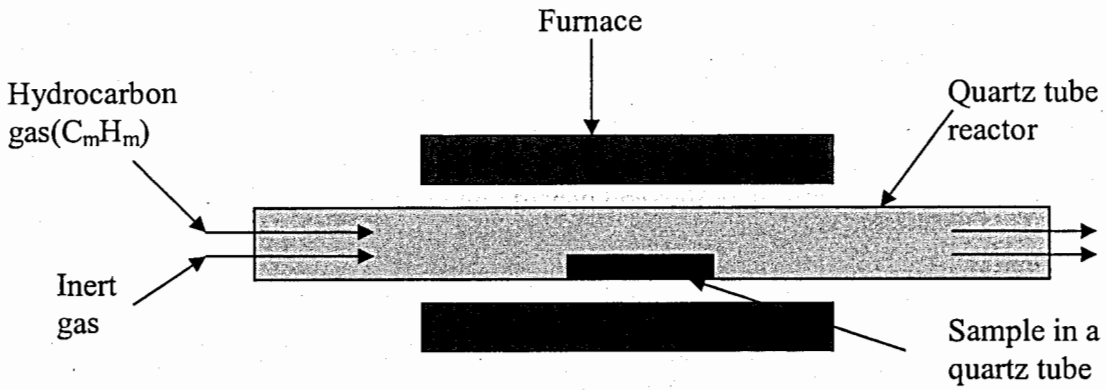

Figure 3. A chemical vapor deposition (CVD) reactor for growing carbon nanotubes. The hydrocarbon gas (C_mH_m) is decomposed in a quartz tube reactor in a furnace at a temperature between 550–1200 °C over metal catalyst. From "Carbon nanotubes fabrication" by C. M. Fabian, 2001.

High pressure carbon monoxide conversion method (HiPCO). The high-pressure carbon monoxide conversion (HiPCO) was said to be a promising new method for bulk production of SWNTs. By this process, catalytic particles are generated in-situ using thermal decomposition of iron pentacarbonyl in a reactor heated to 800-1200 °C. The process is done at a high pressure (~10 atm) to speed up the growth and uses carbon monoxide as the primary carbon source (Fabian, 2001).

Solar vaporization method. Flamant et al. (2001) described the solar method of growing carbon nanotubes when they undertook research with the ultimate goal to scale up a solar process from 2 to 500 kW. Flamant et al. reported that Chibante used a small parabolic mirror to focus solar energy on 0.4 mm and Fields et al. used 6 mm diameter graphite rod respectively. However, Flamant et al. used 6 cm diameter and 10 cm long graphite target. The rod according to Flamant et al. was mounted inside a long pyrex tube of internal diameter 58 mm and 30 cm long and placed coaxially along the optical axis of the parabolic mirror. Figure 4 shows a configuration of a reactor for the solar method of growing carbon nanotubes.

Flamant et al. (2001) described other solar apparatus for growth of carbon nanotubes. However, they indicated that in one such design it was assembled with a water-cooled brass base. This base was then equipped with a filter that functioned to separate the soot from the inert flow. As shown in Figure 4, Flamant et al. also reported the use of a water-cooled heat exchanger located at the back side of the tube to cool the carbon vapor before entering into a 1 m long filter bag.

In operating these solar methods, Flamant et al. (2001) indicated that the reactor was first evacuated to less than 0.25 hPa. It was then later degassed with an inert gas such as helium at 25 hPa. Of great significance to their study were the methodology employed and other major significant theoretical propositions made to achieve the goal of the study. First, Flamant et al. reported that one of the most important parameters in the reactor that governed fullerene growth was the concentration of carbon atom number density to argon number density.

Further Flamant et al. (2001) indicated that there were other factors that influenced yield. The factors outlined as a three process step employed for their study were: (a) vaporization at high temperatures (3400–3500 K) leading to formation of small clusters, (b) expansion of carbon vapor in order to avoid large cluster formation, and (c) fullerenes are formed by allowing clusters to grow in an annealing zone (1500 K).

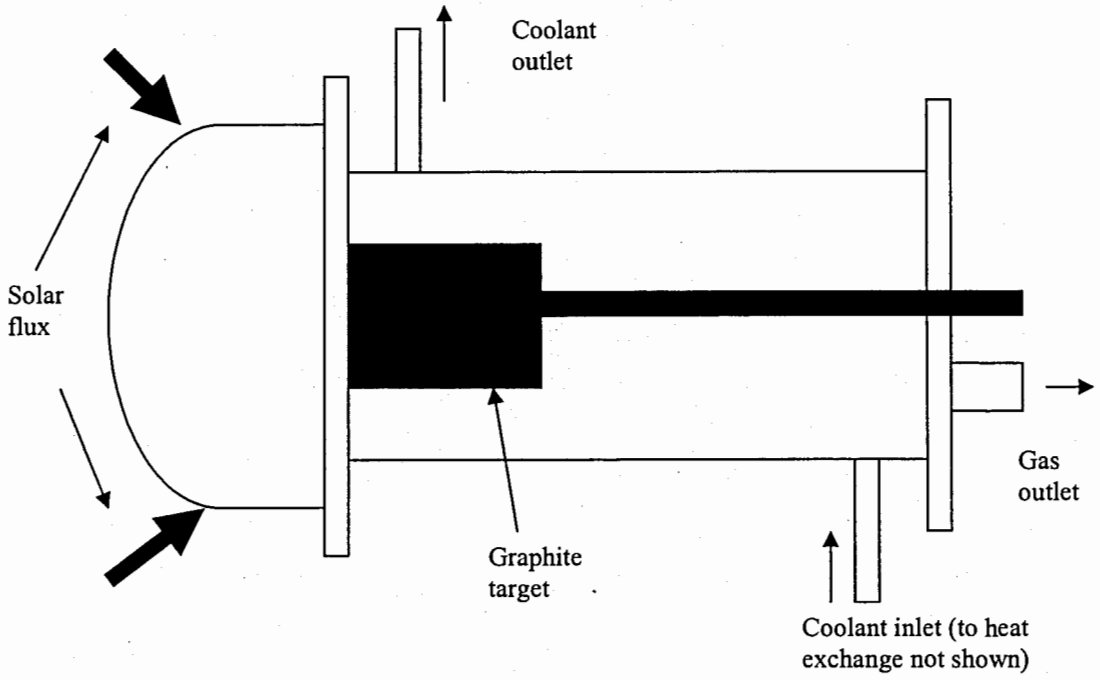

Figure 4. A solar method for growing carbon nanotubes. From "Towards the large scale production of fullerenes and nanotubes by solar energy. *Proceedings of Solar Forum 2001: Solar Energy the Power to Choose,* April 21-25, 2001, Washington, DC" by G. Flamant, J. Giral, T. Guillard, D. Laplaze, B. Rivoire, & J. Robert, 2001.

Furthermore, Flamant et al. (2001) decided to design a reactor concept that will perform according to the three steps outlined and set the following three design goals to be met in order to achieve the purpose of their research. The reactor design goals were:

1. Radiation thermal losses should be minimized in order to reach high surface temperature.
2. In order to avoid carbon deposition on the window where the solar beam enters and to allow easy collection of carbon soot the carbon vapor flow should be directed.
3. The three process steps proposed for formation of fullerene should be incorporated.

When Flamant et al. (2001) employed this procedure they concluded that they exceeded the theoretical predictions. This is a strong indication that improving the design of reactors will contribute to improving yield and productivity of carbon nanotubes as stated in the purpose of this study.

Flame combustion method. Alford, Diener, and Nielson (2000) provided technical description and specification of a reduced-pressure combustion synthesis apparatus for growing carbon nanotubes and fullerenes in a research with the topic synthesis of single wall carbon nanotubes in flames. In that research Alford et al. (2000) described the flame experimental method and results from their experiment. Figure 5 presents the schematic diagram of a flame method for synthesizing carbon nanotubes as described by Alford et al.

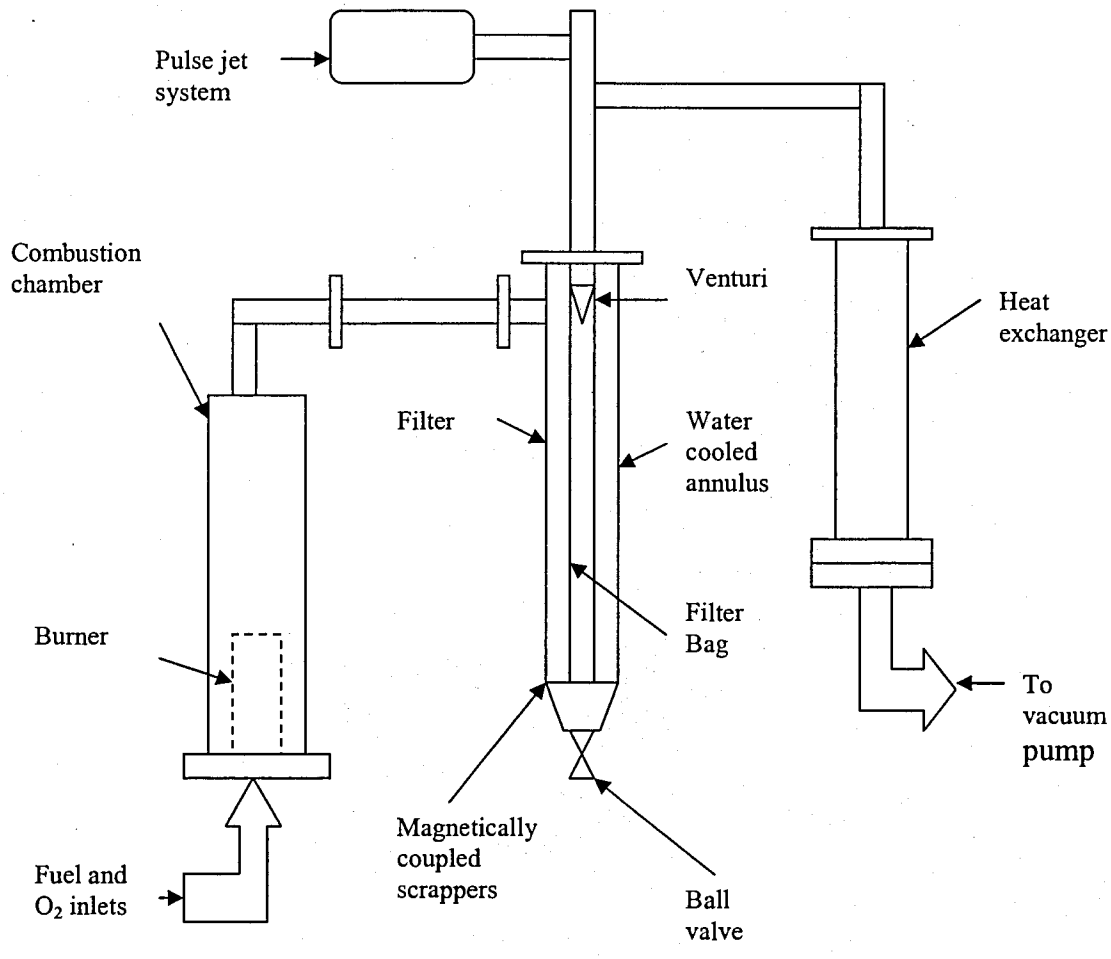

Figure 5. A flame type reactor for growing carbon nanotubes. From "Synthesis of single wall carbon nanotubes in flames" by J. M. Alford, M. D. Diener, & N. Nielson, 2000.

Laser Ablation Method of Growing Carbon Nanotubes

Working principles. The Laser vaporization or ablation process is said to be one of the best methods for producing SWNTs. Figure 6 illustrates a typical example. It is

used to grow and form nanomaterials employing pulsed or continuous laser by evaporating or ablating a carbon target which contains a small amount of metal catalyst (~1 atomic % Ni and ~1% Co) into a background inert gas (~500 Torr of Ar). The inert gas which is also referred to as buffer or carrier gas flows gently through a quartz tube oven heated to a high temperature (~1000 °C). The buffer gas flowing through the chamber carries nanotubes "downstream" and the SWNTs condense from the laser vaporization plume and are deposited on a cooling collector outside the furnace zone (Fabian, 2001; Popov, 2003).

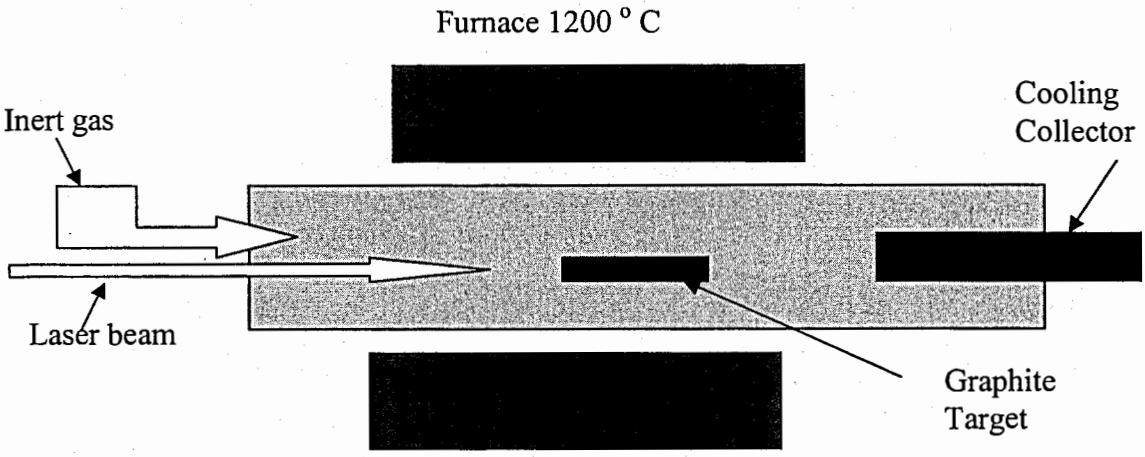

Figure 6. A laser vaporization method with a reactor for producing carbon nanotubes. The laser beam vaporizes the target made of graphite and sometimes with a mixture of metal catalyst such as nickel or cobalt in a reactor with the flowing inert gas under a controlled pressure carries the vaporized material and cooled the nanotubes and deposited outside the reactor. From "Carbon nanotubes fabrication" by C. M. Fabian, 2001.

Popov (2003) reported that in 1996 Smalley and co-workers produced 70 % high yield SWNT by the laser vaporization method using graphite rod target materials with small amounts of Ni and Co at a furnace temperature of 1200 °C. He again indicated that X-ray diffraction and Transmission Electron Microscope (TEM) images showed formed nanotubes bundles or ropes of diameters between 5 to 20 nm with length around 10 to 100 μm. Further, he reported that through van der Walls bonding, the nanotube bundles or ropes formed a two dimensional triangular lattice with lattice constant of 1.7 nm.

Popov (2003) attributed the growth mechanism in a laser vaporization method to the single metal catalyst Ni or Co atom chemisorbs onto the open edge of a nanotube. To prevent formation of fullerene, he explained that the metal catalyst should have sufficiently high electronegativity. He further explained that metal catalyst atoms circulate around the open end of the nanotube and absorb small carbon molecules and convert them to sheet-like graphite. Popov further stated that nanotube grows until too many catalyst atoms aggregate to the end of the nanotube. Finally, the large particles either detach or become over-coated with an appropriate amount of carbon atoms and then poison the catalyst.

According to the account given by Flamant et al. (2001) and Kasuya et al. (2002), several researchers reported that yield and diameters of formed SWNT depend on several factors. Some of these factors are listed as follows:

1. Reactor design
2. Type of metal catalysts
3. Laser power.

4. Carrier/buffer gas pressure
5. Carrier gas flow rate
6. Furnace temperature
7. Residence Time

Reactor/Furnace. The two types of reactors have been used to synthesize SWNT. One group experimented with a reactor with a furnace for external heating. The second group of experimenters used a reactor without external heating. In this second case, the heating temperature only depends on the laser type and power of laser employed (Chen et al., 2002; Fan, Geohegan, Guillorn et al., 2002; Kasuya et al., 2002). Table 1 shows summary data of the characteristic dimensions of existing reactors comprising furnace and quartz tube.

Table 1

Characteristics Dimensions of Existing Reactor: Quartz Tube and Furnace

Quartz tube		Furnace	Reference
Inner diameter (mm)	Length (mm)	Length (mm)	
27	500		Ichihashi et al., 1999
36	600		Ichihashi et al., 1999
50	609.6	304.8	Allard et al., 2002
50	609.6		Fan, Geohegan, Guillorn et al., 2002

Fan, Geohegan, Guillorn et al. (2002) and Fan, Geohegan, Pennycook et al. (2002) used a reactor with external heating. Both Chen et al. (2002) and Kasuya et al.

(2002) ablated a graphite target in a reactor without an external heating to raise the chamber temperature. The reactor used by Chen et al. (2002) had a chamber made of stainless steel, of about 400 mm in diameter and 300 mm high. Chen et al. (2002) and Ichihashi et al. (1999) employed a ZnSe window on the chamber through which the laser beam was focused on the composite target. Fan, Geohegan, Guillorn et al. (2002) and Fan, Geohegan, Pennycook et al. (2002) instead equipped the external heating furnace with a rectangular quartz window of 1 in width and 10 in long. Alternatively, Allard Jr. et al. (2002) employed a 2 inch diameter by 24 inch length quartz tube mounted inside a hinged tube furnace of 12 inch long.

However, Kasuya et al. (2002) suggested that the low yield of SWNT produced with a reactor without using a furnace with external heating could be due to short growth time. On the other hand, Achiba et al. (2003) employed an electric furnace for external heating to synthesis SWNT.

Quartz tube. Achiba et al. (2003), Fan, Geohegan, Guillorn et al. (2002), Fan, Geohegan, Pennycook et al. (2002), Ichihashi et al. (1999), and Kasuya et al. (2002) all used quartz tube glass as a receptacle for placing the graphite target. However, Ichihashi et al. employed double-layered quartz glass tubes. The inner diameter of one of the tubes was 36 mm with a length of 600 mm. The second tube used by Ichihashi et al. had an inner diameter of 27 mm with a length of 500 mm.

Meanwhile, Fan, Geohegan, Guillorn et al. (2002) and Fan, Geohegan, Pennycook et al. (2002) used a single quartz tube which was 2 in ($\approx$50.8 mm) diameter and 24 in ($\approx$ 609.6 mm) long with an O-ring sealed to standard 4.5 in ($\approx$114.3 mm) vacuum

components. Further, Chen et al. (2002) used 2cm (20 mm) mold to serve as the plate or receptacle for the target.

Graphite and metal-catalyst composites. Chen et al. (2002) produced a composite graphite target uniformly mixed with Ni/Co (0.6/0.6 at. %). They indicated that the composite was prepared by pressing and baking at 120 °C for 5 hr under constant pressure. Similarly, Achiba et al. (2003) and Kasuya et al. (2002) used Ni/Co (0.6/0.6 at. %) to synthesize SWNT. Kasuya et al. suggested that Ni/Co nanosized particles in the carbon composite play a crucial role in the segregation of carbon during the formation of SWNTs. They further suggested that the segregation process was governed by factors such as the mobility of carbon and the degree of carbon super-saturation in the Ni/Co particles.

Fan, Geohegan, Guillorn et al. (2002) and Fan, Geohegan, Pennycook et al. (2002) used a 1 in (25.4 mm) diameter graphite target prepared from carbon cement (Dylon GC) containing 1 at.% each of Ni and Co. Fan, Geohegan, Guillorn et al. (2002) and Fan, Geohegan, Pennycook et al. (2002) and Ichihashi et al. (1999) also used a Co/Ni-graphite composite target. Ichihashi et al. (1999) used a pellet-like target with a size of 10 mm diameter and 3-5 mm thick which was placed at the center of a 27 mm tube. The target was further supported by a third quartz glass tube with 10 mm diameter and length of 300 mm. On the other hand, Fan, Geohegan, Guillorn et al. (2002) and Fan, Geohegan, Pennycook et al. (2002) used a 1 in (25.4 mm) diameter graphite composite target that was screwed into a 0.25 in (6.35 mm) graphite rod and rotated during the operation. Fan, Geohegan, Guillorn et al. (2002) and Fan, Geohegan, Pennycook et al.

(2002) mounted the graphite rod along the quartz tube axis through a hole in the collector.

Achiba et al. (2003) and Kasuya et al. (2002) both held the composite graphite with the catalyst and rotated it in the quartz tube. However, Flamant et al. (2001) covered the front part of the reactor with a silvered water-cooled copper plate to surround the graphite composite target.

Vaporization of carbon and metal catalysts. Allard Jr. et al. (2002) indicated that typically, a laser shot vaporizes a small amount of the graphite raw materials, and that approximately, 10^{16} carbon atoms and 10^{14} metal catalyst atoms are vaporized. In addition, Allard Jr. et al. estimated that approximately 5 x 10^{16} carbon atoms and 10^{14} Ni/Co metal-catalyst atoms remained in the vapor phase up to about 100 μs after vaporization of the carbon and metal catalyst composites. Further, the account given by Allard Jr. et al. showed that in an oven or reactor at temperature of around 1200 °C with a gently flowing inert gas at a pressure of approximately 500 Torr., with a single laser shot, the ejected carbon and metal-catalysts materials self-assemble and grow into a high volume fraction of single wall nanotubes with a maximum length of 10 μm.

Allard Jr. et al. (2002) further reported that the atomic and molecular vapors condensed into clusters rapidly and were trapped in aggregates within a plume with a shape of a vortex ring. These group of investigators indicated that, at an oven temperature of 1200 °C, the conversion times of atomic and molecular species to clusters were judged to be approximately 200 μs for carbon and 2 ms for cobalt. Allard Jr. et al. (2002). emphatically concluded that growth of most of the single wall carbon nanotubes occurred

within the spinning vortex ring from the available condensed-phase carbon and metal catalyst nanoparticles during the propagation time within the annealing zone of the furnace.

Furthermore, Allard Jr. et al. (2002) recounted that carbon and metal-catalyst nanoparticles in the plume cool by heat conduction to the carrier gas available in their environment and by thermal radiation. These investigators further indicated that the nanoparticles could also undergo phase transition during the flight, such as vaporization or re-solidification which includes converting amorphous carbon to single wall carbon nanotubes.

In addition, on assumption that the heat conduction to the background carrier gas is the major process responsible for decreasing the temperature of the vaporized nanoparticles, Allard Jr. et al. (2002) indicated that this temperature decrement occurs in the plume at time greater than 1 ms. Also, based on their experimental data, Allard Jr. et al. derived the following governing the differential equation $dT / dt = - A (T-T_{oven})$. Further, Allard Jr. et al. provided the solution to this differential equation as $T(t) = T_{oven} + T_0 e^{(-At)}$ with $A = 0.91$ ms. $T(t)$ is the resulting cooling temperature which is a function of time of the nanoparticles after transferring heat to the surrounding carrier gas, t is the cooling time by which vaporized nanoparticles transfer heat to the carrier gas, T_{oven} is the oven or furnace temperature, which is the temperature attained by the nanoparticles, T_0 is the ambient temperature of the carrier gas, and A is constant estimated as 0.91 ms.

Reactor temperature. As already reported in a previous section two types of reactors have been used to synthesize SWNT. Botton et al. (2002) and Kasuya et al.

(2002) reported that different temperatures produced different diameter SWNTs. These investigators indicated that at higher temperatures thicker diameter SWNTs were formed. Kasuya et al. (2002) explained that the different diameter SWNTs are formed as a result of the segregation of carbon from the composite particles at the different temperatures. Kasuya et al. further indicated that the molten carbon-metal-composite particles were formed in a supersaturated vapor acted as bases for the nucleation and the growth of SWNTs.

Achiba et al. (2003) heated quartz tube to 1200 °C in an electric furnace. In their opinion, their choice of this operating temperature was due to the fact that, it has been found that highest yield of SWNT resulted when either N_2 or Ar carrier gases were used. Achiba et al. further indicated that, the temperature gradient from 1200 ° C to room temperature (RT) in the central area of the furnace was very small however it was larger near the exit. Figure 7 shows an example of a temperature profile in a reactor with an external furnace.

Botton et al. (2002) in using a KrF laser confirmed that the growth temperature or the target surface temperature is the key parameter both for the formation and structural organization of SWNT. Botton et al. indicated that with increase in furnace temperature from 550 to 1150 °C using an excimer KrF laser supported higher yield and thicker bundles associated with shift in the production of larger diameter distribution of SWNT.

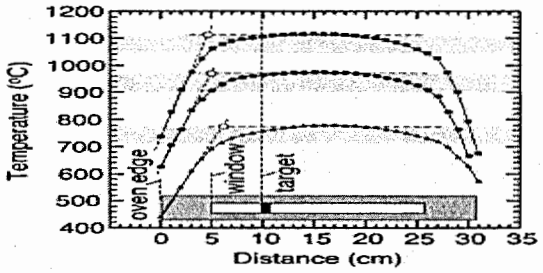

Figure 7. Temperature profiles along furnace axis. From "Time resolved diagnostics of single wall carbon nanotubes synthesis by laser vaporization, *Applied Surface Science* " by Fan, Geohegan, Guillorn, Puretzky, & Schittenhelm, 2002. The diagram shows temperature profiles along the furnace axis measured at 780, 960, and 1100 °C at the center of the furnace. Find at the bottom, an inset showing graphite composite target and window edge positions with reference to the edge of the oven at $d = 0$.

Ambient or carrier or buffer gases. Achiba et al. (2003) experimented with argon (Ar), krypton (Kr), neon (Ne), and nitrogen (N_2) carrier gases also referred to as ambient or buffer gases. They found that the gases systematically change the abundance of single wall carbon nanotubes formed. Achiba et al. therefore reported that, yield or abundance or quantity of SWNT depends on the type of carrier gas used. Achiba et al. indicated that the best abundance was obtained with N_2 at 1000 Torr. Sequentially, second best was Ar at 1000 Torr, followed by Ne at 1500 Torr; and Kr at 800 Torr which produced the least yield.

In addition, it was found that highest purity of SWNT was produced with N_2 at a pressure of 1000 Torr. Again, it was only N_2 that was found to produce thinner SWNT by

a decrement of about 0.2 nm. This decrease in the diameter distribution of the SWNT, Achiba et al. (2003) explained that can also be achieved for rare gases if the furnace temperature is reduced by 50 ° C. Further the reason why N_2 only produced thinner SWNT was explained. Achiba et al. indicated it was due to the higher cooling rate in the N_2, attributed to its diatomic molecule structure and as a consequence its vibrational degree of freedom affected the cooling process of the vaporized carbon by collision.

Achiba et al. (2003) therefore suggested that the choice of carrier gas may sensitively contribute to size of SWNTs due to the effects of the internal freedom of the gas. Achiba et al. further indicated that carbons in N_2 are less amorphous than those in Ar. This supports the fact that choice of carrier gas can affect the structure and purity of grown carbon nanotubes (Achiba et al., 2003).

Conversely, Fan, Geohegan, Guillorn et al. (2002) and Fan, Geohegan, Pennycook et al. (2002) used only Ar gas which was pumped out through a needle valve around a quartz window. They controlled the Ar gas at 100 sccm in order to maintain 500 Torr pressure. Also Achiba et al. (2003) suggested that with an electric furnace at 1200 °C, both N_2 and Ar carrier gases provided the highest yield of SWNT. Achiba et al. thus indicated that an optimum yield of SWNT does not depend of the kind of carrier or ambient gas.

In addition, Achiba et al. (2003) showed that at constant carrier gas flow rate with no variation in the temperature gradient inside the furnace that influenced the SWNT diameter distribution, the carrier gases, Ar, Kr, and Ne except N_2 did not show any significant change in the diameter distribution of SWNT at all pressures. Thus, these

investigators suggested that the molecular mass of the carrier gas did not have strong effect in controlling the mean diameter distribution of SWNT.

Ambient or carrier or buffer gas pressure. At Ar gas pressures between 150 to 760 torr and using CO_2 laser at room temperature, Kasuya et al. (2002) concluded that low yield SWNTs were formed at these Ar gas pressures. They reported that at higher Ar gas pressures, the yield decreased. For example Ar gas pressure of 760 torr did not produce any SWNT except nanohorns. Thus, Kasuya et al. concluded that different Ar gas pressures produced different diameter SWNTs. However, they also concluded that the diameter of SWNT increased at higher Ar gas pressures.

On the other hand, Achiba et al. (2003) set the gas pressures at 100 and 1500 Torr for Argon (Ar), krypton (Kr), neon (Ne), and nitrogen (N_2) carrier gases they employed. Achiba et al. showed that for these four buffer gases they investigated, the yield first increased linearly with pressure, and later exhibited a broad maximum at an optimum pressure except Ne.

Ambient or carrier or buffer gas flow rate. Achiba et al. (2003) reported that other investigators have concluded that the buffer gas flow rate influenced the diameter distribution of SWNTs, and thus influenced the SWNT growth process. Although Kasuya et al. (2002) used Ar gas flow rate of 0.5 l/min, Achiba et al. employed a pumping speed that gave a constant linear velocity (flow rate) at 0.88 cm/s for the carrier gases employed. In the process, they indicated that the temperature gradient history during the growth process inside the furnace for the vaporized carbon and metal species could be identical.

Furthermore, whereas at constant chamber pressure of between 200-400 Torr, Chen et al. (2002) successfully employed Ar gas flow rate of 60 ml/min to synthesize SWNT, Fan, Geohegan, Guillorn et al. (2002) and Fan, Geohegan, Pennycook et al. (2002) controlled the Ar gas at 100 sccm in order to maintain 500 Torr pressure. Conversely, Botton et al. (2002) controlled the Ar gas at 300 sccm and maintained a pressure of 500 Torr.

Residence/growth time. Kasuya et al. (2002) suggested that when using a reactor without a furnace, there was low growth of SWNT which was attributed to short growth time. Kasuya et al. (2002) further indicated that, on assumption that temperature decreases in the SWNT mushroom forming clouds, at Ar gas pressures of 150 to 400 Torr, it took about 1.9 to 2.6 ms to grow SWNT at assumed temperatures of 1400 to 800 °C.

On the other hand, noted in Table 2 are the growth rate limits recommended by Allard Jr. et al. (2002) and Fan, Geohegan, Guillorn et al. (2002) and Fan, Geohegan, Pennycook et al. (2002). These research teams concluded that, using Ar gas flow rate at 100 sccm with 500 Torr pressure, the estimated lower and upper limit for the experimental growth rates for 35-77 nm short length SWNTs at temperatures between 760 to 1100 °C using Nd:YAG laser lie between 0.6 and 5 μm/s. Additionally, Allard Jr. et al. reported that the theoretical estimate of the growth rate reported by Maiti et al. was 82.5 μm/s at temperature of 1500 K. This theoretical value as compared by Allard Jr. et al. is 10 -10^2 times greater than their experimental values. It is, however, difficult to compare these conflicting growth rates since the growth temperatures are varied.

Further, Fan, Geohegan, Guillorn et al. (2002) and Fan, Geohegan, Pennycook et al. (2002) firmly concluded that the majority of the SWNT growth occurred for times more than 20 ms after carbon vaporization when condense phase carbon and metal catalyst clusters and nanoparticles are converted. Allard Jr. et al. (2002) on the other hand reported that, the ejected material spent about 10–20 ms at uniform temperature zone and 100–200 ms in the steep temperature gradient zone as shown in Figure 7.

Table 2

Limits of Growth Rates of SWNT Synthesized by Nanosecond Laser Vaporization of C/Co/Ni Target

Lower limits of growth rates				Upper limits of growth rates			
Oven Temperature Range	Time at uniform temperature T>700 ° C	Most Probable Length	Growth Rate	Oven Temperature Range	Time at uniform temperature T>700 ° C	Most Probable Length	Growth Rate
°C	ms	nm	μm/s	°C	ms	nm	μm/s
750 -700	25	35	1.4	750 -715	20	35	1.8
900 -700	100	74	0.7	950 -900	15	74	5
1100 -700	120	77	0.6	1100 -1050	15	77	5.1

From "Time resolved diagnostics of single wall carbon nanotubes synthesis by laser vaporization, *Applied Surface Science*" by Fan, Geohegan, Guillorn, Puretzky, & Schittenhelm, 2002.

Further Allard Jr. et al. (2002) reported that growth rates of the single wall nanotubes can be estimated using the measured experimental values of the most probable length of the single wall nanotubes, time the vaporized carbon and metal catalyst particles

spent during flight in the uniform temperature zones, and the estimated short time of 4 ms required to cool the vaporized nanoparticles within the plume to the ambient temperature.

Cooling subsystem and carbon nanotube collector. Botton et al. (2002) used a water-cooled copper collector located at the exit end of the furnace. Further, Botton et al. collected the SWNT on the surface of the copper collector. Fan, Geohegan, Guillorn et al. (2002) and Fan, Geohegan, Pennycook et al. (2002) instead used a brass water-cooled collector which was inserted into a quartz tube and positioned outside the furnace. On the other hand, Flamant et al. (2001) employed a water-cooled heat exchanger at the backside of the reactor before allowing the cooled carbon soot to enter into a 1 m long bag filter. In general, these investigators did not discuss the merits and demerits of any of these cooling collectors and their effects on carbon nanotubes.

Summary of methods and reactors for producing carbon nanotubes. Carbon nanotubes have successfully been grown at the laboratory scale level. The improved methods all use different techniques and different type and form of raw materials. However, in general they all concluded the improved techniques are cheap and easy to scale up to the industrial level. Nevertheless, other investigators have reported on the deficiencies applicable to all these techniques. Some of these difficulties include low productivity for laser method; and low yield for flame, arc, and solar, and CVD methods (Chen et al., Chiashi et al., 2002; Flamant et al., 2001; Lai et al., 2001; Li, Xu, Wu, & Zhu, 2002).

The effects of the reactor design, carrier gas, carrier gas pressure and flow rate, and growth temperature on the growth of carbon nanotubes were confirmed. In general,

however, the need to control growth of carbon nanotubes is a weakness applicable to all the methods.

Characteristic Properties of the Carbon and Metal Catalysts Raw Materials for Growing Carbon Nanotubes

Characteristics Properties of Carbon

Carbon is the main raw material for growing carbon nanotubes. It exhibits allotropy and hence exists in more than one form. It is believed that there are four known allotropic forms of carbon. They are diamond, graphite, amorphous, and fullerene carbon. Amorphous carbon, however, is said to be an impure form of carbon which includes varieties of vegetable and animal charcoals such as lampblack, charcoal, soot, gas carbon, and coal (Parkes, 1961).

Amorphous carbon such as charcoal is black and porous with low apparent specific gravity due to the relatively high volume of air entangled in the pores. Due to its porosity, amorphous carbon has very large surface in proportion to its weight and hence exhibits high degree of surface effects. Consequently, due to the large surface, amorphous carbon exhibits adsorption, that is, gas adheres to the surface. Again on account of its large surface area, amorphous carbon is the most reactive of all forms of amorphous carbon (Parkes, 1961).

Graphite is widely distributed all over the world. It also occurs in the form of fine crystals in meteorites. In addition, artificially, graphite is manufactured by heating amorphous carbon at high temperatures by means of an electric furnace. Graphite is dark grey and composed of easily separated sheets with characteristic greasy feel and a lustre

resembling that of a metal. Graphite consists of sheets or planes of linked carbon atoms. This structure accounts for its use as a lubricant (Parkes, 1961).

Graphite crystallizes in hexagonal plates with specific gravity between 2 to 3. It is chemically inactive. When heated in oxygen graphite burns to form carbon dioxide. Graphite is used to make lead pencils, refractory, lubricant for machinery, a coating for iron to prevent rusting, and a coating for goods to be later electrotyped to prevent boiler scale. It is also used largely in making electric furnaces. Graphite conducts electricity very well and is used as electrodes in the electrochemical industries. Hence, it is also used for battery plates and electric-light carbons among others (Parkes, 1961). Located in Appendix A, the characteristic properties of carbon may be found.

Characteristic Properties of Nickel and Cobalt Metal Catalysts

Nickel. Nickel and Cobalt are usually found in association. Nickel is a white and moderately hard metal. The atomic weight is 58.71 and it melts at 1453 ^{o}C and it is magnetic. At ordinary temperatures, nickel is stable in air, but burns in oxygen to form nickelous oxide (NiO). Water does not affect nickel, but it decomposes at red heat. Dilute hydrochloric and sulphuric acids slowly act on nickel. Nitric acid, on the other hand, readily attacks nickel to form nickel nitrate (Parkes, 1961). These are the reasons why these chemicals are used in the purification of single wall carbon nanotubes.

Nickel is used for nickel plating. The alloy forms are used for the production of crankshaft, case hardening, unusual magnets for high speed telephony and telegraphy, and coinage. Finely divided nickel is used as catalyst in most hydrogenation reactions (Parkes, 1961).

Cobalt. Cobalt is usually found in association with nickel mainly in the form of arsenides, for example $CoAs_2$. Cobalt is white, malleable and ductile metal. It is harder than iron. It has weak magnetic properties and melts at 1492 ° C. The bulk form is usually not attacked by air at ordinary temperatures. It however reacts at a red heat. The finely divided state of cobalt is pyrophoric. Cobalt is attacked slowly by hydrochloric and sulphuric acids. It also dissolves fairly readily in nitric acids (Parkes, 1961). Further, these are the reasons why these chemicals are used in the purification of single wall carbon nanotubes.

Cobalt has atomic weight of 58.94. It is used in electroplating. Alnico, one of the alloy forms is used to make outstanding permanent magnets for loudspeakers and magnetos among others. Cobalt oxides are also used for colorless glass and pottery glazes. In addition, cobalt salts are used as driers for the production of paints and varnishes (Parkes, 1961).

Characteristic Properties of Nitrogen and Argon Carrier Gases.

Nitrogen. Nitrogen is a diatomic gas. It is colorless just as argon and it is not as dense as air. It is slightly soluble in water and 100 volumes of water at 0 °C absorb 2.39 volumes of nitrogen. Further, at 20 °C, 1.64 volumes of nitrogen is absorbed. However, at 3500 °C about 5% of nitrogen is dissociated into atoms (Parkes, 1961). Parkes represented this chemical dissociation as N_2 (95%)$\leftrightarrow$2N (5%).

Nitrogen can be condensed to colorless liquid and boils at -195.8 °C at atmospheric pressure. It solidifies as a white snow-like mass melting at – 209.9 °C. The

solid form of nitrogen exists in two forms and has transition temperature of – 209.9 °C and 53.8 cals of molecular heat of transformation (Parkes, 1961).

Nitrogen is not poisonous; it constitutes large proportion of the air we breathe. It is not combustible and can not support ordinary combustion. Because of the great affinity of the nitrogen atoms to be together in its molecule, it makes nitrogen chemical inert, which is its chief characteristics at temperatures below 200° C. However, at and above red heat, most metals combine with nitrogen to form derivatives of trivalent nitrides (Parkes, 1961). Again, Parkes cited magnesium nitride as an example as shown in this chemical reaction as $3Mg + N_2 = Mg_3N_2$.

In addition, nitrogen reacts with oxygen at high temperatures forming nitric oxide to a small extent. Nitrogen can combine with hydrogen at suitable conditions. It can also react with some non-metallic elements such as carbon to form cyanogens (Parkes, 1961).

On a large scale, nitrogen is used to manufacture synthetic ammonia. It is also used in certain industrial processes, where it is used to provide inert atmosphere. For example it is used in metallurgy to prevent oxidation or decarburization (Parkes, 1961).

Argon (Ar). Ar is classified as noble or inert gas. The earth's atmosphere contain about 0.94% of argon. On the Mars' atmosphere, there are 1.6% ^{40}Ar and 5 p.p.m. of ^{36}Ar. Ar is manufactured by fractionation in large quantities from liquid air (Los Alamos National Laboratory Chemistry Division [LANLCD], n.d.; Parkes, 1961).

Argon that occurs naturally has three isotopes. In addition, there are twelve other known radioactive isotopes. The mass number of the three naturally occurring isotopes in

the order of abundance are 40 (99.6%), 36 (0.337%) and 38 (0.063%) (Dubson, Taylor & Zafiratos, 2004).

In terms of uses, at a pressure of about 400 Pa, Ar is used in electric light bulbs and in florescent tubes. It is also used in filling photo tubes and glow tubes. In industry, because of its inertness, argon is used to shield arc welding and cutting. In addition, it is used as blanket for the production of titanium and other reactive elements. It is also used as protective atmosphere for growing silicon and germanium crystals (LANLCD, n.d.).

Argon is a monatomic gas. It is odorless, tasteless and colorless gas. The atomic weight is 39.944 and the density is 19.97. In addition, the atomic number is 18, melting point is -189.2 °C, boiling point is -185.9 °C, critical temperature is -122.4 °C, critical pressure is - 47.996 atm, compressibility (λ) is +0. 0009, and the solubility in one volume of water at 0 °C is 0.0056 (Parkes, 1961).

Argon is preferably more soluble in water than nitrogen and oxygen. Furthermore, it is $2^1/_2$ times more soluble than nitrogen. The electronic configuration of argon is: $1s^2$ $2s^2 2p^6$ $3s^2 3p^6$. It is therefore chemically inert and it is not known to form stable compounds (LANLCD, n.d.; Parkes, 1961).

Summary of characteristics of selected carrier gases. The inert nature of Ar and the chemically inert nature of Nitrogen are the reasons why they were used as buffer or carrier gases in the growth of carbon nanotubes. However, the two gases have very different chemical and physical properties. The characteristic properties of Nitrogen and Argon buffer gases may be found in Appendices B and C respectively. Their striking differences are the reasons these two gases were chosen for investigation in this study.

Static Mixers

Introduction

Static mixers are sometimes referred to as inline or motionless or passive mixers. This type of mixing technique is well suited to laminar flow mixing although it is also used in turbulent flows. In this type of mixers, the fluid is made to pass through a pipe which contains stationary obstacles or blades (COMSOL AB., 2004b).

The static mixer design type can be classified based on variety of factors. It could be classified depending on the shape or configuration of the inner obstacles or blades. It can also be classified based on the position of the inlet (s) for the flow. Furthermore, it can be classified depending on whether the flow is turbulent or laminar. In some types, the blades are straight and others they are twisted (COMSOL AB., 2004b; Devahastin & Mujumdar, 2001; Povitsky, 2002).

Further, some experimenters measured the mixing performance of static mixers by calculating the standard deviation of the concentration. Others evaluated the performance of inline mixers by evaluating the standard deviation of the temperature at the exit (COMSOL AB., 2004b; Devahastin & Mujumdar, 2001).

Devahastin, Mujumdar, and Wang (2004) explained that static or in-line mixer with opposing jets impacting head-on have simple configurations and have been used in industrial applications for rapid mixing of viscous fluids. They can be found in reaction injection molding, thermal drying of solid particles with high water content, fuel combustion, gas or liquid mixing, pharmaceutical crystallization, absorption, catalytic reactions, dust collection, and liquid-liquid extraction (Devahastin et al., 2004).

Devahastin et al. (2004) indicated that despite the proven usefulness of static mixers in industry, fundamental research on opposing jets was very limited. This motivated Devahastin et al. (2004) to launch further scientific investigation into the effectiveness of static mixers with opposing jets using air as the working fluid.

Thus, Devahastin et al. (2004) reviewed several literature including the works of Kudra and Mujumdar (1989) and Tamir (1994). Devahastin et al. (2004) also investigated new design approaches to improve effectiveness of in-line or static mixers based on laminar flow of opposing jet impingement. Devahastin et al. (2004) concluded that by using two-dimensional (2-D) configurations and numerical simulations, the effectiveness of in-line mixers were improved by operating conditions and geometrical configurations.

Devahastin et al. (2004) reported that most studies conducted on static mixers indicated that, several dependent variables could be used, however the one that seem appropriate for their work and was employed by other researchers was temperature. In this respect, the temperature at the cross section of the exit or outlet was measured as passive tracer to evaluate the mixing effectiveness of the mixers. In this case, the mixing effectiveness or the mixing index was obtained by the relation

$$\mathrm{MI} = \frac{\Delta T}{T_b} \times 100\% \tag{1}$$

Where MI is the mixing index, ΔT is the standard deviation based on the bulk temperature of the fluid temperature at any specific location in the exit and T_b is the bulk temperature at that particular location. According to Devahastin et al. (2004) physically, MI measures the extent to which the bulk temperature at any specific station represents

the set of temperatures that comes from it. Hence, MI = 0 % means perfectly flat profile, which is an indication of complete mixing.

Further, Devahastin et al. (2004) reported that several independent variables were employed by different researchers. These independent variables included Reynolds numbers; inlet jet Reynolds number; system geometry; length of mixing channel; ratio of the height of exit channel to the width of the inlet jet; and ratio of the spacing between two inlet jets to the width of an inlet. The control variables employed by most researchers as reported by Devahastin et al. (2004) are laminar flow, turbulent flow, and Reynolds number for identical inlet velocities. Further, usually, the mass flow rate was made constant.

Specifically, Devahastin et al. (2004) indicated that the effects of operating conditions on improving mixing effectiveness can be achieved by unequal inlet momenta of opposing jets obtained by either using equal and unequal slot widths. Also, Devahastin et al. (2004) indicated that the effects of the geometrical configurations were achieved by addition of baffles in the exit channel.

However, Devahastin et al. (2004) noted that when the baffles were introduced, there was pressure loss. In the view of these investigators, the effect of the pressure will be significant for viscous fluids. To minimize the limiting effects of the pressure drop in order to further improve on the mixing effectiveness of static mixers, Devahastin et al. (2004) recommended the use of curved baffles or the use of perforated baffles as a means to reduce the pressure drop without decreasing the effectiveness of static mixers.

Devahastin et al. (2004) verified the results of their study by comparing the numerical results with existing experimental data and flow visualization.

Design Types, Modeling and Computer Simulation Experimental Methods

Laminar multi-jets static mixer design type . Devahastin and Mujumdar (2001) reported a numerical study of mixing in a novel in-line mixer utilizing multiple impinging stream inlets which was operated in the laminar flow regime. The purpose of Devahastin and Mujumdar study was to test a new conceptual design of a modified in-line mixer for viscous fluids such as polymer solutions via a numerical simulation. The conceptual design is as shown Figure 8.

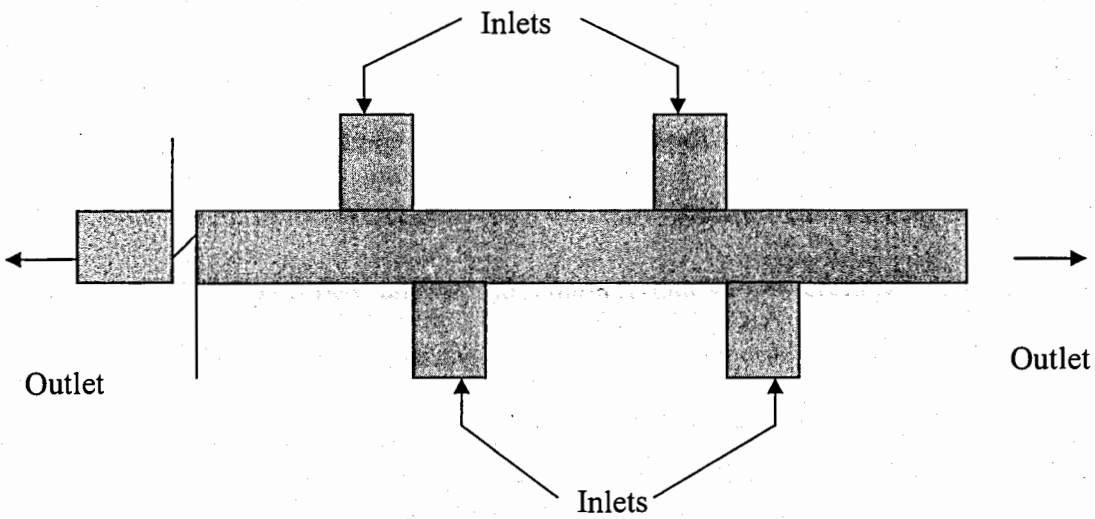

Figure 8. 2-dimensional in-line mixer with multiple impinging inlets. From "A numerical study of mixing novel impinging stream in-line mixer" by Devahastin & Mujumdar, 2001.

In that study, Devahastin and Mujumdar (2001) investigated the main effects of inlet jet Reynolds numbers and the mixer geometry on the mixing characteristics of the proposed design. They further investigated the effects of other several treatment variables. The covariates used by Devahastin and Mujumdar for the geometry are the ratio of the height of the mixer exit channel to the width of the inlet jet and the ratio of the spacing between the inlet jets to the width of the inlet jet.

Devahastin and Mujumdar (2001) concluded that the mixer geometry improved the quality of mixing. Particularly, they reported that offsetting the top and bottom inlet jets effectively improved the mixing quality. According to their account the intense mixing zones between the inlets shown by the stream lines were confirmed.

Devahastin and Mujumdar (2001) concluded that, in general, geometric and operating parameters influence mixing differently at different zones of the mixer. They further concluded that at short axial distance excellent fluid mixing was achieved. In addition, Devahastin and Mujumdar also reported a numerical study by Hosseinalipour and Mujumdar (1997) on flow and mixing characteristics at different temperatures in a two dimensional laminar opposing jets.

According to the Devahastin and Mujumdar (2001) account, Hosseinalipour and Mujumdar (1997) used temperature as the passive mixing tracer and found that increasing the inlet jet Reynolds number delayed the attainment of uniform temperature and hence complete mixing of the two fluids were delayed. This was attributed to the shorter residence time of the fluid in the system caused by the increase in the mean flow rate.

Similarly, Devahastin and Mujumdar utilized fluid temperature as the passive mixing tracer to evaluate their new concept.

To develop the physical modeling equations, namely conservations of mass, momentum, and energy to govern the simulation, Devahastin and Mujumdar made the following assumptions: (a) steady flow, (b) the flow is two dimensional, (c) flow is laminar, (d) flow is incompressible, (e) the fluid is Newtonian, and (f) viscous dissipation is neglected.

Following the aforementioned assumptions, below are the tensor forms of the governing physical equations or models employed by Devahastin and Mujumdar (2001):

Continuity equation:

$$\frac{\partial u_i}{\partial x_i} = 0 \tag{2}$$

Momentum equation:

$$\rho\left(u_i \frac{\partial u_j}{\partial x_i}\right) = -\frac{\partial p}{\partial x_j} + \mu \frac{\partial}{\partial x_i}\left(\frac{\partial u_i}{\partial x_i}\right) + \rho g_j \tag{3}$$

Energy equation:

$$\rho c_p\left(u_i \frac{\partial T}{\partial x_i}\right) = k \frac{\partial}{\partial x_i}\left(\frac{\partial T_i}{\partial x_i}\right) \tag{4}$$

The boundary conditions applied by Devahastin and Mujumdar (2001) to solve the above three Equations 2, 3, and 4 numerically are as follows:

Top inlets:

$$u_1 = 0; u_2 = -u_{2\,jet} \text{ and } T = T_{topjets} \tag{5}$$

Bottom inlets:

$$u_1 = 0; u_2 = u_{2\,jet} \text{ and } T = T_{bottomjets} \tag{6}$$

Top and bottom walls:

$$u_i = 0 \text{ and } \frac{\partial T}{\partial y} = 0 \tag{7}$$

Outlet Conditions:

$$\frac{\partial \phi}{\partial x} = 0 \tag{8}$$

where ρ denotes density, u_i velocity components, T temperature, k thermal conductivity, μ viscosity, C_p specific heat capacity at constant volume, p pressure, g acceleration due to gravity, y position variation along the vertical axis, x position along the horizontal axis, u_1 and u_2 are velocity at inlet 1 and 2, $T_{topjets}$ and $T_{bottomjets}$ are temperature at top and bottom jets, and ϕ all dependent variables (Devahastin and Mujumdar, 2001).

Devahastin and Mujumdar (2001) solved the conservation equations numerically with control-volume-based computational fluid dynamic software called PHOENICS. According to Devahastin and Mujumdar with the software, a numerical method for solving the differential equations for the convective terms in the energy and the momentum equation was discretized applying the hybrid scheme. The discretized equations were then solved by the SIMPLEST algorithm. Devahastin and Mujumdar claimed that, the numerical solution was judged to have converged when the criterion in Equation 9 is found have been met by all the dependent variables:

$$\max \left| \frac{\phi^{n+1} - \phi^n}{\phi_r} \right| \leq 10^{-3} \tag{9}$$

Where ϕ_r denotes the reference value for the dependent variable ϕ. To ensure the reliability of the study, Devahastin and Mujumdar verified their simulation results by comparison with the experimental and numerical results reported by other investigators.

Turbulent multi-jets mixer. Povitsky (2002) presented a relevant paper on a turbulent jet mixing reactor designed to heat up catalytic particles for growth of carbon nanotubes with the title 'improving jet reactor configuration for production of carbon nanotubes'. According to Povitsky, the purpose of the study was to obtain uniformly high temperature for a catalyst following the proposal to employ jet mixing reactors for industrial production of fullerene carbon nanotubes. Figure 9 is a typical jet interaction studied by Povitsky.

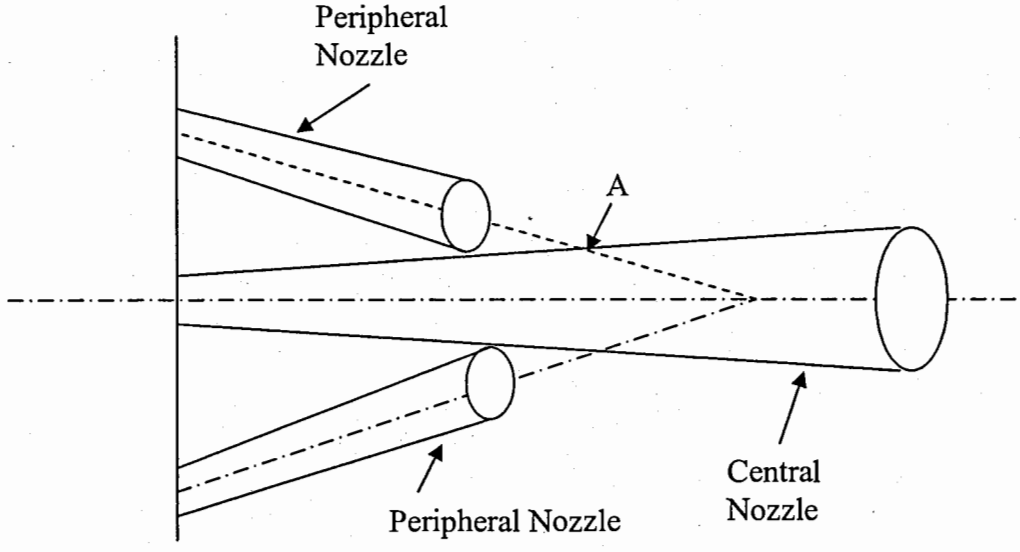

Figure 9. A typical turbulent multi-jets mixer showing jet interaction geometry. From "Improving jet reactor configuration for production of carbon nanotubes, *Computers & Fluids,* 31, 957-976, by Povitsky, 2002. The jets begin to interact at point A.

Povitsky (2002) indicated that other investigators have thoroughly examined the behavior of a single jet and surrounding gas, the effects of co-flowing round jets, jet rotation, and development of jets in a cross-flow stream. However, in the opinion of Povitsky, there was need to conduct detailed computational fluid dynamic (CFD) investigation with thorough discussion of the physics of interacting jets for reactor optimization.

The independent variables utilized by Povitsky (2002) are various configurations of peripheral jets with various numbers of jets, distance between central and peripheral nozzles, angle between the central jet and a peripheral jet, and twisted configuration of nozzles. In his study, Povitsky concluded that optimal configuration of peripheral jets strongly extended the cross-section of the central jet and consequently improved the mixing by the central jet situated in the reactor environment.

The assumptions used by Povitsky (2002) for developing the physical modeling and simulation are (a) the density is independent of pressure when the Mach number $M <$ 0.3, and (b) the source term in Equation 10 is set to zero for mixing chemically inert jets (1000 °C) in order to solve the concentration C of the material in central (cold) jet (200 °C).

Further, the boundary conditions employed by Povitsky (2002) to solve the physical equations during simulation are as follows:

Inlet conditions:

1. The concentration at the central nozzle C was made to be equal to one (1).
2. The concentration of the peripheral nozzles was set to zero(0)

Outlet conditions:

1. $\partial F / \partial x = 0$

In addition, the size (20 μm) and mass of catalyst particles were considered small and hence have zero (0) velocity relative to the gas. As a result, the concentration field C according to Povitsky (2002) showed similar spatial distribution for the catalyst particles. Also, the boundary conditions of the temperature field were made to be similar to the concentration field. According to Povitsky, the temperature field did not affect the governing equations.

Following the assumptions, the physical governing equation employed by Povitsky (2002) to govern the CFD model and simulation was the Navier-Stokes equations of gas dynamics with turbulence model for describing mixing of jets. The transport equation for the system was defined by Povitsky as

$$\frac{\partial}{\partial xi}\left(\Gamma \frac{\partial F}{\partial x_i}\right) - \frac{\partial(\rho U_i F)}{\partial x_i} + S_F = 0 \qquad (10)$$

where $F = U_i$, k, ϵ, C, T are the main variables, and U_i are velocity components of the jets, k the kinetic energy of the turbulence, ϵ the turbulent dissipation, C the mass concentration of material in the central (cold) jet, T is the temperature, S_F is the source term, and Γ denotes the transport coefficient.

According to Povitsky (2002), the standard k-ϵ model was used to predict the turbulent transport. Hence, the turbulent viscosity and transport coefficient were stated as

$$\Gamma = \frac{\mu_{eff}}{\mathrm{Pr}_F}, \qquad (11)$$

$$\mu_{eff} = c_{\mu}\rho k^2 / \varepsilon, \tag{12}$$

where C_{μ} is the coefficient of the k-ϵ model, and Pr_F is the Prandtl number for F. Povitsky (2002) defined the source term rate of turbulence energy generation (Q) as

$$Q = \mu_{eff}\left(\frac{\partial U_i}{\partial x_i}\right)\left(\frac{\partial U_i}{\partial x_j} + \frac{\partial U_j}{\partial x_i}\right) - \frac{2}{3}k\rho\left(\frac{\partial U_i}{\partial x_i}\right) \tag{13}$$

Further, following from the boundary conditions, with the assumed concentrations, the local density was computed by Povitsky (2002) with the following relation

$$\rho = C\rho_{cold} + (1 - C)\rho_{hot} \tag{14}$$

where ρ_{cold} denotes the density of the central jet and ρ_{hot} is the density of the peripheral jet. In addition, applying the assumptions for the temperature field, Povitsky solved the temperature field with zero source term using Equation 10.

Further, to solve partial differential Equation 10, Potvisky (2002) used numerical methods. Povitsky discretized Equation 10 by utilizing the finite volume method and a structured numerical grid to solve for the dependent variable.

Laminar static mixer. COMSOL (2004b) developed a simulation model for a laminar static mixer. The purpose of the modeling and simulation of their experiment was to study the mixing of one species dissolved in water at room temperature. The design of the inner baffles was made of three twisted blades with alternate rotations. This is shown in Figure 10.

With this type of laminar static mixer design, COMSOL (2004b) reported that the two solutions (dissolved specie and water) nearly achieved constant concentration at the

outlet. In addition, COMSOL (2004b) reported that after observing several slices of the cross section of the mixer after simulation, it was noticed that most of the mixing took place at the section where the twisted baffles or the blades changed direction.

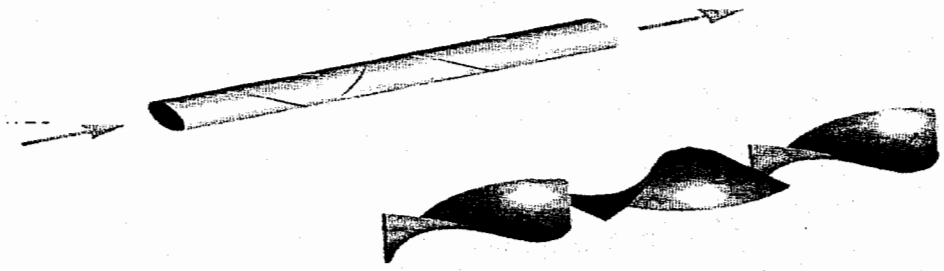

Figure 10. Laminar static mixer showing twisted blades or baffles type of design. From "*FEMLAB 3.0: Model library" by* COMSOL, 2004b.

The characteristics dimensions of the laminar static mixer used by COMSOL (2004b) are radius R, length of pipe 14R, and the length of each blade 3R. In this study, COMSOL (2004b) assumed that the flow was laminar and fully developed with given average velocity. At the outlet, COMSOL (2004b) set a constant reference pressure of zero (0) Pa.

Further assumptions made by COMSOL (2004b) in order to be able to use the appropriate governing equations are:

1. The change in concentration of the dissolved species in the water did not affect the properties of the fluid (water).
2. A discontinuous concentration profile existed at the inlet of the mixer in order to be able to study the mixing performance.

3. Transport by diffusion is neglected in the normal direction of the cross-section of the pipe, and hence at the outlet, and thus the mass transport is mainly driven by convection.
4. With low Reynolds Numbers, the Navier-Stokes equation will not require very dense mesh.

In addition, the governing equations employed by COMSOL (2004b) for the laminar static study are as follows:

Following from assumption 1, the momentum balance for stationary Navier-Stokes equations in 3D was given by:

$$-\nabla \cdot \eta(\nabla u + (\nabla u)^T) + \rho(u \cdot \nabla)u + \nabla p = 0$$

$$\nabla \cdot u = 0 \tag{15}$$

where η represents the dynamic viscosity ($kgm^{-1}s^{-1}$), u velocity vector (ms^{-1}), ρ density of fluid (kgm^{-3}), and p is the pressure (Pa), and superscript T in Equation 15 denotes transpose. Similarly, following assumption 2, the inlet concentration was defined by:

$$c|_{inlet} = \begin{cases} c_0 & x<0 \\ 0 & x \geq 0 \end{cases} \tag{16}$$

Finally, from assumption 3, the resulting mass balance from the mass flux due to the diffusion and convection was given as

$$\nabla \cdot (-D\nabla c + cu) = 0 \tag{17}$$

where D is the diffusion coefficient (m^2s^{-1}) and c is the concentration ($mol\ m^{-3}$). Additionally, following from the fourth assumption, the Navier-Stokes equation was first solved with a coarse mesh and then later mapped onto a finer mesh.

In the computer model using Navier-Stokes equation, COMSOL (2004b) used three types of boundary conditions. At the inlet, the inflow/outflow velocity boundary condition was used with fully developed velocity set. The other two velocity components were set to zero. At the outlet, COMSOL (2004b) used the outflow/pressure condition and set it to zero. COMSOL (2004b) then set all other boundaries to the no slip boundary condition.

On the other hand, for the diffusion and convection (mass flux) Equation 17, COMSOL (2004b) used three types of boundary conditions. At the inlet, concentration was set at $c_0 = c_0 * (x < 0)$. At the outlet, the convective flux boundary condition was used. All other boundaries were set at the insulation/symmetry condition which means that the temperature at these boundaries are constant throughout the simulation.

In this study, however, in order to show reliability of the results, COMSOL (2004b) obtained streamlines which clearly confirmed that the twisted mixer blades induced twisting motion in the fluid which was responsible for the mixing.

Summary of static mixers.

Examples of static mixer design types in terms of configuration of static mixers have been demonstrated. In addition various classifications of static mixers have been stated. Further, the various independent variables used by the independent investigators have also been given.

Different levels of physical equations for CFD modeling were used to govern the flow by each of the investigators. Different assumptions and boundary conditions were also used. In addition researchers used 2-D and others used 3-D geometric models.

Furthermore, all the investigators applied different numerical methods to solve for the dependent variables.

The researchers measured the mixing effectiveness either by determining the temperature deviation or using concentration. The researchers either used only stream lines or a combination of stream lines with results from an existing experiment to validate their simulation.

However, COMSOL (2004b) did not clearly show the variables that were being manipulated. In addition, calculation of the mixing performance was not shown, but was directly obtained from the simulation results.

Fluid Devices With Capabilities of Mixing Fluids

Diffuser

A diffuser has positive pressure gradient, that is, $\frac{\partial P}{\partial x} > 0$. As a consequence, the boundary layer grows rapidly. An example of a diffuser is shown in Figure 11. If the angle of divergence is too large, separation will occur. At the point of separation, the flow breaks away from the surface and creates a wake. As a result, separation will lead to a diffuser with poor performance (Brighton & Hughes, 1999).

Alternatively, if the angle of divergence is too small, an excessive length is required to obtain a given pressure. This results in large friction losses. To overcome these problems, it was suggested that the design of diffusers should be one of compromise of length and angle of divergence. As a result, in the design of a mixer the interest is in separation to facilitate mixing (Brighton & Hughes, 1999).

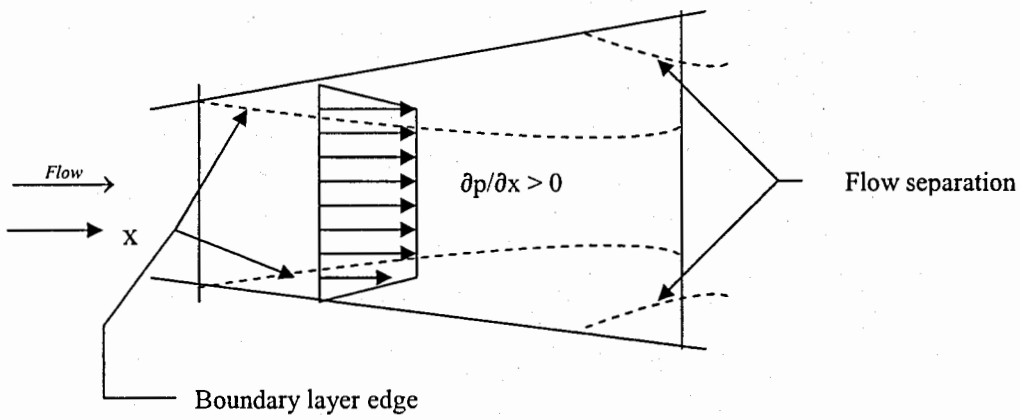

Figure 11. Schematic showing subsonic diffuser characteristics. From "Schaum's outlines: fluid dynamics" by Brighton & Hughes, 1999.

Converging Nozzle Flow

Brighton and Hughes (1999) provided characteristics to be considered for the design of a nozzle. An example is a nozzle is shown in Figure 12. According to Brighton and Hughes (1999) a nozzle involves flow with a decreasing favorable pressure gradient, that is, $\frac{\partial P}{\partial x} < 0$ in the direction of flow. As a result, the boundary layer remains relatively small and separation is not a problem in nozzle flows. Thus the design problem of nozzles is simpler than that of diffusers (Brighton & Hughes, 1999).

Brighton and Hughes (1999) derived relevant equations for the design of converging nozzle by assuming the fluid is an ideal gas, one dimensional and steady flow, and isentropic. Isentropic mean flow is adiabatic and frictionless with no discontinuities in the flow properties. Such isentropic flows according to Brighton and Hughes (1999) occur in external and internal flows with some specific conditions. The

condition for external flows occur in regions of small velocity and temperature gradient and internal flows such as nozzles and diffusers occur where change of flow conditions is mainly due to change in the area. The continuity equation of the nozzle was given as

$$\dot{m} = A_2 V_2 \,/\, v_2 \tag{18}$$

where $\dot{m}$ is the mass flow rate, A is the cross–sectional area, V is the flow velocity, and v is the specific volume which is $1/\rho$. The energy equation was given in terms of enthalpy as

$$\frac{1}{2}\left(V_2^2 - V_1^2\right) = h_1 - h_2 \tag{19}$$

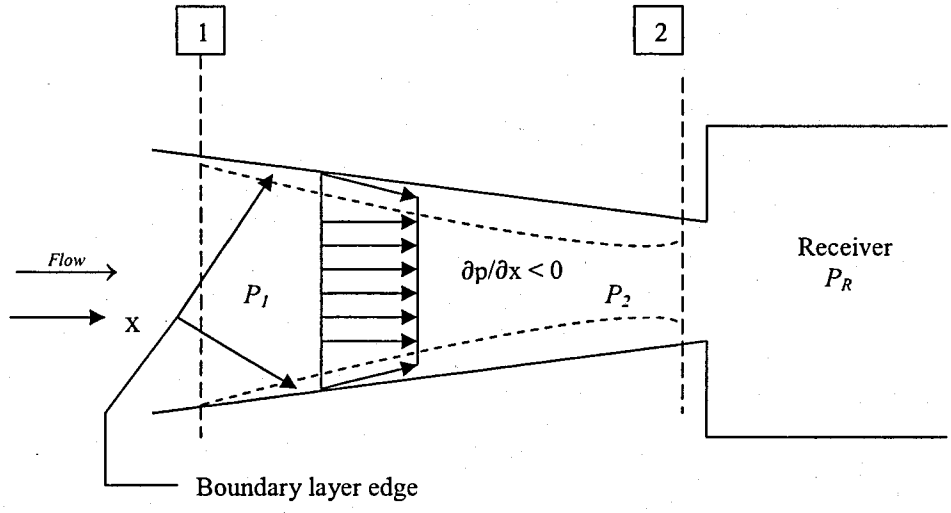

Figure 12. Schematic showing subsonic nozzle characteristics. From "Schaum's outlines: fluid dynamics" by Brighton & Hughes, 1999.

Further on assumption that $V_1 << V_2$, and using isentropic and property relationships, equation (19) was re-written as

$$V_2 = \left\{ \frac{2k}{k-1} p_1 v_1 \left[1 - \left(p_2 / p_1 \right)^{(k-1)/k} \right] \right\}^{1/2} \tag{20}$$

Combining Equations 18 and 20, and the isentropic relationship $\left(p_1 v_1^k = p_2 v_2^k \right)$ with $k = c_p/c_v$, the ratio of specific heats, and where c_p and c_v being the specific heat capacities at constant pressure and volume respectively, Brighton and Hughes (1999) arrived at

$$\dot{m} / A_2 = \left\{ \frac{2k}{k-1} \frac{p_1}{v_1} \left[\left(p_2/p_1 \right)^{2/k} - \left(p_2/p_1 \right)^{(k+1)/k} \right] \right\}^{1/2} \tag{21}$$

Additionally, Brighton and Hughes (1999) argued that if the inlet conditions are assumed to be constant, then the mass flow rate will only change as a result of changes due to only pressure P_2. Brighton and Hughes (1999) indicated that there is discrepancy between the actual and the predicted results. The actual results agree very well with those predicted from the point where $P_R / P_1 = 1.0$ down to the receiver pressure where the mass flow attains its maximum (Brighton & Hughes, 1999).

According to Brighton and Hughes (1999) a further reduction in receiver pressure (P_R) does not change the mass flow rate. They further noted that experimentally, the throat pressure P_2 is never less than maximum mass flow, and this minimum throat pressure was referred to as the critical pressure P_c. This critical pressure is obtained by differentiating Equation 21 and equating the result to zero. This resulted in

$$\left(p_2/p_1 \right)_{\max flow} = p_c/p_1 = \left[2/(k+1) \right]^{k/(k-1)} \tag{22}$$

Brighton and Hughes (1999) concluded that by combining Equations 20 and 22, where the pressure is critical, the Mach number (M) is found to be equal to unity.

Potential Flow Solution for Flow Past an External Object and Effect of Pressure Gradient on Boundary Layer Growth

Flow past an aerofoil object. The potential flow solution for flow past an object usually predicts a decreasing pressure over the front portion of the body where as at the rear portion the pressure increases. Figure 13 is an example of flow past an aerofoil. As shown in the schematic diagram, the boundary layer at the front portion is thinner and thicker at the rear portion with possible separation occurring (Brighton & Hughes, 1999).

Brighton and Hughes (1999) indicated that if the rear body is too "blunt," separation will occur due to the fact that the pressure gradient $\partial p/\partial x$ will become too large as shown in Figure 13. On the other hand, as shown in the Figure 14, if the rear is gently streamlined, separation is prevented and a tear drop shape is formed.

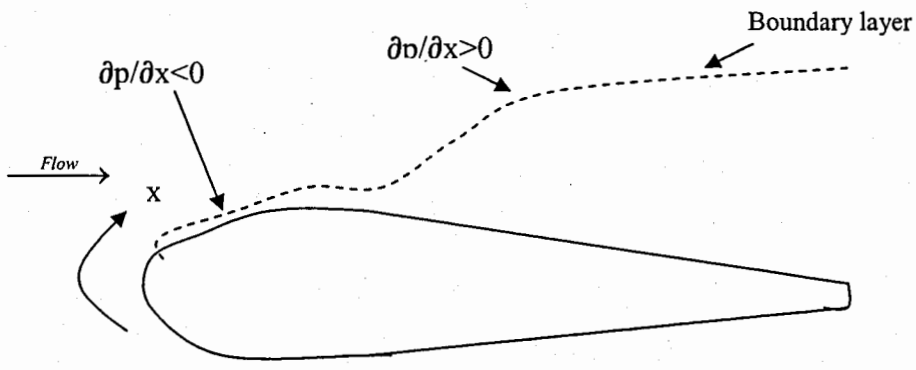

Figure 13. Schematic showing effect of pressure gradient externally on the boundary layer growth. From "Schaum's outlines: fluid dynamics" by Brighton & Hughes, 1999.

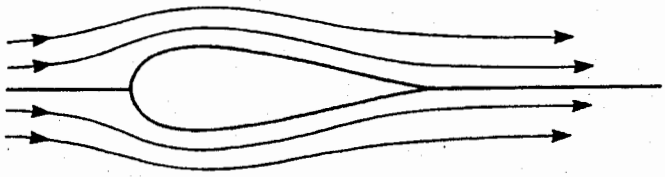

Figure 14. Schematic showing streamlined flow over a tear drop shape without separation. From "Schaum's outlines: fluid dynamics" by Brighton & Hughes, 1999.

Flow past over cylinder at different Reynolds numbers. Further, Brighton and Hughes (1999) provided characteristics effect of separation of flow over cylinders with different Reynolds numbers. These are illustrated in the Figures 15 to 18. As shown in Figures 16 to 18, at the point where separation takes place, the flow breaks away from the surface and creates a wake. Beyond the separation, flow actually reverses along the surface and gives rise to eddies and vortices in the wake (Brighton & Hughes, 1999).

According to Brighton and Hughes (1999) account, the wake structure critically depends on Reynolds number of the free stream flow which in turn depends on the characteristic dimension of the object. Following from this dependency on Reynolds numbers, Brighton and Hughes (1999) explained that at very low Reynolds numbers, Re $<< 1$ as shown in Figure 15, the flow is termed creeping or viscous flow.

Under such condition, according to Brighton and Hughes (1999) the boundary layer becomes very thick and the viscous effect is felt far out into the main flow. Under this circumstance, there is no potential flow region and also there is no definite wake. Further, at the front and back, the flow pattern is found not to be symmetrical as demonstrated in Figure 15.

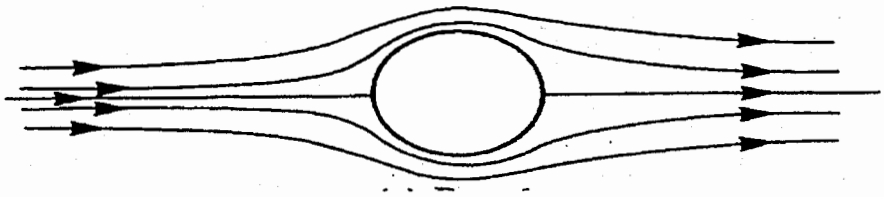

Figure 15. Flow past cylindrical bodies at Reynolds number, Re << 1. From "Schaum's outlines: fluid dynamics" by Brighton & Hughes, 1999.

As shown in Figures 16 to 18, a pair of bound vortices appears in the wake. Consequently, with increasing Reynolds numbers, the vortices form and shed alternately from side to side and thus form what is termed a von Karman vortex street. Brighton and Hughes (1999) indicated that this is an important phenomenon, and hence if such periodic behavior is coupled with a mechanical system of the object, a self sustained oscillation can result. If resonance conditions occur in the process, catastrophic effect may arise (Brighton & Hughes, 1999).

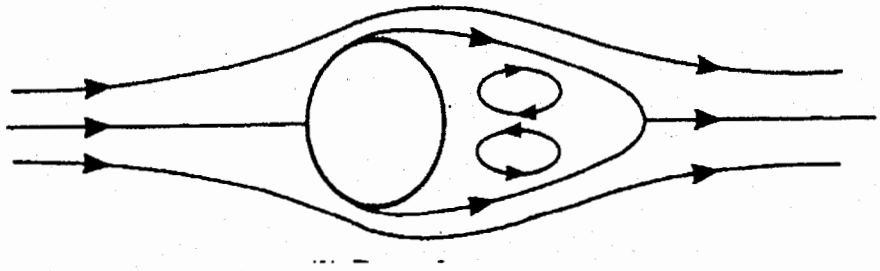

Figure 16. Flow past cylindrical body at Reynolds number, Re ≈10. From "Schaum's outlines: fluid dynamics" by Brighton & Hughes, 1999.

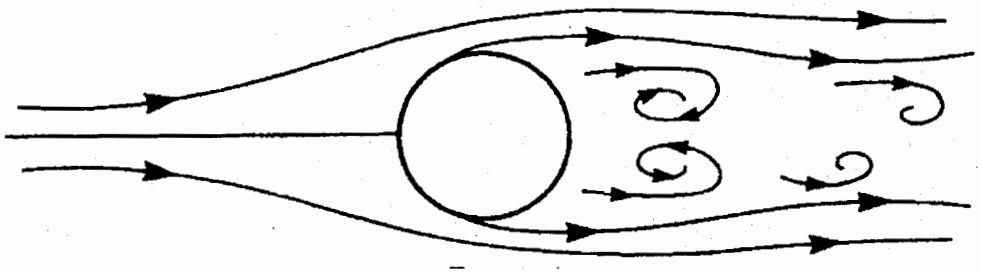

Figure 17. Flow past cylindrical body at Reynolds number, Re ≈60. From "Schaum's outlines: fluid dynamics" by Brighton & Hughes, 1999.

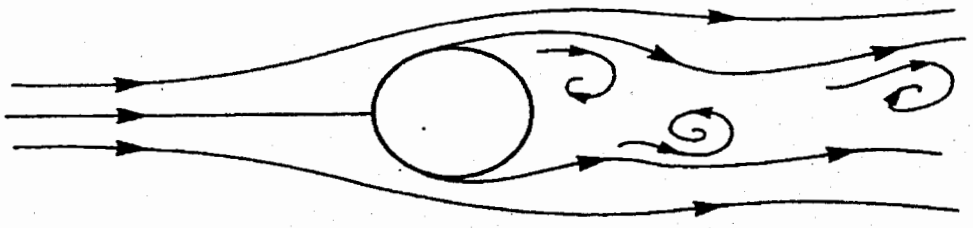

Figure 18. Flow past cylindrical body at Reynolds number, Re ≈1000. From "Schaum's outlines: fluid dynamics" by Brighton & Hughes, 1999.

Further, because of the interaction of the wake and potential flow region, the actual separation position is difficult analytically to calculate. Brighton and Hughes (1999) explained that the wake changes the pattern of potential flow and the associated pressure gradient along the surface, and that the pressure gradient along the surface and the turbulence level in the boundary layer affects the position of the separation point. Consequently, as the turbulence level increases, the position of the separation point travels toward the trailing or rear edge (Brighton & Hughes, 1999).

Further, the roughness of the surface and the level of turbulence in the free stream outside the boundary layer affect the level of turbulence in the boundary layer. In general, if the body is blunt in the rear, because of boundary layer thickening or separation, the wake becomes appreciable. However, besides the front portion where the boundary is thin, according to Brighton and Hughes (1999) the potential flow solution in general is incorrect over bodies with wake. They further suggested that for cylindrical bodies with laminar boundary layer with Reynolds number $Re < 5(10)^5$, the position of the separation point is located at 81 ^{o} from the stagnation point (Brighton & Hughes, 1999).

Internal Flow

There are two factors or conditions that differentiate internal flows from external flows. They are (a) at the entry region and (b) when the flow is fully developed. At the entry region of an internal flow, there is a boundary layer and a uniform free stream that accelerates according to the rate at which the boundary layer grows. Secondly, when the flow is fully developed, the velocity varies wholly over the channel (Brighton & Hughes, 1999).

Entrance Flows

Entry at a laminar flow. For a laminar flow in the entry region of a tube, the velocity is found to be uniform at the entrance. Thus, the boundary layer grows with distance from the entrance to the extent that flow becomes fully developed. Assuming a frictionless flow, and applying the continuity equation, it is noticed that the core must accelerate. Consequently, employing the Bernoulli's equation along a streamline in the

free stream region, it is further observed that the pressure decreases (Brighton & Hughes, 1999).

Brighton and Hughes (1999) suggested that, for the flow to become fully developed, Boussinesq found a relation that must be met for the laminar development length X_L which is stated as $X_L = 0.03$ Re D. X_L is the laminar development length after which the flow becomes fully developed, D is the drag force diameter; Re is the Reynolds number (Brighton & Hughes, 1999).

Entry at turbulent flow. Alternatively, the flow in the entry region of a turbulent flow occurs when the Reynolds number is large, that is Re > 2300. Fully developed flows can be identified by several criteria. They are pressure drop, mean velocity distribution, or turbulence quantities. According to Brighton and Hughes (1999), the actual lengths for these criteria are significantly different (Brighton & Hughes, 1999).

For instance, in general, the pressure gradient attains a fully developed value after three (3) or four (4) diameters of the entrance length, that is, $X_L = (3 - 4)\ D$. On the other hand, the mean velocity becomes fully developed after 30 to 60 diameters of the entrance length, that is, at $X_L = (30 - 60)\ D$. The turbulence quantities, however require greater lengths. Brighton and Hughes (1999) hinted that the criterion used most frequently in literature is when the mean velocity profiles do not change with distance in the flow direction (Brighton & Hughes, 1999).

Fully Developed Flows

Transition. Flows in a pipe could be laminar or turbulent. When the flow is laminar it is well ordered and smooth. On the other hand, when the flow is turbulent it

usually assumes a chaotic fluctuating motion. In general, the characteristic of the flow is determined by the Reynolds number and the roughness of the wall of the pipe (Brighton & Hughes, 1999).

By illustration, for laminar flows, when the flow rates are of small values, a dye in the flow forms a smooth line. On the other hand, during turbulent flows, when the flow rate is increased, a point is reached when the dye introduced breaks up into uneven or bumpy or rough patterns (Brighton & Hughes, 1999).

According to Brighton and Hughes (1999), for transition from laminar to turbulent, the Reynolds number is estimated as 2300. Nevertheless, under some special conditions according to Brighton and Hughes (1999), transition has taken place at higher Reynolds numbers at about 40,000.

Laminar flow in a circular tube, Poiseuille flow. Brighton and Hughes (1999) indicated that flow in circular pipe is also referred to as Poiseuille flow. Brighton and Hughes (1999) applied the momentum equation of motion and boundary condition and integrated directly twice to obtain the following derivations for Poiseuille flow:

$$0 = -\frac{dp}{dx} + \mu\left(\frac{d^2u}{dr^2}\right) \tag{23}$$

The first integration gives

$$\mu\left(\frac{du}{dr}\right) = \frac{dp}{dx}r + C_1 \tag{24}$$

Using the condition that at $r = 0$, $du/dr = 0$, and hence $C_1 = 0$. This resulted in

$$\mu\left(\frac{du}{dr}\right) = \frac{dp}{dx}r \tag{25}$$

Integrating Equation 25 gives

$$\mu u = \frac{dp}{dx}r^2 + C_2 \tag{26}$$

Further, using the condition that at $u = 0$ and $r = R$, $\Rightarrow C_2 = \frac{dp}{dx}R^2$. By substitution, this further resulted in

$$u = \frac{1}{4\mu}\frac{dp}{dx}(r^2 - R^2) \tag{27}$$

To obtain the flow rate Q, the velocity was integrated over the cross section of the tube as

$$Q = \int_0^R 2\pi r u dr = \frac{1}{8\mu}R^4\frac{dp}{dx} \tag{28}$$

Turbulent flow. The velocity distributions for fully developed flow in a pipe is approximated by the power law velocity as

$$u/_{U\max} = (y/R)^{1/n} \tag{29}$$

where y is the distance measured from the pipe wall towards the center, R is the radius of the tube. The exponent $1/n$ weakly varies with Reynolds numbers from 1/6 to 1/10 for Reynolds numbers between $4x10^3$ to $3x10^6$ (Brighton & Hughes, 1999).

Temperature and Pressure Effects on Mixing of Gases and Vapors

Salzman (2004) indicated that entropy is a measure of disorder. Thus as entropy increases it is an indication of increase of disorder. Salzman derived the relevant entropy equations that govern the mixing of gases.

To understand gas mixing, Salzman (2004) suggested that one has to visualize a container divided into two compartments. One compartment has n_1 moles of ideal gas 1 at a pressure, p and temperature, T. Also in the other compartment, n_2 moles of another ideal gas 2 at the same pressure and temperature. If the partition is removed the gases will diffuse into each other and the system will then attain a state where both gases become uniformly distributed throughout the container. According to Salzman (2004), this is an irreversible process and hence, the entropy will increase.

After extensive derivation, Salzman (2004) arrived at the following equations for entropy change under the assumption that one gas expands reversibly and isothermally but the other gas remains undisturbed. Starting from $dU = T\,dS - p\,dV = 0$ or $dS = (p\,dV)/T + dU/T$, he arrived at

$$\Delta S_{mix} = -R\left(n_1 \ln X_1 + n_2 \ln X_2\right) \tag{30}$$

or

$$\Delta S_{mix} = -n\,R\left(X_1 \ln X_1 + X_2 \ln X_2\right), \tag{31}$$

where ΔS_{mix} is entropy of mixing, R is the Boltzman constant, n_1 is the number of moles of ideal gas 1, n_2 is the number of moles of ideal gas 2, $n = n_1 + n_2$ is the total number of moles, $X_1 = n_1/n = V_1/(V_1+V_2)$ is the mole fraction of gas 1, $X_2 = n_2/n = V_2/(V_1+V_2)$ is

the mole fraction of gas 2. Also, $V_1 = n_1 R T / p$ and $V_2 = n_2 R T / p$ are the partial volumes for gas 1 and 2 respectively.

Salzman (2004) further suggested that if the two gases being mixed are not under the same initial pressure, the following steps can be introduced. One can first expand or compress one of the gases to bring it to the pressure of the other gas. Secondly, one can mix the gases and subsequently compress or expand the mixture to bring it to the correct final volume and pressure.

Additionally, Salzman (2004) suggested that if the two gases are not at the same temperature and pressure, one could first use the heat balance to find the final temperature. One then follows this up with reversible cooling and heats the two gases individually to the same temperature, then expanding or contracting the gases, mixing the gases, and then expanding or contracting the mixture to the appropriate volume. Salzman indicated that entropy change in Equation 31 can be extended to more than two gases as follows:

$$\Delta S_{mix} = -n R \left(X_1 \ln X_1 + X_2 In X_2 + X_3 \ln X_3 + \cdots\right) \tag{32}$$

Salzman (2004) interpreted the entropy mixing relations as follows:

1. An isothermal expansion allows molecules greater room to travel around but the molecules become less localized.
2. When the temperature is increased, the average speeds of molecules increase. The molecules become more disordered in momentum or velocity space.
3. Mixing either gases or liquids intermingle or spread the molecules among each other and thus increases the disorder.

4. Entropy is increased during a phase change from solid to liquid or solid to gas, or from liquid to gas.

Salzman (2004) went on to note that vaporization of liquids has positive entropy of vaporization. This is because gases are more disordered than liquids. Salzman further indicated that the entropy of vaporization for many substances at their boiling point are approximately 86 J/K except water and helium. Salzman referred to this phenomenon as Trouton's rule.

As explained by Salzman (2004) the process of vaporization creates a mole of disordered gaseous molecules from a mole of well ordered solid or liquid molecules. Thus, Salzman further identified that gases are more disordered than solids and liquids. On the other hand, liquids are also more disordered than solids. Salzman again observed that gases are normally found at the atmospheric pressure because that is their boiling point.

Statistical Thermodynamics and the Kinetic Theory of the Ideal Gas Law

This section presents the derived kinetic equations of the ideal gas law, the distribution of velocities of the gas molecules, and transport processes in gases. The transport processes in gases are related to diffusion, thermal conductivity and viscosity.

Pressure of Gas on the Wall.

When molecules strike a unit area of the wall of a container, the pressure on the wall is given by Kittel and Kroemer (1980) as:

p = (*momentum change per molecule*) x (*number of molecules striking unit area per unit time*) (33)

From the above relation, the ideal gas law was derived by Kittel and Kroemer (1980) as:

$$p = nM\left\langle v_z^{\,2}\right\rangle = n\tau = (N/V)\tau;\ \text{or}\ \ pV = N\tau\ \ \text{or}\ pV = Nk_BT \tag{34}$$

where p is the pressure of the gas; $n = N/V$ is the number of molecules per unit volume, N is the total number of molecules, V is the volume of the container; M is the mass of one molecule, v_z is the velocity of the particle or molecule normal to the wall; $\tau = k_B T$ is the fundamental temperature that has dimensions of energy (J), $k_B = 1.381 \times 10^{-23}$ J/K (it is called the Boltzman constant) and T is the temperature in Kelvin (Kittel & Kroemer, 1980).

Maxwell Distribution of Velocities

The probability distribution of the classical velocity was obtained by transforming the energy distribution function of an ideal gas into a classical velocity distribution function. This was achieved by equating the classical kinetic energy ½ $M v^2$ to the quantum orbital energy

$$\varepsilon_n = \frac{\hbar^2}{2M}\left(\frac{\pi n}{L}\right)^2 \tag{35}$$

The Maxwell velocity distribution was then obtained as

$$P(v) = 4\pi(M2\pi\tau)^{3/2} v^2 \exp(-Mv^2/2\tau) \tag{36}$$

where n is the quantum orbital number, and $P(v)$ is the probability that a particle has its speed in dv at v. From the Maxwell velocity distribution, the mean square thermal velocity, mean speed and the most probable speed of a molecule were given as $v_{rms} = (3\tau/M)^{1/2}$, $\bar{c} = (8\tau/\pi M)^{1/2}$, $v_{mp} = (2\tau/M)^{1/2}$ respectively (Kittel & Kroemer, 1980).

Atom Mean Free Paths, Collision Cross Sections and Collision Rates.

Consider two atoms, each with diameter d. The two atoms will collide if their centers pass within a distance of d from each other. Consequently, an atom of diameter d which travels a distance L will sweep a volume of $\pi d^2 L$. Hence, if the concentration of atoms is n, then the average number of atoms in this volume is $n\pi d^2 L$. Thus, the number of collisions in the volume will be $n\pi d^2 L$ (Kittel & Kroemer, 1980).

Consequently, the mean free path, which is the average distance between collisions was given by Kittel and Kroemer (1980) as

$$l = \frac{L}{n\pi d^2 L} = \frac{1}{n\pi d^2} \tag{37}$$

Where l is the mean free path, which is the average distance traveled by an atom between collisions, n is the number of atoms per unit volume, and d is the diameter of the atom. Further, if the atom diameter is d, then the collision cross section (σ_c) of the atom and the associated collision rate (σ_r) are respectively given by Kittel and Kroemer (1980) as:

$$\sigma_c = \pi d^2 \tag{38}$$

$$\sigma_r = \frac{v_{rms}}{l} \tag{39}$$

The effect of reducing pressure on the concentration of atoms was discussed by Kittel and Kroemer (1980). At a pressure of 10^{-6} *atm* or 1 *dyne* cm^{-2}, concentration of atoms is reduced by 10^{-6} *atm* and the mean free path is increased by 25 cm. As a result, at 10^{-6} *atm*, the mean free path might not be small when compared with dimensions of the

apparatus. During this condition, the state of the atoms is referred to as high vacuum region or Knudsen region (Kittel & Kroemer, 1980).

Transport Processes

Transport processes are concerned with a system which is not in thermal equilibrium and it is also not in equilibrium steady state, but it is under constant flow from one point of the system to another point. Under this situation, there is a linear region in most transport processes such that the flux is directly proportional to the driving force (Kittel & Kroemer, 1980). This relation is called the linear phenomenological law and provided the driving force is not too large, this relationship is the flux and it is defined as:

Flux = (coefficient) x (driving force) (40)

We can therefore define the flux density of a quantity A as J_A = flux density of A = net quantity of A transported across unit area in unit time. The net transport is the transport in one direction minus the transport coming from the opposite direction. The following subsections describe various transport laws in relation to the foregoing phenomenon (Kittel & Kroemer, 1980).

Particle diffusion. Particle diffusion is concerned with transport of particles. At a constant temperature, consider a system such that one end is in diffusive contact with reservoir at chemical potential μ_1. Consider that the other end is also in diffusive contact with a reservoir at chemical potential μ_2. Consequently, if reservoir *1* has a higher chemical potential, the particles in the system will flow through the system from reservoir *1* to *2*. Thus, the particle flow in the direction just described will increase the total entropy of the system (Kittel & Kroemer, 1980).

Now, following from the above principles, consider particle diffusion due to the difference in chemical potential caused by the difference in the particle concentration. In this case, the flux density J_n becomes the number of particles passing through a unit area in unit time. Under this particular circumstance, the driving force of the isothermal diffusion is usually taken as the gradient of the particle concentration along the system. It is referred to as the Fick's law and the relation is stated as (Kittel & Kroemer, 1980):

$$J_n = - D \text{ grad } n \tag{41}$$

where D is the particle diffusion constant or diffusivity. The particle diffusivity is model for transport problems and the diffusivity is given by

$$D = \frac{1}{3} \bar{c} l \tag{42}$$

According to Lide (2002) diffusion coefficient is inversely proportional to pressure when fluid especially gases are in region such that binary collisions dominate.

Thermal conductivity. This is the transport of energy by particles. The Fourier's Law describes the energy flux density in terms of the thermal conductivity as

$$J_u = K grad \tau \tag{43}$$

where J_u is the energy density flux, and K is the thermal conductivity. The thermal conductivity is also defined as

$$K = D \hat{C}_v = \frac{1}{3} \hat{C}_v \bar{c} l = \eta \hat{C}_v \rho \tag{44}$$

where $\hat{C}_v = \partial \rho_u / \partial \tau$ is the heat capacity per unit volume, ρ_u is the energy density; η is the viscosity, and $\rho = n M$ is the mass density. The thermal conductivity of gases is independent of pressure. Further, at very low pressures the mean free path is limited by

the apparatus dimensions instead of the intermolecular collisions (Kittel & Kroemer, 1980).

Viscosity. Viscosity is concerned with the transport of momentum by particles. It can be conceived as resistance to flow of or through a medium. Substances which are less viscous are less resistance to pass through because they have weaker intermolecular interactions. That is, the energy of the van der Waals forces in the less viscous substances is much lower than the energy of the viscous substances that have more or stronger bonds (Kittel & Kroemer, 1980).

Technically, the concept of viscosity of a gas is attributed to transfer of momentum between moving and stationary molecules. Consequently as temperature increases, molecules more frequently collide and therefore transfer a greater amount of their momentum. Viscosity is therefore a measure of the diffusion of momentum parallel to the flow velocity and transverse to the flow velocity gradient. For a gas flowing with a velocity (v_x) in the x direction and the flow velocity in the z direction, the viscosity coefficient η is defined by the relation

$$X_z = -\eta \frac{dv_x}{dz} \tag{45}$$

where X_z is the shear force exerted by the gas on a unit area of the $x\,y$ plane normal to the z direction. The viscosity can be expressed as

$$\eta = D\rho = \frac{1}{3}\rho \bar{c} l = M \bar{c} / 3\pi d^2 \tag{46}$$

where D is the diffusion coefficient, l is the mean free path, d is the molecular diameter, and n is the concentration and $\rho = n\,M$ is the mass density (Kittel & Kroemer, 1980).

The viscosity is independent of the gas pressure. However, at very high pressures, this independence fails when the molecules are nearly always in contact. Similarly, the independence fails at very low pressures when the free path becomes longer than the dimensions of the apparatus (Kittel & Kroemer, 1980; Nieto de Castro, Dymod & Millat, 1996).

Further, while the viscosity of solids and liquids decreases as temperature increases, on the other hand, the viscosity of gases increases as temperature is increasing. This is due to the fact that as the temperature of a gas rises, the gas then has more collisions. In other words, as a gas is heated, the movement of the molecules increases and the probability of one gas molecule interacting with another then increases (Kittel & Kroemer, 1980; Nieto de Castro et al., 1996).

Thus heating a gas translates into an increase in intermolecular activity and attractive forces which is opposite to the effect of heating a liquid or solid. Consequently, a gas molecule will encounter more friction with its neighboring molecules and hence further increases the viscosity (Kittel & Kroemer, 1980; Nieto de Castro et al., 1996).

Thermal Conductivity and Viscosity of Monatomic Fluid-Argon

Nieto de Castro, Dymod and Millat (1996) indicated that the thermal conductivity (k), a transport property for monatomic fluid such as Argon has two main components, a background contribution $\bar{k}$ and critical enhancement Δk_c of the form $k = \bar{k} + \Delta k_c$. Nieto de Castro et al. (1996) provided detailed derivations for both the background contribution $\bar{k}$ and critical enhancement Δk_c but have not been presented in this report. In general,

however, Nieto de Castro et al. indicated that the excess thermal conductivity Δk of simple fluids depends weakly on temperature. In addition, Nieto de Castro et al., however, expressed that for more accurate engineering functions, the critical thermal conductivity enhancement Δk_c for general application is temperature dependent.

Similarly, Nieto de Castro et al. (1996) indicated that the conceptual and mathematical relation of the viscosity (η), also a transport property for monatomic fluid, in Argon has similar components to the thermal conductivity. Hence, the viscosity (η) and its background contribution $\bar{\eta}$ and critical enhancement $\Delta\eta_c$ are expressed in the form $\eta = \bar{\eta} + \Delta\eta_c$ and the background contribution is also decomposed as $\bar{\eta} = \eta^{(0)}(T) + \Delta\eta(\rho,T)$. Where $\Delta\eta(\rho,T)$ is the excess viscosity. Similarly, Nieto de Castro et al. again provided detailed derivations for these relations but then have not been presented in this report. Nieto de Castro et al. suggested that similar to the thermal conductivity, viscosity of monatomic fluid, argon is also dependent on temperature and density.

Thermal Conductivity and Viscosity of Diatomic Fluid-Nitrogen

Nieto de Castro et al. (1996) expressed that nitrogen, a diatomic molecule, is one of the stable and simplest molecule that behaves as a typical polyatomic molecule compared to the structureless monatomic fluids such as argon. Nieto de Castro et al. stated that conceptually, the thermal conductivity of diatomic fluids such as nitrogen can be expressed as $k = k^{(0)}(T) + \Delta k(\rho,T) + \Delta k_c(\rho,T)$. Similarly, $k^{(0)}(T)$ denotes the thermal conductivity in the diatomic dilute-gas (low density) transport property limit at

temperature T, and $\Delta k(\rho,T)$ is the excess thermal conductivity contribution at density ρ and temperature T, and Δk_c is critical thermal conductivity enhancement.

Nieto de Castro et al. further concluded that in general the transport properties including thermal conductivity and its critical enhancements for nitrogen have validity in the range from 70 to 1100 K with a maximum pressure of 100 MPa which is equivalent to maximum density of 30 mol L^{-1}. Further, Nieto de Castro et al. indicated that at higher temperatures, the range of the pressure and hence the density is reduced.

Once again, Nieto de Castro et al. (1996) showed that the viscosity of diatomic fluid, nitrogen, can be conceptually and mathematically expressed in a similar pattern as the thermal conductivity of diatomic molecule, nitrogen. Hence, the general viscosity expression showing dependence on temperature and density was given as $\eta = \eta^{(0)}(T) + \Delta\eta(\rho,T) + \Delta\eta_c(\rho,T)$. With regards to the critical enhancement $\Delta\eta_c$ for the viscosity, Nieto de Castro et al. came to a conclusion that it has very small contribution to the viscosity and hence for most practical purposes it is sufficient to consider it as zero.

Partial Differential Equation and Finite Element Analysis.

Partial differential equation (PDE) is similar to ordinary differential equation (ODE), but the difference is that, in the case of PDE the dependent variable is a function not only for one, but of several independent variables. Conceptually, given a function $u = u(x_1, x_2, \ldots, x_n)$, the PDE in u is formulated as an equation which relates any partial derivates of u to each other and / or to any of the independent variables $x_1, x_2, \ldots, x_n$ and the dependent variable u (Coleman, 2005).

Coleman (2005) illustrated some of the acceptable forms of mathematical notations for PDEs. For lower order PDE we can write

$$u_x = \frac{\partial u}{\partial x}. \tag{47}$$

An example of the higher order PDEs is

$$u_{xy} = \frac{\partial}{\partial y}\left(\frac{\partial u}{\partial x}\right) = \frac{\partial^2 u}{\partial y \partial x}. \tag{48}$$

Coleman (2005) further indicated that for practical purposes, the order of differentiation is not of great significance and that the following PDEs are equivalent $u_{xzyx} = u_{zxxy} = u_{yxzx}$

In general for PDEs, we always wish to solve for the dependent variable u which is not often known. Thus, the solution to a PDE is any function $u = u(x_1, x_2, ..., x_n)$ which satisfies the PDE identically. As a consequence, all possible values of the independent variables $x_1, x_2, ..., x_n$ must satisfy the PDE (Coleman, 2005).

There are several numerical methods available for solving partial differential equations. These are: (a) finite difference approximations with its explicit and implicit scheme techniques, (b) spectral methods, and (c) finite element method.

The finite element method is very powerful and most popular method for solving PDEs numerically. Compared to the finite difference approximations and spectral methods, the disadvantage of finite element method is that it is difficult to implement. On the other hand, the advantage outweighs the disadvantage. This is because, it is broadly applied.

The similarities between the finite element methods and the others are that the first step is to break the domain into subdivisions. The difference is however significant,

and that makes the finite element method powerful. These are: (a) the subdivisions for the finite element method need not be rectangular, and hence can be applied to any domain with an arbitrary shape, and (b) the approximating sum is not smooth but continuous piecewise polynomial function.

Summary of Literature Review

To minimize threats to internal validity a comprehensive literature review was conducted in order to communicate clear understanding of the experimental factors being investigated and the appropriate experimental conditions. Hence, initially, the amazing mechanical and electronic properties and usefulness of carbon nanotubes were described. Also the methods and reactors for producing carbon nanotubes were described. More detailed explanations of laser methods for growing carbon nanotubes were provided since that formed the sample for this study.

Similarly, the characteristics of the two selected carrier gases, that is, nitrogen and argon were described. It was noted that there are striking differences in these two gases and hence they are good candidates for the type of carrier gases being considered as one of the main factors for this study. Further, static mixers sometimes referred to as inline or motionless or passive mixers were reviewed. Design types, kinds of variables and simulation methods employed by other investigators were noted.

Furthermore, temperature and pressure effects on mixing of gases and vapors were considered. It was noted that manipulating pressure and temperature enhances mixing of gases as recognized by Salzman (2004). Additionally, to understand the atomic and molecular behavior of the carrier gases in combination with the other experimental

conditions statistical thermodynamics and the kinetic theory of the ideal gas law were reviewed. In this review, transport properties such as diffusion, thermal conductivity and viscosity of the carrier gases and how they were affected by temperature and pressure were explained.

Also, since most of the governing equations for modeling static mixers and fluid flow were developed using partial differential equation (PDEs) this was also reviewed. Hence, the mathematical treatments regarding problem definition, assumptions, and boundary conditions were studied. Moreover, the numerical methods such as the finite element methods used in finding PDE solutions to most fluid flow and thermal simulation experiments were described.

CHAPTER 3

METHODOLOGY

Introduction

The purpose of the methodology is to describe in detail how the study was conducted. This indicates the methods chosen to ensure validity and reliability of the results. The methodology was broken into the following subsections (a) research design, (b) apparatus/materials, and (c) procedures (American Psychological Association [APA], 2001).

The research design section which follows describes the subjects; population; sample; type of experimental method; choice of variables and their levels and type of treatments given. The apparatus/materials section describes briefly, the computer and software used and their role in the simulation experiment. The procedure subsection provides a summary of the phases and steps employed to complete the study. Issues related to experimental control are also described (APA, 2001; CTE, 1987; Creswell, 2003; Fraenkel & Wallen, 2003; Kim, Liu, & Sung, (in press); Non-linear Engineering (NE), 2005). The steps employed in the procedure section included:

1. Description of method of data collection.
2. Conceptual design of three types of static mixer design configurations employed with the capabilities of improving the existing reactors for achieving improved carbon vapor and carrier gas mixing/concentration ratios as precondition for controlling growth and maximizing yield of carbon nanotubes (COMSOL AB., 2004b; COMSOL AB., 2004d).

3. Description of physical and computer simulation models developed for the static mixers in relation to known practice in industry. The description encompasses simulation development, evaluation, conclusion and validation (Banks & Carson II, 1984; COMSOL AB., 2004b; COMSOL AB., 2004d)
4. Description of the computer simulation experimentation and data generation procedures (Banks & Carson II, 1984; COMSOL AB., 2004b; COMSOL AB., 2004d)
5. Description of the descriptive and inferential statistical methods employed for summarizing data and for generalizing to the target population (Banks & Carson II, 1984; CTE, 1987; Dunn & Everitt, 1983; Elliot, 2000; Fraenkel & Wallen, 2003; Longnecker & Ott, 2001; SPSS Inc., 1999).

Research Design

Subjects

Population. The target population was reactors employed by production methods specifically used for growing carbon nanotubes. These included reactors used in laser, solar, arc discharge, flame combustion, chemical vapor deposition, and high-pressure carbon monoxide conversion methods.

Sample. The sample consisted of reactors used in laser vaporization method for synthesizing single wall carbon nanotubes.

Type of Research Method.

A quantitative type of experimental research method was employed. However, specific types of research method were applied to specific research questions or hypotheses. The generic experimental research method employed was a factorial design with four factors. Three of the four factors were given two levels of treatment, and one factor was given three levels of treatment. The four factors and their levels were (a) three types of static mixer designs, (b) two types of carrier gas, (c) two sets of reactor operating temperature, and (d) two sets of carrier gas inlet pressure. Only main effects of the four factors were investigated, and possible interactions were deferred to future studies.

To investigate the main effects four-way analysis of variance (4-Way ANOVA) was used to answer the research questions and research hypotheses. Specifically, 4-Way ANOVA was found sufficient to answer research questions 1 and 2. In addition, the coefficient of determination output from the 4-Way ANOVA results was found sufficient to answer research hypothesis 1. However, in addition to the foregoing, the Tukey's honest significance difference (HSD) procedures were employed to answer research hypotheses 2 to 5.

Experimental and Measuring Units

Three types of particular static mixer designs (that is different internal configurations with same external characteristic dimensions) served both as the experimental and measuring units. These design types were the baffle type static mixer (concept design 1), aerodynamic type static mixer (concept design 2), and existing reactor (concept design 3).

Variables.

Dependent variable. The mixing index or effectiveness obtained from the mixing ratio of the carrier gases flowing through the static mixers served as the output or dependent variable. The mixing ratios were measured indirectly from temperatures at the cross section of the exit of the static mixers. They were then multiplied by 100% to obtain the mixing effectiveness or index (Devahastin et al., 2004).

Ideally to measure the mixing ratio between the carbon-metal catalyst vapors and the carrier gases as the dependent variable requires three phase fluid flow. This would have made the experiment very complicated. And hence as an exploratory experiment only a single type of carrier gas was simulated. Future studies may investigate two and three phase gas flow involving all the gases that take place in the mixing.

Independent variables. These are categorical and quantitative discrete variables that were manipulated. The categorical variables were the three types of static mixer designs and the two types of carrier gases. The quantitative discrete variables were the two sets carrier gas inlet pressures and two sets of reactor operating temperatures.

To ensure that results of the study are useful, most of the input data used were based on values established in existing literature. This was found to be one of the current directions of most modeling and simulation experiments in the field of nanomanufacturing (NSF).

Control variables. These were the variables kept constant throughout the simulation experiment. They were the carrier gas inlet flow rate and inlet temperature. The inlet flow rate was originally set at 100 sccm which is approximately 0.006 m/s as

used by Fan, Geohegan, Guillorn et al. (2002) and Fan, Geohegan, Pennycook et al. (2002) since the dimensions of the reactor being modeled was chosen to have similar characteristic diameter. The inlet temperature was set at 300 K assumed to be the room temperature at which the gas will enter into the reactor mixing zone.

However, the original flow rate did not lead to convergence for some of the treatment conditions, and hence by systematic reduction, 0.0045 m/s was found suitable for all the treatment conditions. In addition, the vapor zone of the existing laser vaporization type reactor was considered as a control variable and was developed as static mixer design concept (3) without baffles or inner blades.

Description of Variables and Their Levels.

Type of static mixer design. This is a categorical variable. Three levels of static mixer design configurations were chosen. This was because to improve the design of a reactor as suggested by Flamant et al. (2001), there was the need to improve the configuration of the reactor. In this respect three different design configurations were chosen as the levels. The main characteristic dimensions were the same so that only the effects of the inner configuration designs in the form of partial barriers were investigated.

Type of carrier gas. This is also a categorical variable. Nitrogen and argon gases were chosen as the two types carrier gases because they have different characteristic properties. In Appendices B and C the characteristic properties of the two gases are described.

For example, argon is a monatomic gas whilst nitrogen is diatomic gas. Argon is chemically inert but some percentage of nitrogen dissociates into atoms at about 3500 °C

according to Parkes (1961). In addition, the densities, the transport properties such as the thermal conductivity and viscosity of the two gases are different under the same temperature and pressure conditions.

In fact, Achiba et al. (2003) concluded that molecular mass of carrier gas does have influence on the quantity of carbon nanotubes produced. Consequently, it was considered that all the characteristics properties of the carrier gases that have a relationship with the molecular mass could influence the purity and quantity of carbon nanotubes and need to be further understood.

Levels of carrier gas inlet pressures. It was reported by several investigators that below and beyond certain buffer gas pressures there is low or no growth of carbon nanotubes. Inlet carrier gas pressure was therefore considered very important in the carbon nanotube growth process. Many investigators experimented with different pressures. Two pressures that have been successfully used to grow carbon nanotubes were selected. Hence, the two levels of pressures selected and employed were 500 Torr and 1000 Torr (Chiashi et al., 2002, Flamant et al., Lai et al., 2001; Li et al., 2002).

In addition, it was reported that pressure has no significant effects on the transport properties (that is thermal conductivity and dynamic viscosity). Hence, the inlet pressure effects on the carrier gases thermal conductivity and dynamic viscosity transport properties were neglected (Kittel & Kroemer, 1980; Nieto de Castro et al., 1996; Salzman, 2004).

Levels of reactor operating temperatures. In the growth of carbon nanotubes, using the laser method, carrier gas enters into the reactor at ambient temperature. Two

types of reactors have been used for the laser method of growing carbon nanotubes. Some investigators successfully grew carbon nanotubes using only laser power and others grew carbon nanotubes using a furnace for annealing purposes (Achiba et al., 2003; Botton et al., 2002; Kasuya et al., 2002).

However, in the reactor where the static mixer is to be installed, the carbon in vaporized form was melted at 3500 °C, that is the melting point of carbon (Parkes, 1961). This means, in the reactors which only use laser power, there is the possibility that the carrier gases could attain this extreme temperature and hence it was expected to have an effect on mixing. Alternatively, those investigators who used a furnace for annealing indicated that the most appropriate annealing temperature for growth of carbon nanotubes is 1200 °C. Flamant et al. (2001), confirmed that 1200 °C is most suitable annealing temperature for the growth of carbon nanotubes (Flamant et al., 2001).

Hence, in this study, these two extreme temperatures effect on the mixing ratio were investigated as reactor operating temperature variable. This is because, as suggested by Parkes at 3500 °C, some nitrogen may dissociate and may impact the mixing ratio and consequently the growth of carbon nanotubes. A study was not yet found that addressed the possible dissociation of nitrogen and its effect on the mixing ratio and the growth process of nanotubes. Hence, in this study, two levels of reactor operating temperatures, that is 1200 and at 3500 °C were employed. As result, the temperature at the walls of the mixers was set at these two levels, namely 1200 °C and at 3500 °C (Flamant et al., 2001; Parkes, 1961).

Although it was reported that temperature has effects on the transport properties of gases, in this study, the effects of the reactor temperature on the carrier gas transport properties were neglected. However, in this study, the effect of the reactor temperature on carrier gas density variation and therefore the mixing ratio were included in the modeling (COMSOL AB., 2004f; Kittel & Kroemer, 1980).

Controlled inlet carrier gas flow rate. Different flow rates were successfully used to grow carbon nanotubes by other investigators. The flow rate of 100 sccm which is approximately 0.6 cm/s or 0.006 m/s used by Fan, Geohegan, Guillorn et al. (2002) and Fan, Geohegan, Pennycook et al. (2002) was originally adopted for the experiment. This was done to ensure that the modeling and simulation replicates proven laboratory results. However, the original flow rate did not lead to convergence for some of the treatment conditions, and hence it was reduced to 0.0045 m/s so that it was the same for all treatment conditions.

Controlled carrier gas inlet temperature. Investigators reported that carrier gases were at ambient conditions. This implied the initial temperature with which the carrier gases enter into the reactor was at room temperature, assumed to be 25°C (298K ≈300K). In this experiment, 300 K was chosen and was kept constant throughout the experiment. Since, the pressure is reported to have little significant effect on viscosity and thermal conductivity, the fundamental transport properties for the two carrier gases were appropriately chosen at this initial carrier gas inlet temperature (Achiba et al., 2003).

Validity and Reliability.

Internal validity. The literature review on the static mixers with their design types, modeling and simulation methods; properties of the argon and nitrogen carrier gases; theoretical underpinnings of gas mixing and effects of temperatures and pressures on the mixing of gases were thoroughly understood. This was to ensure that levels of independent variables could lead to a useful outcome of the experimental result (COMSOL AB., 2004b; Devahastin & Mujumdar, 2001; Povitsky, 2002).

External validity. The gaseous zone of the vaporized carbon and metal catalyst vapors of the single wall carbon nanotubes production reactors used in the laser vaporization method was the position chosen for installation of the static mixers. This was to ensure that the results of this study could be generalized to all other single wall and multi-wall carbon nanotubes production methods that either use raw gaseous carbon sources or vaporized graphite materials with or without catalyst materials (Fan, Geohegan, Pennycook et al., 2000; Fan, Geohegan, Pennycook et al., 2002).

In addition, the flow patterns for the most significant differences were recorded to further help validate the results of the simulation experiment. The use of stream lines to validate mixing or concentration ratio or mixing index have been used by other investigators (COMSOL AB., 2004b; Devahastin & Mujumdar, 2001; Povitsky, 2002).

Reliability. The main computer software used for the simulation experiment was FEMLAB™ multi-physics modeling and simulation software. It was originally intended to use Flow 3D™ modeling and simulation software to verify the results obtained. But this could not be done due to time limitations. The main modeling and simulation

application software used have been reported by the developers to be reliable by matching several bench marks and comparing them with other software outputs (COMSOL AB., 2004a).

However, to ensure the model built and the governing physical equations are reliable, existing experimental data for the carrier gases were simulated in the reactor without a static mixer, considered as the concept design 3 and results compared with two proposed static mixer concepts 1 and 2. In addition, stream line pattern for the flow for each experimental treatment were recorded and qualitatively compared with quantitative values to ensure that it agreed with theoretical expectations (COMSOL AB., 2004a).

It was expected that if the quantitative results of the simulation agree with the qualitative stream line flow patterns, we can conclude further that the computer model built for the simulation was reliable. In addition, the mesh used for the finite element analysis was tested to ensure that there was convergence and that there was no variation in mesh size that would affect the results of the experiment. Since variation in mesh size could also influence the experimental results, efforts were made to ensure that the same mesh sizes were generated for all the static mixer design types and the accompanying experimental treatments. However, future studies could construct a prototype to verify the results of this simulation experiment.

Apparatus/Material

The main materials/apparatus used for the study were personal computers at the Department of Industrial Technology Computer Laboratory with the appropriate

computer-aided-design (CAD) and computational fluid and thermodynamic (CFD) software, and the computers at the Rod Library with the appropriate statistical software.

The FEMLAB™ was the main software used to perform the required computational fluid and thermodynamic (CFD) modeling and simulation. SAS™ statistical software was used for the major descriptive and inferential statistics. However, Microsoft Excel™ was also used to support exploratory descriptive statistics (COMSOL AB., 2004c).

Originally, FEMLAB™ Chemical Engineering Module was intended to be used for the simulation experiment. This could not be purchased in time and hence the generic FEMLAB™ platform developed by COMSOL AB. and purchased by the Department of Industrial Technology with GRASP scholarship support from the College of Natural Sciences (all of the University of Northern Iowa) was used with success.

Procedures

Appropriate physical/mathematical and computer models for static mixer, argon and nitrogen carrier gases, levels of inlet gas pressures, levels of reactor operating temperature, the constant gas inlet flow rate, and the constant inlet temperatures were developed and computer simulation experiments set up for the flow of the carrier gases. Three temperature points at the cross section of the exit (at center, 50% from the center and extreme inner wall of the reactor) were obtained from the simulation.

The differences or deviations of these temperatures from the bulk temperature were calculated. The ratio of each temperature deviation to the bulk temperature was determined and three data points were obtained for each experimental run. This was

termed the mixing ratio. The percentages were then calculated, and this was termed the mixing index or effectiveness. The best results of the either mixing ratios or mixing indices are those closer to zero (Devahastin & Mujumdar, 2001; Povitsky, 2002)

To arrive at conclusions from the results that can be generalized, inferential statistics at significance level of .05 was applied to either establish significant differences or significant relationships between the variables of interest as defined by the research question or the research hypothesis (CTE, 1987; Elliot, 2000; Longnecker & Ott; SPSS Inc., 1999).

Static Mixers: Conceptual Designs, Physical and Computer Modeling

Static Mixers: Design Types and Model Definition

Choice of static mixers. Since static mixers were known to result in successful mixing in reactors, two types of designs were chosen for improving the existing reactors (Devahastin & Mujumdar, 2001; COMSOL AB., 2004e). In the existing reactor, the proposed mixing zone without mixer for the laser vaporization method of growing carbon nanotubes was considered as a static mixer since temperature and pressure treatment of flowing gases could enhance mixing (Salzman, 2004). However, the main purpose of the existing reactor was to serve as a control variable with which to compare the two proposed static mixer designs intended to improve the existing reactors.

The two static mixer design configurations intended to improve the internal design configuration of existing reactors have been presented in Figures 19 and 20. The existing reactor considered also as static mixer due to the likely effect of temperature and pressure on the mixing ratio has been presented in Figure 21 (Salzman, 2004).

The static mixer design concept 1 named the baffled type design was chosen because they are well known in the process in industry. In addition, aerodynamic type static mixer concept 2 was chosen, because, many aerodynamic bladed static mixers have been investigated and were found effective. Further, the two static mixers were chosen because of the differences in their internal design configurations. Additional reasons for selecting these two types of static mixers have been presented in the subsequent two sections.

The physical and computer models were developed to study mixing ratio and/or mixing index due to flow of two carrier gases, namely Argon and Nitrogen in the static mixers. The two gases have different chemical and physical characteristics. In this simulation model, the carbon-metal catalyst vapors were not modeled. This was done to simplify the modeling and simulation experiment. Using single fluid flow to determine effectiveness of static mixers has been successfully used by other investigators including Devahastin et al. (2004).

Hence, since a single fluid was used in this study, temperature was chosen as tracer to represent carbon-metal catalyst vapors and carrier gas mixing ratio. The mixing indices were determined by computing the percentage of the mixing ratios (that is ratios of deviations of the temperatures from the bulk temperature to the bulk temperature given by Equations 63 and 64) at the exit of the mixers (Devahastin et al., 2004).

Static mixer concept 1-baffle type mixer. The baffle type of static mixer (Figure 19) was chosen because of its simplicity. In addition, according to COMSOL AB. (2004e), baffled reactors are very common in the process industry. Further, COMSOL

AB. (2004e) indicated that the stationary baffles introduce turbulence which in turn promotes mixing within the reactor. The baffled reactor can also be easily constructed and cleaned as compared to twisted baffles that will be expensive to construct and difficult to clean.

Baffled mixers are known to be effective in reactors. Hence, in this study since the interest is only to investigate the effectiveness of inner configurations, the dimensions and positions of the baffles were fixed. However, future studies will examine variations of characteristic dimensions of the heights and distances of baffles and also the location of the inlet and outlet baffles at say 25%, 50% and 75% to establish whether there would be further significant differences with respect to growth of carbon nanotubes.

Static mixer concept 2- aerodynamic type mixer. Although some investigators had established the effectiveness of the aerodynamic type static mixers (Figure 20), they used many blades. In this study, only one aerodynamic bladed static mixer was chosen. This was done in order to exploit both aerodynamic capabilities and simplicity of cleaning such a shape. Hence, if the single aerodynamic proved effective in mixing, it will be a better choice for the reactors because it will be easy to clean. Also in this study, all the characteristic dimensions were fixed and overall dimensions were made to be similar to that of the baffle type mixer. Similarly, in future studies radii, maximum height and the length of the aerodynamic blade could be varied at 25%, 50% and 75% to investigate additional differences in their effectiveness.

Static mixer concept 3 – existing reactor without static mixer. In the existing reactor, the mixing zone without mixer was considered as a static mixer (Figure 21) since

temperature and pressure treatment of flowing gases could enhance mixing (Salzman, 2004). However, the main purpose of the existing reactor was to serve as a means for comparison with the two proposed designs.

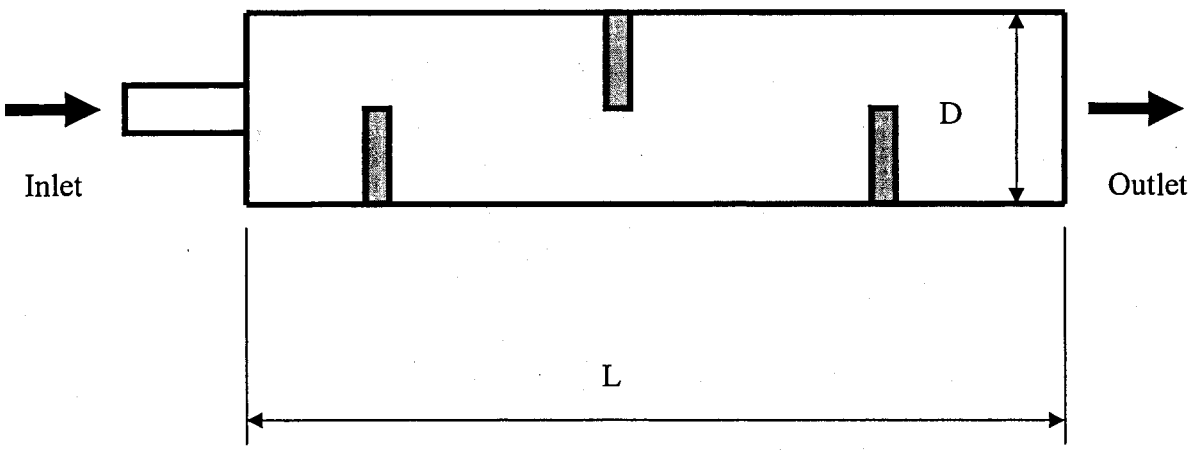

Figure 19. Schematic diagram of a reactor modeled to show integration of baffle type static mixer (static mixer concept 1). The diagram is not to scale. The three baffled type mixer is intended to improve the mixing ratio of the reactor. At the front edge of the modeled reactor is a model of size of a typical graphite target raw material of size 25 x 25 mm. The overall size of the carbon vapor zone without the graphite projecting at the front proposed to be the mixing zone was chosen to be $D = 50$ mm and $L = 50$ mm estimations adapted from Fan, Geohegan, Pennycook et al. (2000), Fan, Geohegan, Pennycook et al. (2002) and Fan, Geohegan, Guillorn et al. (2002) specifications. With the graphite target included the overall dimension of reactor was 50 x 75 mm, and height of baffles at 25 mm.

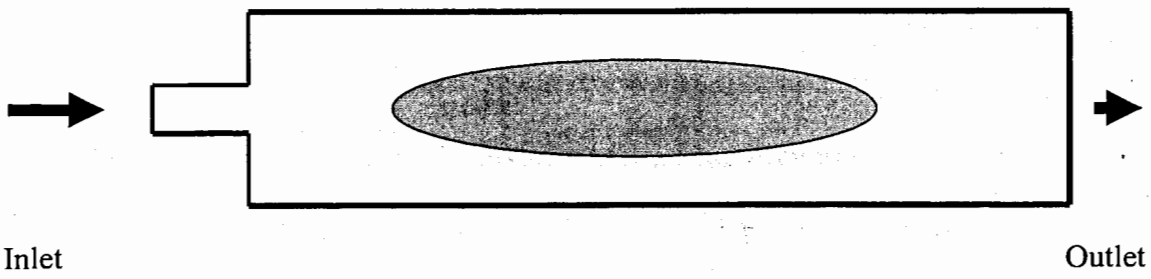

Figure 20. Schematic diagram of a reactor modeled to show integration of single bladed aerodynamic mixer (static mixer concept 2). The one bladed aerodynamic type mixer was chosen because of the merit of ease of cleaning. It has same overall dimensions as the baffle type static mixer, but with maximum blade thickness of 25 mm. Except that the inner configurations are different. Future improvement could include truncating the trailing end to facilitate wake generation (Brighton & Hughes, 1999).

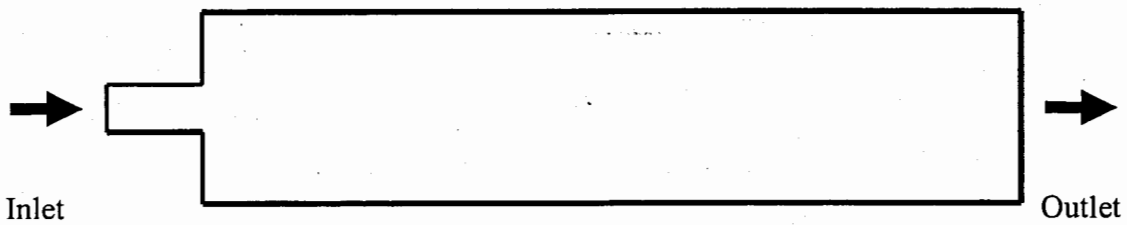

Figure 21. Schematic diagram of existing reactor modeled without static mixer (static mixer concept 3). It has same overall dimensions as the baffle and single bladed aerodynamic types of static mixers, except that it has no internal blades, however, it was considered as static mixer concept 3 because mixing can also be achieved through treatment of inlet pressure and operating temperatures (Salzman, 2004).

Model Problem Definition

The 2D geometries in Figures 19 and 20 show the design improvement being proposed to study the effects of static mixer, carrier gases, reactor operating temperature and buffer inlet pressure on the mixing ratio of carbon nanotube growth reactors. The proposed mixing zone of the existing reactor is illustrated by Figure 21.

The overall fixed diameter or height of the reactor and hence the mixer D was made 50 mm and the overall length of each static mixer was also 50 mm excluding the graphite target modeled with size 25 x 25 mm. When the graphite target was included, the modeled reactor had the overall width of 50 mm and overall length of 75 mm. The heights of the inlet and outlet baffles for the baffle type reactor were kept constant at 25 mm.

Since the Mach number ($M < 0.3$), that is flow velocity divided by the velocity of sound is less than one, the flow was assumed to incompressible. The inlet flow rate was initially controlled at constant flow rate of 0.006 m/s. However, it could not converge for some of the treatments and hence to ensure that same conditions were applied it was then reduced to 0.0045 m/s. The carrier gas inlet temperature was made constant and was set at 300 K. The two levels of pressure in Pascal and two levels of reactor temperature in Kelvin were then applied according to the experimental design.

Since small variations in temperature invoke density changes, employing modeling terminology, the non-isothermal flow application mode was adopted (COMSOL AB., 2004f). According to COMSOL AB. (2004f), this application mode is similar to the Incompressible Navier-Stokes application mode, however, the continuity,

momentum and energy equations contain the density term. The relevant physical modeling equations consistent with commercial software platform used including notations have been presented in a later section. However, future studies should consider small variations due to effects of higher temperatures on viscosity and thermal conductivity of the two different gases as expounded by Nieto de Castro et al. (1996) on the mixing ratio and consequently growth of carbon nanotubes.

Physical/Mathematical Modeling

The physical models, that is, the mathematical equations governing the flow of carrier gases through the mixers have been presented. The physical models were developed in order to capture the effects of the static mixer, and pressure and temperature variation effects on density changes of the argon and nitrogen carrier gases (COMSOL AB., 2004f). Thus assumptions were made in order to be able to obtain temperature distribution at the outlet of the mixing chamber of the reactor and the accompanying appropriate qualitative fluid flow pattern or stream lines to validate the flow. The properties of nitrogen and argon carrier gases used for the simulation are as in Table 3.

Table 3

Properties of Carrier Gases Used for the Computer Modeling and Simulation

Properties/Parameters	Units	Argon (Ar)	Nitrogen (N_2)
Dynamic viscosity, η	Kg/ms (Pa.s)(at 300K and 0.1MPa=1atm)	22.9×10^{-6}	18.0×10^{-6}
Density, ρ	Kg/m^3 (@ 274K and 101.33Pa =1atm)	1.7824	1.2506
Molar mass, M	Kg/mol	0.039962384	0.028
Gas constant, R	J/mol.K	8.31441	8.31441
Heat capacity, C_p	J/mol.K(@300K and 0.1MPa=1atm)	20.8	29.2
	J/Kg.K(@ 300K and 0.1MPa=1atm)	520.49	1042.86
Thermal conductivity	W/mK (@300K and 0.1MPa=1atm)	17.9×10^{-3}	25.8×10^{-3}

From "*Handbook of chemistry and physics*" by D. Lide, 2002

Assumptions. Using single-phase carrieg gas fluid flow, the following assumptions underlying the development of the physical equations or models were made in order to simplify the modeling and also to capture the effect of variation of temperature and pressure on the density of gases (COMSOL AB., 2004f):

1. Flow at the inlet is fully developed and hence becomes Poiseuille flow (Brighton & Hughes, 1999).
2. The changes in the heat capacity, *Cp* is small and hence it was taken to be constant (COMSOL AB., 2004f; Kittel & Kroemer, 1980).
3. Thermal conductivity is independent of pressure but varies with temperature but it was taken to be constant (Nieto de Castro et al., 1996). (This should be investigated at future studies).
4. Viscosity is independent of pressure but varies with temperature but it was also taken to be constant. (Nieto de Castro et al., 1996). (Additionally, this should be investigated at future studies).
5. The argon and nitrogen gases were considered Newtonian fluids (Brighton & Hughes, 1999; Devahastin & Mujumdar, 2001).
6. Effects of viscous dissipation were neglected (Brighton & Hughes, 1999; Devahastin & Mujumdar, 2001).
7. 2-Dimensional geometry of the static mixers could give adequate representation of the model because the static mixers are cylindrical (Devahastin & Mujumdar, 2001; Povitsky, 2002).

Following from the above assumptions, the following generalized conservation equations in the differential equation tensor form were applied to the fluid flow in the mixer and the associated boundary conditions have been stated (Brighton & Hughes, 1999; Coleman, 2005; COMSOL AB., 2004f):

From assumption (1), the fully developed Poiseuille flow that enters the inlet of the static mixer was given as (Brighton & Hughes, 1999; COMSOL AB., 2004f):

$$n \bullet V = u_{\max} 4s(1-s) \tag{49}$$

Assumptions (2) to (6) were employed to derive the Equations (50) to (52). These conservation equations have been stated below (Brighton & Hughes, 1999; COMSOL AB., 2004f):

Continuity or conservation of mass equation:

$$\frac{\partial \rho}{\partial t} + \nabla \bullet (\rho V) = 0 \tag{50}$$

Conservation of momentum equation:

$$\rho \frac{\partial V}{\partial t} - \nabla \cdot \eta(\nabla V + (\nabla V)^T) + \rho(V.\nabla)V + \nabla p = \rho g \tag{51}$$

Conservation of energy equation:

$$\nabla \bullet (\rho C_p TV - k\nabla T) = 0 \tag{52}$$

From the ideal gas law, the density, pressure, temperature, and molar mass relationships for the carrier gases have been stated as (COMSOL AB., 2004f; Kittel & Kroemer, 1980):

$$\rho = \frac{pM}{RT} \tag{53}$$

The term $n \cdot V$ in Equation 49 is the velocity normal to the surface of the control volume; the first term in Equation 50 is the rate of change of mass within the control volume and it is said to be equal to the mass flux crossing the control volume, which is the second term in Equation 50; Equation 51 obeys the Newtonian second law of motion and the first and third terms in Equation 51 constitute the total rate of change of linear momentum which is equal to the sum of acting forces which comprise of the second (viscous force associated with the nature of the fluid) and fourth (pressure force which acts normal) terms on the left of Equation 51, and the volume or body force term at the right of Equation 51.

Boundary Conditions

The following boundary conditions were derived following similar approach adopted by COMSOL AB. (2004f) and Coleman (2005):

Inlet boundary condition. With respect to Equation (52), the temperature at the inlet with which a carrier gas entered into the static mixer is denoted as $T_{o,\,in}$. This initial condition is represented mathematically as:

$$T = T_{o,in} = 300 \text{ K } (\sim 25\ ^{\circ}\text{C}) \tag{54}$$

Further, considering Equation (51), the pressure at the inlet with which each carrier gas entered into the static mixer is denoted as $p_{o,\,in}$. This is stated as:

$$p = p_{o,in} = 500 \text{ Torr } (0.0667 \text{ MPa}); \ 1000 \text{ Torr } (0.1333 \text{ MPa}) \tag{55}$$

Outlet boundary condition. Employing a similar argument made by COMSOL AB. (2004f) and Coleman (2005), at the outlet, the following conditions have been presented:

With respect to Equation (50), the tangential velocity vector is zero COMSOL AB., 2004f). Furthermore, non-slip condition was applied at all other conditions (COMSOL AB., 2004f; Brighton & Hughes, 1999). These two conditions have been respectively stated as:

$$t \bullet V = 0 \tag{56}$$

$$V = 0 \tag{57}$$

In addition, considering Equation (51) the pressure normal to the boundary at the outlet is also zero (COMSOL AB., 2004f). This was also given as:

$$p = 0 \tag{58}$$

Furthermore, considering Equation (52), for energy balances where the outlet temperature is unknown, COMSOL AB (2004f) suggested that for such boundary condition, it is useful to consider convection dominated energy balance at the outlet. In this case, COMSOL AB (2004g) and Coleman (2005) proposed that first one should assume that the heat flux due to conduction across the boundary is zero. This conductive heat transfer boundary condition was then stated as (COMSOL AB., 2004f and 2004h):

$$n \bullet q = -k\nabla T = 0 \tag{59}$$

Secondly, COMSOL AB (2004f) and COMSOL AB (2004h) further suggested that for convection when the outlet temperature is not known, the convective boundary condition is given by the heat flux equation:

$$n \bullet q = \rho C_p T V \bullet n \tag{60}$$

This means that, only the convective flux, the first term in Equation (52) will be allowed to exit the domain (COMSOL AB., 2004f; COMSOL AB., 2004g).

All other boundaries condition. Similarly, as applied by COMSOL AB. (2004f) and stated by Brighton & Hughes (1999) in connection with conservation of mass equation, a non-slip condition was applied at all other boundaries at the walls of the mixer. Therefore, regarding Equation (49), the velocity becomes zero at the boundaries and this was stated as (COMSOL AB., 2004f):

$$V = 0 \tag{61}$$

In addition, the two temperatures due to the reactor at the walls of the mixer is denoted as $T_{w,\,react}$. This is represented mathematically as:

$$T = T_{w,react} = 1473\text{K } (1200^{\circ}\text{C}); \; 3774.3\text{K } (3500\ ^{\circ}\text{C}) \tag{62}$$

Each of these two temperatures was used in combination with the treatment conditions as indicated in the sampling plan.

Mesh development. To ensure the simulation performed correctly according to the modeling, the aspect ratios of the meshes for the alternative static mixer design concepts were made the same. This was done to ensure that they do not affect performance of any of the treatment conditions. To ensure that the baffle mixer worked correctly with respect to the finite element method, the technique used to construct the 2D baffle mixer by COMSOL AB. (2004e) in their study of residence time in a 2D and a 3D turbulent reactor employing a baffle type mixer was adopted.

Calculation of Mixing Ratios (MR) and Mixing Indices (MI).

Quantitatively, the mixing in the proposed vapor mixing zone of the laser type reactor for determining the mixing ratio between the carbon-metal vapor and the nitrogen carrier gas were measured by representing the gases with the single carrier gas and using

temperature as a tracer of the mixing/concentration ratio. The ratio between the deviations of the temperature at specific locations of the cross section at the exit of the mixer to the expected bulk temperature at the exit was used as the representative of the mixing/concentration ratio. The formula for the mixing ratio and the mixing indices used are stated respectively as follows:

The mixing ratio is given as (Devahastin et al., 2004):

$$MR = \frac{\Delta_T}{T_B} \tag{63}$$

The mixing index or effectiveness is given as (Devahastin et al., 2004):

$$MI = \frac{\Delta_T}{T_B} \text{ x } 100\% \tag{64}$$

where MR is the mixing ratio, MI is the mixing index, Δ_T is the deviation of the temperature at the specific radial locations of cross section of the exit channel, and T_B is the expected mean temperature referred to as the bulk temperature at the exit of the mixer. COMSOL AB. (2004h) provided a formula for estimating the bulk temperature at the exit cross-section of the mixers. This is given by the expression (COMSOL AB., 2004h):

$$T_B = \langle T \rangle = \frac{\int Tudy}{\int udy}, \tag{65}$$

where T denotes the temperature distribution along the vertical (y) axis at the outlet of the mixers, u represents the distribution of x-direction velocity along the vertical (y) axis at the outlet of the mixers, and dy is the incremental distance at the outlet of the mixer by which the temperature and velocity varied.

Qualitatively, to verify the results and the performance of the mixers, the fluid flow patterns or streamlines were observed. At the discussion of the report, commentary was given on these flow patterns or stream lines observations to validate the quantitative mixing ratio or indices results.

Statistical Methods

Introduction

This statistical analysis was motivated by the fact that, to control growth and increase both yield or volume and productivity of synthesized carbon nanotubes, there was the need to achieve the right mixing or concentration ratio between carbon-metal catalyst vapors and carrier gas as a pre-condition. Most existing designs for producing nanotubes do not claim to have a mixing chamber for mixing carrier gases and carbon-metal catalyst vapors. Since prototyping will be expensive, simulation and statistical analysis to measure the mixing effectiveness and understand the role of the static mixers in carbon nanotubes (CNT) reactors without incurring too much cost was pursued.

This statistical method was therefore used to help establish whether there were significant differences between the proposed CNT reactor improvements and the existing reactor designs, and also to establish whether there were significant differences within each of the main variables being investigated. The statistical procedures were applied in stages, and conclusions were made for each stage and recommendations made whether to stop at that stage or continue to subsequent stage(s).

Sampling Plan.

Data for the analysis was first obtained for nitrogen carrier gas which was made to flow through each of the three types of static mixers under the proposed treatments and the controlled conditions. Three temperature data points at three exit locations were obtained and the mixing ratios and/or mixing indices computed as discussed earlier.

Following the same procedure a second set of data was collected using only argon under the same treatment and controlled conditions. The two sets of data from the nitrogen and the argon gases in combination with the treatment conditions were transferred into a full factorial experimental design. This is shown in Table 4. The raw data in Table 4 shows both the positive and negative percentage mixing ratios (indices).

Statistical Modeling Techniques

Although one could have examined interaction effects between the factors, this was deferred to future studies, and only main effects were investigated. Conclusions were drawn from the four way-analysis of variance (4-way ANOVA) to find whether the observed differences were significant at $\alpha = .05$ significant level. Further, to find whether each of the main factors is significant in predicting the mixing ratio the results from the (4-way ANOVA) were found sufficient to test those hypotheses. In order to find whether the specific differences between the levels of each of the main factors were significant, the Tukey's HSD post-hoc procedure was adopted.

To assess the strength of relationship between the main factors and whether they could be used to explain differences in the mixing ratios or indices, the coefficient of determination (r^2) was evaluated. The criterion lies in the interval $0 < r^2 < 1$. The

coefficient of determination (r^2) measured the fraction of variability in the dependent variable that is explained by the four independent variables. It was applied, because, there were more than one covariate. Additionally, it is often used to measure effect size. In general if the overall p-value is less than .05 significant level, either significant differences or strength of relationship was confirmed. That is the null hypothesis was rejected. Alternatively, when the obtained overall p-value was found greater than .05 significant level, the null hypothesis was supported or confirmed. The statistical programs used to generate the statistical outputs written in SAS have been given in Appendices D to F.

Statistical Model Checking Diagnostics.

The following assumptions for the 4-Way Analysis of Variance (4-Way ANOVA) were checked to have been met:

1. Independence of samples: The error term or residuals should be independent, once the samples are independent.
2. Normality: The residuals should be normally distributed. With these plots, using the normal probability plots, large residuals and consequently outliers can be identified.
3. Constance of variance: check patterns in the plot of predicted versus residual. With these plots, outliers can be identified.
4. Zero expectation: The expectation of the residuals for all observations should be zero. Here, unusual observations could be identified. This was to be verified by checking for large and influential residuals. If outliers were

identified, the Cook's distance would have been used to check the influential data.

The sequence plot of residuals, normal probability plot of the residuals, and scatter plot of predicted values against the residuals were the techniques used to check assumptions numbers 1, 2, and 3 respectively. The diagnostic test for checking multiple regression models was generated to check assumption 4. However, this was not evaluated because the first three assumptions were met.

Initially, when the assumptions were checked with the absolute original percentage mixing ratios or mixing indices data, the assumptions were not met. Consequently, the data were transformed using logarithm of 10. This was again checked and the assumptions for the 4-way ANOVA were met. Hence, the answers to the two research questions and the five research hypotheses were based on the statistical procedures applied to the transformed raw percentage mixing ratios or mixing indices data.

Table 4.

Raw Data for Mixing Indices (Mixing Ratios) due to Static Mixer Design Types, Carrier Gases, Carrier Gas Inlet Flow Pressure, and Reactor Operating Temperature

Observation No.	Mixer design concepts (Baffle type=1; Aerodynamic type=2, Existing Reactor =3)	Type of carrier gas(Nitrogen=1; Argon=2)	Inlet carrier gas pressure	Reactor Operating Temperature	Deviation of Temperature /Bulk Temperature at Exit of Mixers
			P_{in}/ Torr	T_{react} / °C	MI=MR x100% = $\Delta t/T_B$ x100%
1	1	1	500	1200	0.001
2	1	1	500	1200	0.003
3	1	1	500	1200	-0.022
4	1	1	500	3500	0.001
5	1	1	500	3500	0.002
6	1	1	500	3500	-0.014
7	1	1	1000	1200	0.002
8	1	1	1000	1200	0.010
9	1	1	1000	1200	-0.062
10	1	1	1000	3500	0.0008
11	1	1	1000	3500	0.003
12	1	1	1000	3500	-0.02
13	1	2	500	1200	0.04
14	1	2	500	1200	0.70
15	1	2	500	1200	0.02
16	1	2	500	3500	0.0006
17	1	2	500	3500	-0.007
18	1	2	500	3500	-0.01
19	1	2	1000	1200	0.002
20	1	2	1000	1200	0.01
21	1	2	1000	1200	-0.07
22	1	2	1000	3500	0.0008
23	1	2	1000	3500	-0.01
24	1	2	1000	3500	-0.02
25	2	1	500	1200	1.6
26	2	1	500	1200	-0.6
27	2	1	500	1200	-3.5
28	2	1	500	3500	0.63
29	2	1	500	3500	-0.20
30	2	1	500	3500	-1.35
31	2	1	1000	1200	3.5
32	2	1	1000	1200	-1.2
33	2	1	1000	1200	-7.3
34	2	1	1000	3500	1.3
35	2	1	1000	3500	-0.4
36	2	1	1000	3500	-7.3
37	2	2	500	1200	1.7

(table continues)

Observation No.	Mixer design concepts (Baffle type=1; Aerodynamic type=2, Existing Reactor =3)	Type of carrier gas(Nitrogen=1; Argon=2)	Inlet carrier gas pressure	Reactor Operating Temperature	Deviation of Temperature /Bulk Temperature at Exit of Mixers
			P_{in}/ Torr	T_{react} / °C	MI=MR x100% = $\Delta t/T_B$ x100%
38	2	2	500	1200	-0.6
39	2	2	500	1200	-3.6
40	2	2	500	3500	0.6
41	2	2	500	3500	-0.2
42	2	2	500	3500	-1.4
43	2	2	1000	1200	3.6
44	2	2	1000	1200	-1.2
45	2	2	1000	1200	-7.6
46	2	2	1000	3500	3.6
47	2	2	1000	3500	-0.4
48	2	2	1000	3500	-2.8
49	3	1	500	1200	0.20
50	3	1	500	1200	-0.03
51	3	1	500	1200	-0.61
52	3	1	500	3500	-0.13
53	3	1	500	3500	-0.02
54	3	1	500	3500	-0.44
55	3	1	1000	1200	0.42
56	3	1	1000	1200	-0.07
57	3	1	1000	1200	-1.30
58	3	1	1000	3500	0.198
59	3	1	1000	3500	-0.033
60	3	1	1000	3500	-0.618
61	3	2	500	1200	0.199
62	3	2	500	1200	-0.034
63	3	2	500	1200	-0.621
64	3	2	500	3500	0.14
65	3	2	500	3500	-0.02
66	3	2	500	3500	-0.4
67	3	2	1000	1200	0.3
68	3	2	1000	1200	-0.05
69	3	2	1000	1200	-0.9
70	3	2	1000	3500	0.20
71	3	2	1000	3500	-0.03
72	3	2	1000	3500	-0.6

Note: Number of replications=3x2x2x2x3 = 72

CHAPTER 4

RESULTS, ANALYSIS OF DATA AND DISCUSSIONS

In this chapter, validation of the simulation results based on single phase-carrier gas flow, the results subsection summarizes data collected based on the single phase carrier gas flow and the statistical treatments, and the analysis of data component is used to qualify results and draw inferences for subsequent action(s) that can be generalized to multi-phase fluid flows. On the other hand, in the discussion section, the obtained results are evaluated and their implications in support of the original research questions and hypotheses or otherwise are stated. Further, in the discussion section, the similarities and differences between the results of this research and the work of other investigators presented in the literature review chapter that validated the results and confirmed the conclusions of this study are also presented.

Validation of Simulation Results.

Based on single-phase carrier gas flows, the streamlines shown in Appendices J to L exhibiting Figures J1 to L4 demonstrate the validation of the computer simulation experiment. As illustrated by Figures J1 to J4, the vortices formed in the baffle type mixer supported the reason why the baffle type in-line mixer showed effective mixing indices. Further, the smaller vortices shown in the existing reactor without a mixer (Figures K1 to k4) illustrate why it performed better than the aerodynamic type mixer.

More importantly, the aerodynamic type mixer (Figures L1 to L4) only showed streamlines without any separation or wake or vortices formation. This gave sufficient evidence demonstrating that vortex formation was responsible for the mixing

effectiveness of improved reactor and also explains why the aerodynamic mixer could not perform well comparatively because of the absence of vortex formation. This confirms that both the commercial application software platform used and the model built truly operated correctly and that the quantitative mixing ratio or index results of the static mixers in the carbon nanotubes reactor have been validated.

The above validation procedure using stream lines is consistent with similar simulation validations completed by Devahastin et al. (2004) and Devahastin and Mujundar (2001) who used temperature as a tracer to determine the mixing effectiveness, and COMSOL AB. (2004b) who alternatively used concentration as a measure of the concentration or mixing ratio of the static mixer.

Additionally, comparison of the temperature profiles in Appendices G to I further validate the simulation results. This is because as illustrated by the plots (Appendices G to I), the temperature profiles are different for each of the static mixers. The simulation was therefore able to capture the effects of the different configurations of the various passive mixers modeled as exhibited by the temperature distributions at their exits. This is significant because, the purpose of this study, that is, improving the design of the carbon nanotube growth reactors with static mixers is to modify their internal configurations in terms of form and shape to enhance mixing between carbon and metal catalyst vapors and carrier gases.

Results and Analysis of Data

Description of Raw Data

The goal of the research was to build a computer simulation model to investigate the effects of four main factors on the mixing ratio of carbon nanotubes growth reactors. This was determined by calculating the mixing indices of the static mixers taking into account all the treatment conditions. The main factors investigated were three types of static mixers, two types of carrier gases, two levels of carrier gas inlet pressures and two levels of reactor temperatures under the same carrier gas inlet flow velocity (0.0045 m/s) and inlet temperature (300 K).

The types of static mixers investigated were the baffled type static mixer, a single bladed aerodynamic type static mixer, and the existing reactor without a static mixer. Also, the types of carrier gases investigated were nitrogen and argon. Further, the levels of inlet carrier gas pressures used were 500 Torr (66,650.0 Pa) and 1000 Torr (133,300.0 Pa). Similarly two levels of reactor temperatures used in the mixing zone of the reactor were 1200 °C (1473.4 K) and 3500 °C (3773.4 K).

Tables 5 and 6 show the calculated raw data for the mixing indices (mixing ratios x 100%) obtained for the study based on simulation of types of carrier gases and types of static mixers for the two levels of carrier gas inlet pressures and the two levels of reactor temperatures at the mixing zone of the laser vaporization reactor. The controlled conditions which were kept constant from which the results were generated are the carrier gas inlet linear velocity at 0.0045 m/s and the carrier gas inlet temperature at 300 K.

Table 5 demonstrates the calculated mixing indices raw data based on simulated nitrogen carrier gas flowing through the three types of static mixers being evaluated under the same levels of carrier gas inlet pressure and reactor temperature expected at the mixing zone. In columns 1 and 2 are shown respectively the two levels of carrier gas inlet pressures and the two levels of the reactor temperatures in the proposed mixing zone of the carbon-metal catalyst vapors and carrier gases. In addition, column 3 shows the bulk temperature at the exit estimated using an integral formula built into the commercial application simulation software platform used.

Furthermore, columns 4, 7, and 10 show respectively the estimated three temperatures at the center, fifty percent from the center and the extreme inner wall of the exit of the mixer/reactor. These three temperatures were extracted from the application software. The temperature profiles at the exit of static mixers for various treatments generated by the application software are available in Appendices G to I as Figures G1 to I4.

Then columns 5, 8, and 11 portray the differences between the bulk temperature and the extracted temperatures at the exit of the reactor mixing zone/static mixers. The differences were obtained by subtracting the extrapolated temperatures from the bulk temperature. In addition, columns 6, 9, and 12 show the calculated mixing indices obtained as percentage mixing ratios due to nitrogen carrier gas in the presence of the other three factors, namely, types of static mixers, carrier gas inlet pressures and reactor temperatures being investigated.

Similarly, Table 6 shows the calculated mixing indices obtained as percentage mixing ratios of the raw data based on simulated argon carrier gas flowing through the three types of static mixers being evaluated under the same levels of carrier gas inlet pressures and reactor operating temperature conditions. The descriptions of the items in the columns of Table 6 are the same as those in Table 5. However, the extrapolated temperatures at the exit of the reactor are obtained from argon gas carrier gas (refer to Appendices G to I).

Descriptive Statistics

The mean absolute percentage mixing ratios (a measure of the mixing indices of static mixers due to carrier gas inlet pressures and reactor temperatures) according to the nitrogen and argon carrier gases are shown in Table 7. The results in Table 7 demonstrate considering only nitrogen carrier gas under the same nitrogen inlet pressure of 500 Torr. and at 1200 °C (1473.4 K) and 3500 °C (3773.4 K) reactor temperatures, the baffle type mixer (1) has the lowest mixing index followed by the existing reactor without mixer (3) and the highest being the aerodynamic type mixer (2). This is an indication that using nitrogen gas, the baffle mixer performs better followed by the existing reactor and thus the aerodynamic provided the worst performance.

Also, for nitrogen, under the same conditions but at higher pressure of 1000 Torr and higher reactor temperature the results for the static mixers showed a similar pattern as at lower pressure. Furthermore, considering only nitrogen and comparing performance of baffle mixer at the same temperature, the results show that at lower pressures all the static mixers perform better than at higher pressure.

Table 5.

Raw Data for Mixing Indices (Percentage Mixing Ratio) for Nitrogen Carrier Gas and Types of Static Mixers

Gas inlet pressure	Reactor temperature	Bulk temperature	Temperature at exit (Ti) in kelvin (K) at the carbon-metal catalyst vapors and carrier gas zone of the laser type reactor								
			1st reading at the center of reactor			2nd reading at 50% from center of reactor			3rd reading at wall from the center of the reactor		
$P_{n,\,in}$ (Torr)	$T_{reac,}$ (K)	$T_{B,}$ (K)	T_1	$dt_1 = T_B - T_1$	$MI_1 = (dt_1/T_B)*100$	T_2	$dt_2 = T_B - T_2$	$MI_2 = (dt_2/T_B)*100$	T_3	$dt_3 = T_B - T_3$	$MR_3 = (dt_3/T_B)*100$
1	2	3	4	5	6	7	8	9	10	11	12
					Static mixer 1-baffled type design						
500	1473.15	1473.1	1473.06	0.01	0.001	1473.02	0.1	0.003	1473.4	-0.3	-0.02
500	3773.15	3772.9	3772.87	0.02	0.001	3772.81	0.1	0.002	3773.4	-0.5	-0.01
1000	1473.15	1472.5	1472.46	0.03	0.002	1472.33	0.1	0.010	1473.4	-0.9	-0.06
1000	3773.15	3772.6	3772.56	0.03	0.001	3772.47	0.1	0.003	3773.4	-0.8	-0.02
					Static mixer 2-aerodynamic type design						
500	1473.15	1420.0	1397.3	22.70	1.6	1428.5	-8.5	-0.6	1470.3	-50.3	-3.5
500	3773.15	3720.2	3696.83	23.35	0.6	3727.74	-7.6	-0.2	3770.2	-50.0	-1.3
1000	1473.15	1366.9	1319.18	47.69	3.5	1382.79	-15.9	-1.2	1467.2	-100.3	-7.3
1000	3773.15	3667.7	3620.95	46.79	1.3	3683.13	-15.4	-0.4	3767.1	-99.4	-2.7
					Static mixer 3- existing reactor without static mixer						
500	1473.15	1463.7	1460.9	2.9	0.2	1464.2	-0.5	-0.03	1472.6	-8.9	-0.6
500	3773.15	3755.6	3760.3	-4.8	-0.1	3756.4	-0.9	-0.02	3772.0	-16.4	-0.4
1000	1473.15	1452.9	1446.7	6.1	0.4	1453.9	-1.1	-0.07	1471.8	-18.9	-1.3
1000	3773.15	3748.3	3740.9	7.4	0.2	3749.5	-1.2	-0.03	3771.4	-23.2	-0.6

Note: Constant gas inlet flow rate with linear velocity u = 0.45cm/s or 0.0045m/s) and inlet temperature Tin=25 °C (298K = 300K)

Table 6.

Raw Data for Mixing Index (Percentage Mixing Ratio) for Argon Carrier Gas and Types of Static Mixers

Gas Inlet Pressure	Reactor Temper-ature	Bulk Tempera -ture	Temperature at Exit (Ti) in Kelvin (K) at the carbon-metal catalyst vapors and carrier gas zone of the laser type reactor								
			1st Reading at the Center of Reactor			2nd Reading at 50% from center of Reactor			3rd Reading at wall from the Center of the Reactor		
$P_{n,\,in}$ (Torr)	$T_{reac,}$ (K)	T_B/K	T_1	$dt_1 = T_B - T_1$	$MI_1 = (dt_1/T_B)^* 100$	T_2	$dt_2 = T_B - T_2$	$MI_2 = (dt_2/T_B) *100$	T_3	$dt_3 = T_B - T_3$	$MR_3 = (dt_3/T_B) *100$
1	2	3	4	5	6	7	8	9	10	11	12
					Static mixer 1-baffle type design						
500	1473.15	1473.7	1473.0	0.66	0.04	1473.0	0.70	0.05	1473.4	0.31	0.02
500	3773.15	3772.9	3772.9	0.02	0.0006	3773.2	-0.27	-0.007	3773.4	-0.52	-0.01
1000	1473.15	1472.43	1472.4	0.03	0.002	1472.3	0.16	0.01	1473.4	-0.97	-0.07
1000	3773.15	3772.6	3772.5	0.03	0.0008	3773	-0.44	-0.01	3773.4	-0.83	-0.02
					Static mixer 2-aerodynamic type design						
500	1473.15	1419.3	1395.2	24.09	1.7	1427.2 6	-7.98	-0.6	1470.2	-50.94	-3.6
500	3773.15	3718.8	3694.8	23.98	0.6	3726.5	-7.77	-0.2	3770.1	-51.36	-1.4
1000	1473.15	1363.8	1314.7	49.07	3.6	1380.2	-16.40	-1.2	1467	-103.21	-7.6
1000	3773.15	3664.9	3616.8	48.08	1.3	3680.7	-15.82	-0.4	3767	-102.12	-2.8
					Static mixer 3- existing reactor without static mixer						
500	1473.15	1463.5	1460.6	2.9	0.20	1464.0	-0.5	-0.03	1472.6	-9.1	-0.62
500	3773.15	3755.4	3750.1	5.29	0.14	3756.3	-0.9	-0.02	3772.0	-16.6	-0.44
1000	1473.15	1459.5	1455.4	4.1	0.28	1460.2	-0.7	-0.05	1472.3	-12.8	-0.88
1000	3773.15	3747.8	3740.3	7.6	0.20	3749.1	-1.3	-0.03	3771.4	-23.6	-0.63

Note: Constant gas inlet flow rate with linear velocity u = 0.45cm/s or 0.0045m/s) and inlet temperature Tin=25 °C (298K = 300K)

Similarly, the results in Table 7 show that considering only argon carrier under the same argon inlet pressure and at 1200 °C (1473.4 K) and 3500 °C (3773.4 K) reactor temperatures the baffle type mixer (concept 1) shows the lowest mixing index followed by the existing reactor without mixer (concept 3) and highest being the aerodynamic type mixer (concept 2). Further, considering only baffle mixer (1) for nitrogen and argon gases, under the same levels of reactor temperature, the baffle mixer performs better at lower inlet pressure than at higher pressure for both nitrogen and for argon. This is also an indication that the baffle mixer performed better at lower pressure than at higher pressure.

The mean of absolute mixing indices according to the four main factors is shown in Table 8. The results showed that comparing types of carrier gases, for any given mixer, the nitrogen carrier gas performed better than the argon carrier gas, but the effectiveness was the same when using the existing reactor. As noted in Table 8, under the same conditions the baffle type static mixer (mixer1) performed better at the higher pressure than at lower pressure. The bar chart in Figure 22 further summarizes data in Table 8.

On the other hand, under the same conditions the aerodynamic type mixer (mixer 2) and the existing reactor (mixer 3) performs better at the lower carrier gas inlet pressure than at the higher pressure. Furthermore, under the same conditions all the static mixers perform better at the higher reactor operating temperature than at lower temperature.

Table 9 shows the overall means and standard deviation by type of static mixer designs. The results showed that the overall mean for mixer (concept 1), the baffle type

static mixer is the lowest followed by existing reactor without mixer (concept 3) and the highest mean being aerodynamic mixer (concept 2). The results of overall means indicated that the baffle type mixer performed better overall than the existing reactor which in turn performed better than the aerodynamic type mixer. Pictorially, Figure 23 further summarizes the data in Table 9 with a bar chart.

Table 7

Mean Absolute Mixing Indices of Static Mixers Due to Nitrogen and Argon Carrier Gases

Level of gas inlet Pressure	Mean mixing index (percentage mixing ratio)		
	Baffle mixer 1	Aerodynamic mixer 2	Existing reactor mixer 3
	Nitrogen carrier gas		
	Reactor Temperature at T_{reac}=1200 °C (1473.4K)		
500	0.009	1.9	0.3
1000	0.02	4.0	0.60
	Reactor Temperature at T_{reac}=3500 °C (3773.4K)		
500	0.005	0.7	0.2
1000	0.01	1.5	0.3
	Argon carrier gas		
	Reactor Temperature at T_{reac}=1200 °C (1473.4K)		
500	0.3	1.9	0.3
1000	0.03	4.1	0.6
	Reactor Temperature at T_{reac}=3500 °C (3773.4K)		
500	0.007	0.7	0.20
1000	0.01	2.3	0.3

Note: Sample size n = 3. The mean calculation is based on absolute values of the raw data.

Table 8

Mean of the Absolute Mixing Indices According to the Four Main Factors

Type of mixer	Overall mean for mixing indices		Sample size, n
	Type of carrier gas		
	Nitrogen	Argon	
Mixer 1	0.01	0.07	12
Mixer 2	2.0	2.3	12
Mixer 3	0.3	0.3	12
	Inlet gas pressure		
	500 Torr	1000Torr	
Mixer 1	0.07	0.02	12
Mixer 2	0.8	3.0	12
Mixer 3	0.2	0.4	12
	Reactor temperature		
	1200 °C	3500°C	
Mixer 1	0.08	0.008	12
Mixer 2	3.0	1.3	12
Mixer 3	0.4	0.2	12

Note: The mean calculation is based on absolute values of the mixing indices (percentage of the mixing ratios raw data). Mixer 1= baffle type static mixer; mixer 2=aerodynamic type static mixer; and mixer 3=existing reactor without static mixer.

Table 9

Overall Absolute Mixing Indices (Percentage Mixing Ratio) Mean for Type of Static Mixer

Mixer type	Overall mean	Standard deviation
Baffle (mixer 1)	0.04	0.1
Aerodynamic (mixer 2)	2.31	2.3
Existing reactor (mixer 3)	0.3	0.3

Inferential Statistics

Diagnostic tests of 4-Way ANOVA with absolute mixing indices data and transformation of the sample data. Initially normal probability plot for the 4-way ANOVA model based on absolute mixing indices were obtained. The plot does not show a straight line (Figure 24). It was therefore concluded that the sample data does not meet the normality assumption and hence the absolute mixing indices data is not normally distributed. This leads to a further conclusion that absolute percentage mixing ratio data need to be transformed to enable a more rigorous statistical analysis that will either support or not support the original research questions and hypotheses.

In addition, the plot of the residual of the absolute percentage mixing ratios (mixing indices) data against the expected means of the absolute percentage mixing ratios (mixing indices) was obtained. The plot revealed a pattern in the distribution of the variance (Figure 25). The plot demonstrated that at lower means the variances are narrowly spread. The spread then increases in the middle and widely spread at higher mean values. Hence, due to the prominence of the pattern of the variances, one concluded that constant variance assumption is not met. This confirms the conclusion drawn from checking the normality assumption that the absolute percentage mixing ratio (mixing indices) sample data need to be transformed for effective statistical analysis. As a consequence, the subsequent statistical analysis will be based on transformed data using logarithm of 10 (log 10).

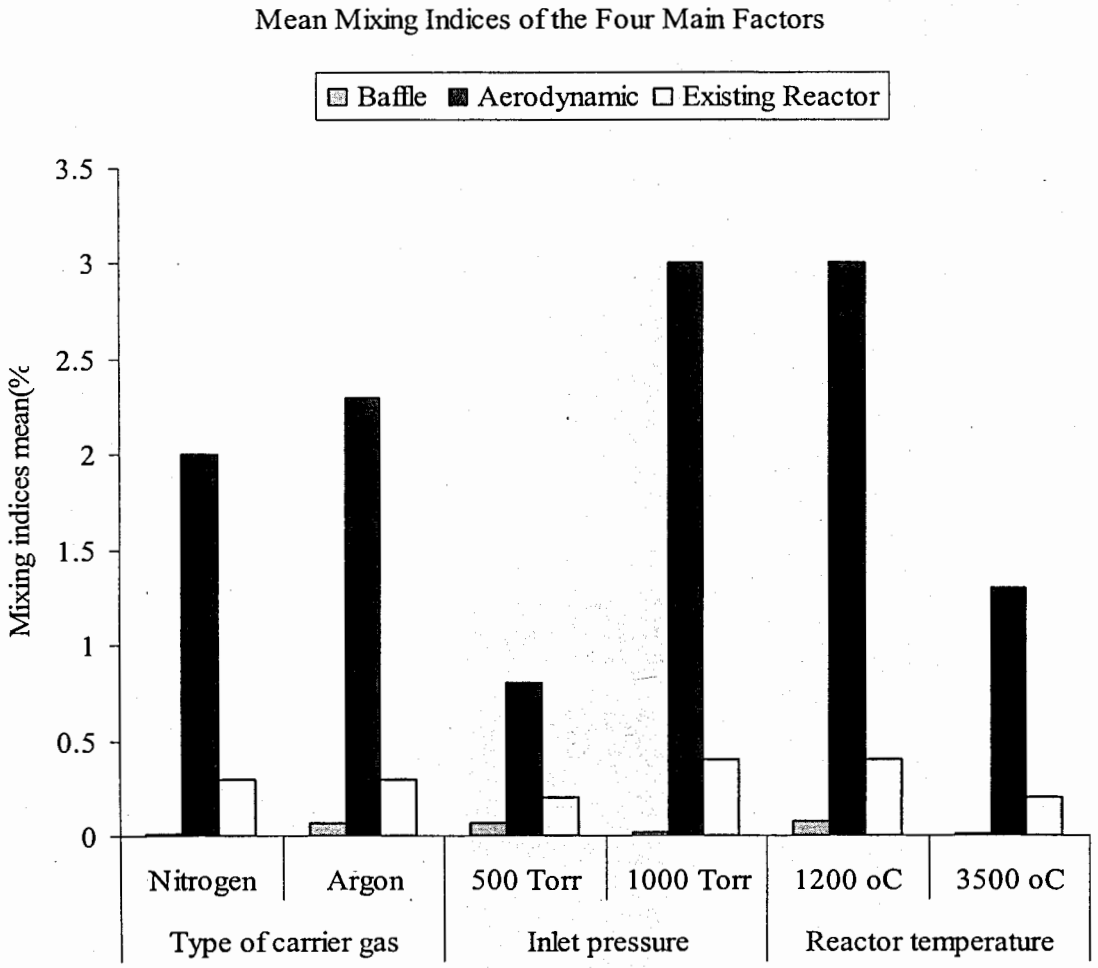

Figure 22. Bar chart comparing mean of the mixing indices of the four main factors. The figure demonstrates how the mean of the percentage mixing ratio of all the four factors developed by comparing static mixers according to the other three factors namely type of carrier gas, carrier gas inlet pressure and reactor operating temperature. The figure shows consistency of performance for static mixers according to each of the other three factors. The consistency of performance breaks down for the baffle type mixer which performs better at higher pressure and higher temperature and the others performed otherwise.

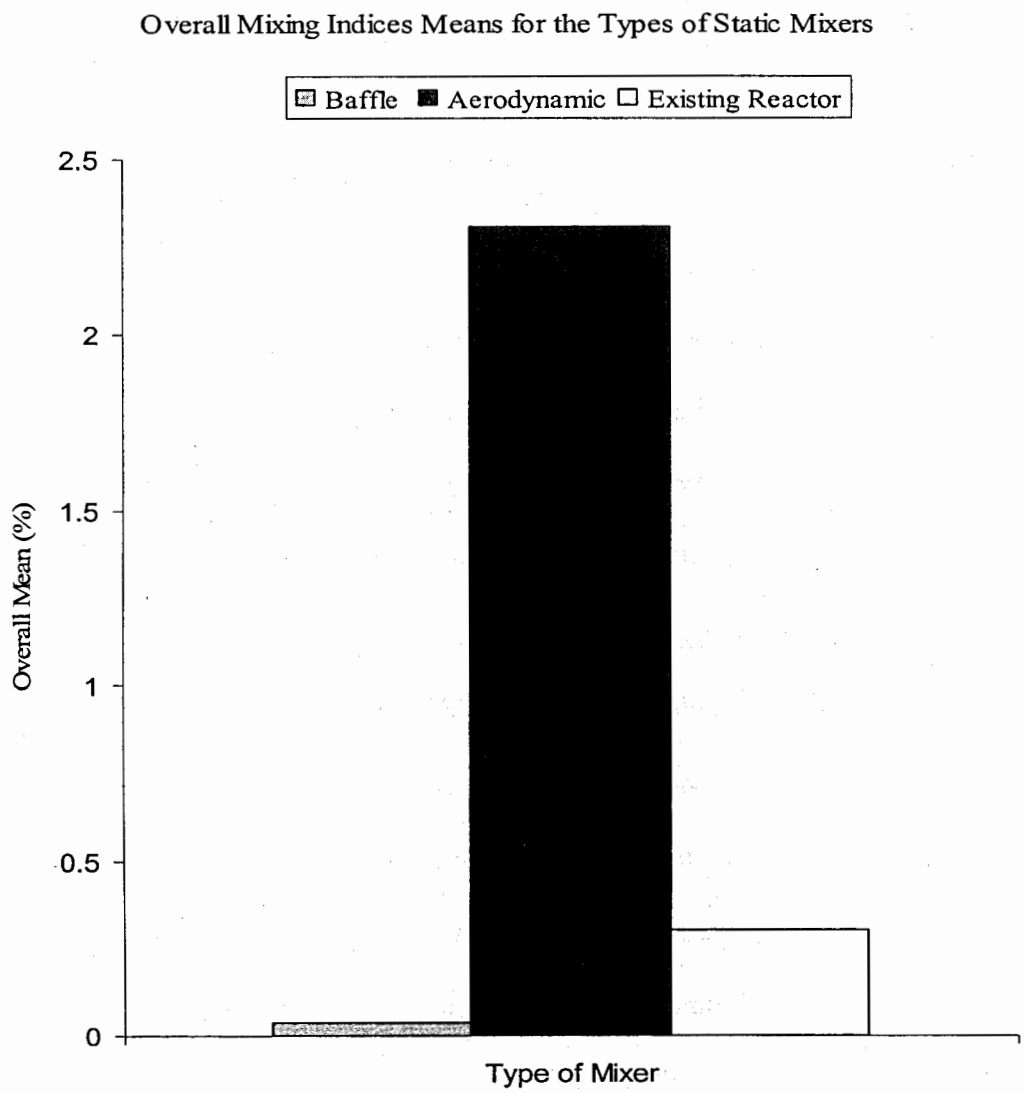

Figure 23. Bar chart comparing mean of the mixing indices of the static mixers. This figure illustrates the overall absolute percentage mixing ratio means according to types of static mixers. When the percentage mixing ratio is low the better the performance of the static mixer. In addition, the figure reveals that, the baffle type mixer performed better than the existing reactor which also performed better than the aerodynamic mixer.

The sample data was transformed to a new variable by applying log 10 because the variances associated with the original percentage mixing ratio variable across treatments are not equal. As suggested by Longnecker (2001), the square, inverse, natural logarithm was tried to obtain a good transformation. By further trial and error, applying log 10 was found to be more appropriate because it was able to stabilize the variances as shown in Figures 26 and 27. Additionally, this outcome was confirmed by the fact that according to Longnecker (2001) when the plot as shown in Figure 25 indicates a relation that is the variability increases as the predicted dependent variable, then one should try using log of the dependent variable as the transformation.

Test for the significant effects of the four main factors on the logarithm 10 mixing index data. Table 10 shows the ANOVA on four-variable model for the combined four main factors (including interaction effects) based on transformed absolute mixing ratio (mixing indices) data with log 10. As already mentioned the four factors are type of static mixers, type of carrier gas, level of carrier gas inlet pressure and level of reactor mixing zone operating temperature. From Table 10, row 2 columns 5 and 6 show the F-tests (F = 7.51) and the p-value (p = .0001). This means that at .05 significance ($\alpha = .05$), there are significant differences between the four factors. One can therefore confirm that there are significant differences in the effects of the four main factors on the mixing indices and consequently the mixing ratios. Table 11 on the other hand illustrates the ANOVA for the main effects where the interactions are pooled into error.

Table 10.

ANOVA on Four-Variable Model

Dependent Variable: log 10 of percentage mixing ratio (mixing index)

Source	DF	Sum of Squares	Mean Square	F Value	Pr > F
Model	23	69.83232792	3.03618817	7.51	<0.0001
Error	48	19.39829288	0.40413110		
Corrected Total	71	89.23062080.			

R-Square	Coeff Var	Root MSE	Mixing ratio Mean
0.782605	-66.94288	0.635713	-0.949635

Note. The statistical analysis is based only on log10 of the absolute percentage mixing ratios. The coefficient of determination is given as R^2= 0.782605. The values for the model, error and the corrected total were based on combined main and interaction effects.

Test of the significant effect of each the four main factors on the mixing index means. It is shown in Table 11 that at .05 significance (α = *.05),* the mixer term is significant at (p-value = .0001). This confirms that the mixer term has significant effect on the mixing ratio. Similarly at .05 significance (α = *.05),* the reactor temperature term shows significant effect on the mixing ratio (p-value = .005).

On the other hand, at .05 significance, gas term is not significant (p-value = .66). Similarly, at .05 significance, pressure term is not significant (p-value = .22). These values mean that type of gas and inlet pressure effects are not confirmed.

Table 11.

ANOVA on Main Effects Model.

Dependent Variable: log 10 of the percentage mixing ratio (mixing index)

Source	DF	Type I SS	Mean Square	F Value	Pr > F	η^2
Mixer	2	61.21955487	30.60977743	75.74	.0001	.72
Gas	1	0.07733677	0.07733677	0.19	.6637	.00
Pressure	1	0.61723188	0.61723188	1.53	.2225	.00
Temperature	1	3.54470692	3.54470692	8.77	.0047	.04
Error	48	19.39829288	0.40413110			
Total	53	84.85712332				

Note. The statistical analysis is based only on log10 of the absolute percentage mixing ratios. The values for the error term were transferred from the overall ANOVA model in table 10. This error term included pooling the interactions into error. Table 11 is part of Table 10. However, table 11 is separated from Table 10 in order clearly isolate the specific main effects which are the focus of this research.

Additionally, the eta-squared (η^2) which is a measure of the magnitude of effect reflecting the importance of the differences between means for the type of mixer term is .72. This is followed by the reactor temperature term with a value of .04. Alternatively, the eta-squared (η^2) values for the type of carrier gas and carrier gas inlet pressure are all .00.

One can therefore conclude from these statistical tests that, the type of mixer and reactor temperature factors have significant effects on the mixing ratio. Further, one can confirm that, the type of carrier gas and inlet pressures have no significant effects on the mixing ratio.

Furthermore, the eta-squared (η^2) values again confirm that the type of static mixer is the only important factor that has greatest effects on the mixing ratios or mixing effectiveness or mixing index of carbon nanotube growth reactors. However, since reactor temperature has significant effects, the importance of the type static mixer has to be combined with the significant effects of the reactor temperature.

Test of the strength of relationships between the four main factors on the mixing index data. Table 10 further illustrates that the coefficient of determination is $R^2 = .78$. Since the coefficient of determination is high and it is approaching one, one can conclude that there is strong relationships between the four main factors, namely, type of static mixers, type of carrier gas, level of carrier gas inlet pressure and level of reactor mixing zone operating temperature.

The value of the coefficient of determination further indicates that the proportion of variability of the mixing ratios (mixing indices) can be attributed to the four main factors. Furthermore, the coefficient of determination of $R^2 = .78$ could be used as a measure of the effect size. Thus, one can again conclude that the combined factors are statistically important and could be used to predict the mixing ratio or mixing index. However, to develop a predictive model based on the size of the coefficient of determination the only statistically significant factors to be considered are the type of static mixers ($p = .0001$) and level of reactor operating temperature ($p = .005$)

Test of significant differences in the mixing index means between the types of static mixers. H_o: There are no significant differences between the mixing ratio means due to type of static mixers. H_a: There are significant differences between the mixing

ratio means due to type of static mixers. The Tukey's HSD procedure was applied to establish significant differences between the mixing index means due to types of static mixers. The result of the Tukey's HSD procedure is shown in Table 12. The results in Table 12 indicate that, at significant level of $\alpha = .05$, there are statistically significant differences in mixing ratio (mixing indices) means between the types of static mixers. The null hypothesis was therefore rejected.

Comparing the logarithmic mixing index means of the three types static mixers indicate that, the baffle type static mixer (concept 1) has the lowest mean followed by the existing reactor without static mixer (concept 3) and highest being the aerodynamic type static mixer (concept 2). Re-stating the means in absolute percentage mixing ratio (mixing index) means terms shows that the said differences in the means of the static mixers are baffle type static mixer (concept 1) = 0.04%; the existing reactor without static mixer (concept 3) = 0.3% and aerodynamic type static mixer (concept 3) = 2.3%.

Test of significant differences in the mixing index means between the levels of reactor temperature. H_o: There are no significant differences between the mixing ratio means due to level of reactor temperature. H_a: There are significant differences between the mixing ratio means due to the level of reactor temperature. The Tukey's HSD procedure was again applied to establish differences between the mixing ratio means due to level of reactor temperature. The result of the Tukey's HSD procedure is shown in Table 13. The results in Table 13 indicate that, at significant level of $\alpha = .05$, there were significant differences in mixing ratio means between the level of reactor temperatures. Thus the null hypothesis was also rejected.

Table 12.

Comparison of the Mixing Index Means of the Type of Static Mixers

Tukey's Studentized Range (HSD) Test for mixing ratio

Alpha	0.05
Error Degrees of Freedom	48
Error Mean Square	0.404131
Critical Value of Studentized Range	3.42026
Minimum Significant Difference	0.4438

Tukey Grouping	Mean	N	mixer
A	0.1140	24	2
B	-0.8280	24	3
C	-2.1349	24	1

Note: This test controls the Type I experimentwise error rate, but it generally has a higher Type II error rate. Means with the same letter are not significantly different. The mean values are stated in log10.

Similarly, comparing the logarithmic mixing ratio (mixing index) means of the two levels of reactor temperatures indicated that, higher level reactor temperature (3500 °C) shows lower mixing ratio mean compared to the lower level reactor temperature (1200 °C). Similarly, re-stating the means in absolute mixing indices values show that the differences in the means of the levels of reactor temperatures are the reactor temperature at 3500 °C is 0.6% and the lower level reactor temperature at 1200 °C is 1.1%.

Diagnostic tests of the 4-Way ANOVA with log 10 mixing index data. In Figure 26 the normal probability plot is shown as generated from SAS outputs for the ANOVA models shown in Tables 10 and 11. Figure 27 noted the plot of the residual against the normalized score. The plot appeared as an approximate straight line. One can therefore conclude that the transformed sample mixing indices data meets the normality assumption and hence the logarithmic percentage mixing ratio or mixing index data is normally distributed. Also, Figure 27 illustrated the plot of the residual of the logarithmic percentage mixing ratio data against the expected logarithmic percentage mixing ratio means, yhat. The figure shows a scattered distribution of the variances. The plot therefore shows that the variances are spread about the mean.

Table 13

Comparison of the Mixing Index Means of the Levels of Reactor Temperature

Tukey's Studentized Range (HSD) Test for mixing ratio

Alpha	0.05
Error Degrees of Freedom	48
Error Mean Square	0.404131
Critical Value of Studentized Range	2.84352
Minimum Significant Difference	0.3013

Tukey Grouping	Mean	N	temperature
A	-0.7278	36	1200
B	-1.1715	36	3500

(table continues)

NOTE: This test controls the Type I experimentwise error rate, but it generally has a higher Type II error rate. Means with the same letter are not significantly different. The mean values are stated in log10.

Due to the prominence of the constancy of the spread of the residuals, one concludes that constant variance assumption is met. This confirms the conclusion drawn from checking the normality assumption. As a consequence, the homogeneity assumption has been met. Thus the 4-way ANOVA models in Tables 10 and 11 are reliable to be used as basis for the statistical inferences.

Discussions

The results of this study are varied. The results support the first research question and part of the second research question. However, some of the results support the null hypotheses and others support the alternative hypotheses. The answers to these research questions and hypotheses are presented in the subsequent sections. Alternative explanations from literature in support of the findings or otherwise are also presented for each of the hypotheses.

Research Questions

Research question one. In general static mixers showed improvement in the mixing ratio. Specifically, a static mixer in a carbon and metal catalyst vapor zone of a laser vaporization reactor for synthesizing carbon nanotubes showed significant effects on the mixing ratio of the single phase carrier gases. Consequently a static mixer can improve the mixing ratio between carbon-metal catalyst vapors and carrier gases.

Specifically, considering conclusion drawn from hypothesis three, the baffle type static mixer shows significant improvement on the mixing ratio as compared to the existing reactor without a static mixer. The effectiveness of the baffle mixer is supported by existing literature. This further indicated that improving the inner configuration of reactors will improve the mixing ratio. Additionally, improving the inner configurations further means improving the shape, form, and characteristic dimensions of the inner configuration of the carbon nanotube growth reactors can improve achieving uniform atomic distances between carrier gases, carbon and metal catalyst vapors.

In the case of laser and solar methods this can then be expected to lead to consistent plume formation, steady cooling, homogeneous nucleation, identical growth, and standard diameter and length of carbon nanotubes. Consequently, the purity of carbon nanotubes can be improved and can lead to higher yield and translated into improved productivity of laser vapor method and other methods of growing carbon nanotubes.

Although the baffle static mixer appears simple to fabricate, its cleaning to ensure efficient operation will be a challenge that needs to be addressed. Due to the possible cleaning problem, there is still the need to explore the aerodynamic type static mixer by increasing the number blades or obstacles instead of the one blade used for this study. This is because the aerodynamic type design appears easy to clean.

Research question two. As shown in Table 10, at .05 significant level with overall probability of $p = .0001$, statistically, the combined four main factors, namely type of static mixer, type of carrier gas, level of carrier gas inlet pressure, and level of reactor

temperature have significant effects on the mixing ratio for the single phase flowing carrier gases at controlled carrier gas inlet flow rate and reactor operating temperature.

However, from Table 11, at .05 significant level, considering the individual factors, statistically it is only the type of static mixer ($p = .0001$) and the levels of reactor temperatures ($p = .005$) that have significant effects on the mixing ratio; the type of carrier gas ($p = .66$) and levels of carrier gas inlet pressure ($p = .22$) have no significant effect on the mixing ratio.

This further strongly supports emphasis on simplicity and effectiveness of static mixers used in industrial processes. Integrating a static mixer into an existing reactor together with the appropriate reactor temperature will improve the mixing ratio and consequently the purity, yield and productivity of carbon nanotubes. Equally integrating a static mixer into an existing reactor together with the appropriate reactor temperature (1200 and 3500 °C) will improve the mixing index particularly for laser, arc and flame methods of synthesizing carbon nanotubes.

As a result of this, the furnace annealing temperature of 1200 °C used in laser, solar and CVD as indicated by Fabian 2001 and Flamant et al. (2001) actually play a significant role in the growth of carbon nanotubes. Additionally, a reactor temperature of 3500 °C required for melting and vaporizing the carbon raw material when using the laser, arc and solar methods of synthesizing carbon nanotubes has a significant effect on the mixing index and hence contributed to recognizing the laser method as the one with the highest yield and the solar method as one of the methods with higher productivity as discussed by Flamant et al. (2001).

Statement of Hypotheses

Hypothesis one. At .05 significant level with coefficient of determination of $R^2 =$ .78, statistically there are strong relationships between the independent variables, namely type of static mixer, type of carrier gas, carrier gas inlet pressures, and reactor operating temperatures on the mixing ratio at constant carrier gas inlet flow rate (0.0045 m/s) and inlet temperature (~25 °C ≈300 K). As result of this, statistically, the combination of these factors can be used to explain variations in the mixing ratio. However, to predict the mixing index using these factors, type of static mixer and reactor temperature should be the only two factors be used in any predicting model, since they have significant effects on the mixing ratio/index (research question two),

Hypothesis two. At .05 significant level, statistically there are no significant differences in the mixing ratio means between types of carrier gases (argon and nitrogen). This further means that under the same type of static mixer, carrier gas inlet pressures (500 or 1000 Torr), and reactor temperatures (1200 or 3500 °C) at constant carrier gas inlet flow rate (0.0045 m/s) and inlet temperature (300 K), using either argon or nitrogen carrier gas do not make significant difference in the mixing ratios.

Consequently, under the same experimental conditions, type of carrier gas will have same effect on the mixing ratio and consequently the same effect on the purity, yield and productivity during carbon nanotubes formation. This result agreed with the Achiba et al. (2003) suggestion that with an electric furnace at 1200 °C both N_2 and Ar carrier gases provided highest yield of SWNT, and that the optimum yield of SWNT does not depend of the kind of carrier gas.

Hypothesis three. There are significant differences at .05 significant level between types of static mixer on the mixing ratio for a given type of carrier gas (Argon and Nitrogen), carrier gas inlet pressures, and reactor operating temperatures at constant carrier gas inlet flow rate and inlet temperature. The significant differences in the mixing indices (percentage mixing ratios) means of the static mixers at the .05 significant level are baffle type static mixer (concept 1), MI = 0.04%; the existing reactor without static mixer (concept 3), MI = 0.3% and aerodynamic type static mixer (concept 2), MI = 2.3%. Specifically, the baffle type static mixer with the lowest overall percentage mixing index mean indicates it is the most effective static mixer compared to the existing reactor and the aerodynamic type mixer.

In other words, the existing reactor without a static mixer (MI = 0.3%) is less effective than baffle type mixer (MI = 0.04%); but more effective than the aerodynamic type mixer (MI = 2.3%). Although the aerodynamic mixer (MI = 2.3%). showed less effectiveness than the existing reactor without a static mixer (MI = 0.3%), as mentioned earlier, presumably it can be improved by increasing the number of blades, instead of using only one blade.

The best effective mixing performance by the baffle type static mixer is supported by some fluid theories proposed by Brighton and Hughes (1999), and pressure and temperature effects on mixing of fluids have also been elucidated by Salzman (2004). According to Salzman (2004) under the same temperature and pressure entropy mixing can be enhanced through expansion and contraction. This expansion and contraction is achieved by the design arrangement of the baffle type static mixer. In addition, as

indicated by Brighton and Hughes (1999) in the baffle type mixer, the baffles appear "blunt," and hence separation occur generating wakes and vortices (Figures J1 to J4).

Further, Brighton and Hughes (1999) explained that because the rear of an aerofoil is gently streamlined, separation is prevented and a tear drop shape is formed. This can be seen in the streamline for the aerodynamic type mixer (Figures K1 to K4) and it further explains the reasons for its low mixing effectiveness. The conditions laid down by Brighton and Hughes (1999) for wakes and vortices formation that suggest that if the rear for the aerodynamic body was to be blunt could facilitate boundary layer thickening or separation for appreciable wake and vortex formation and consequently effective mixing was not met. This in addition to the appropriate Reynolds number could explain the low mixing effectiveness of the aerodynamic type mixer. The foregoing explanations are supported by Appendices J to L containing Figures J1 to L4, where wakes are formed in the baffle type and the existing reactor but not in the aerodynamic type reactors.

Hypothesis four. At .05 significant level, there were significant differences between levels of reactor temperatures (1200 and 3500 °C) on the mixing ratio using the same type of static mixer, type of carrier gas (Argon and Nitrogen), and levels of carrier gas inlet pressures at constant carrier gas inlet flow rate and inlet temperature. At higher reactor temperature of 3500 °C, the lower percentage mixing ratio indicated better mixing ratio at higher temperature than at lower reactor temperature at 1200 °C.

This means that the temperature for vaporizing carbon does have a significant effect on the mixing ratio for the laser vaporization method of growing carbon nanotubes. Consequently, at higher temperatures the yield of carbon nanotubes can be improved.

This may explain the reason why as reported by most investigators, the laser method of synthesizing carbon nanotubes has the highest yield as compared to all other methods of growing carbon nanotubes.

The better mixing effectiveness at higher reactor operating temperature (3500 °C) supported the fact the higher temperatures have a significant effect on the density and hence variations in temperature cause significant variations on the density changes of the carrier gases. Hence with fixed molecular mass and the density variations have significant effect on the mixing ratio. Consequently, since the temperature has effects on the density, one can infer that the transport properties such as thermal conductivity and viscosity that have similar relationships with temperature can vary themselves at high temperatures and hence can also affect the mixing ratio.

This position is supported by the Kittel and Kroemer (1980) explanation that as temperature increases molecules more frequently collide and therefore transfer a greater amount of their momentum. This therefore increases the viscosity of the carrier gases which is attributed to transfer of momentum between moving and stationary molecules. Consequently, with an increase in temperature a carrier gas molecule encounters more friction with its neighboring molecules and hence further increases the viscosity. As a result higher temperature has a significant effect on the mixing ratio. Salzman (2004) suggested that when the temperature is increased the average speeds of molecules increase and that the molecules become more disordered in momentum. This also explains why the higher temperature showed better mixing performance than at lower temperature.

Hypothesis five. There are no significant differences between levels of carrier gas inlet pressures (500 and 1000 Torr) on the mixing ratio under same type of static mixer, type of carrier gas (Argon and Nitrogen), and levels of reactor temperatures at constant carrier gas inlet flow rate and inlet temperature. This means carrier gas pressure ranges (500 vs 1000 Torr) have the same effect on the mixing ratio.

Additionally this result partially supported Achiba et al.'s (2003) claim that at constant carrier gas flow rate with no variation in the temperature gradient inside the furnace that influenced the SWNT diameter distribution, the carrier gases Ar, Kr, and Ne except N_2 did not show any significant change in the diameter distribution of SWNT at all pressures. Furthermore, this result is supported by Kittel and Kroemer's (1980) explanation that the thermal conductivity of gases is independent of pressure. This confirms that levels of pressures (500 and 1000 Torr) employed for this study did not affect the thermal conductivity and hence pressure is not a significant factor in the predicting mixing ratios of carrier gases and carbon-metal catalyst vapors.

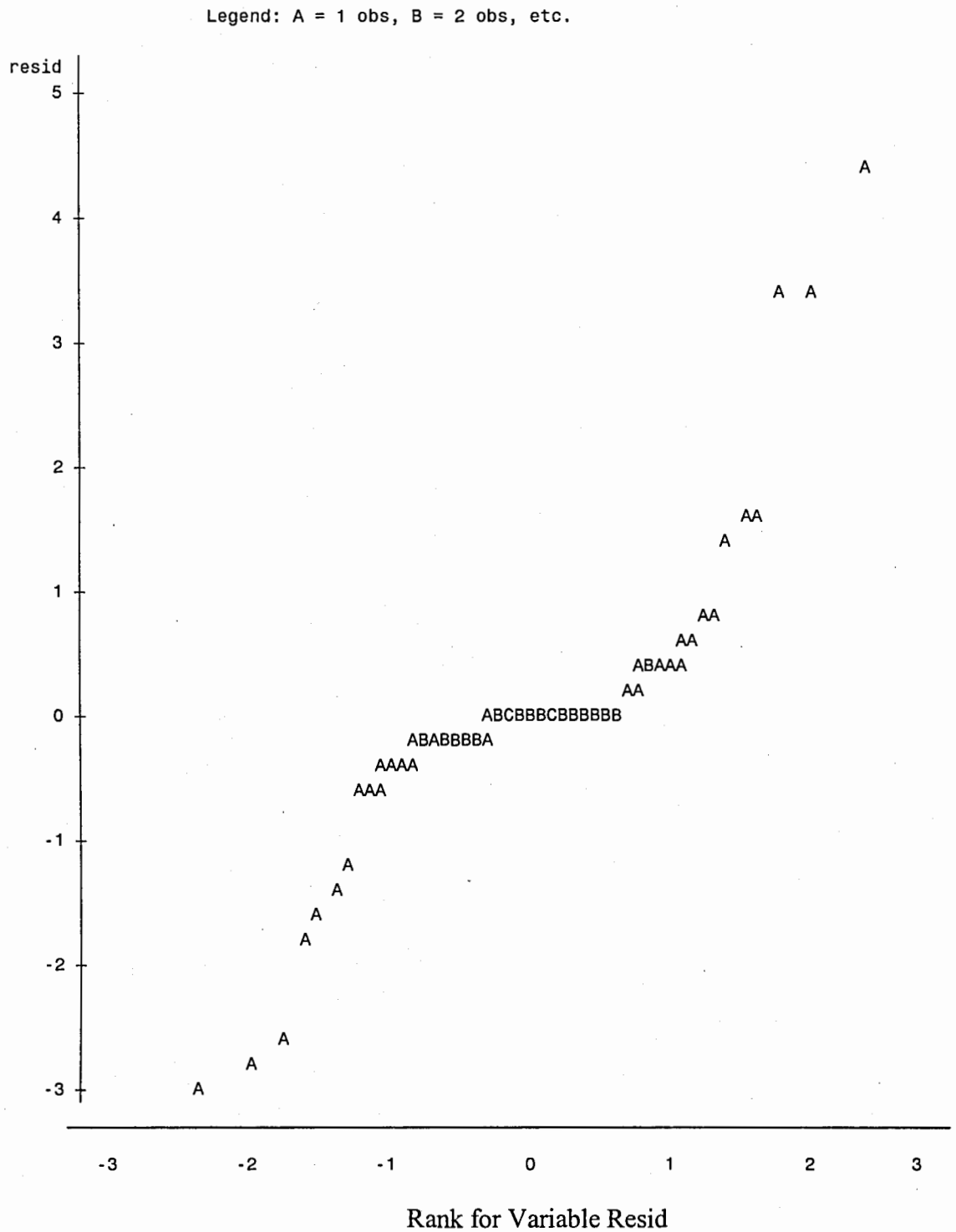

Figure 24. The plot of the residual against the normalized score (Plot of resid * nscore) for absolute percentage mixing ratio data (mixing indices).

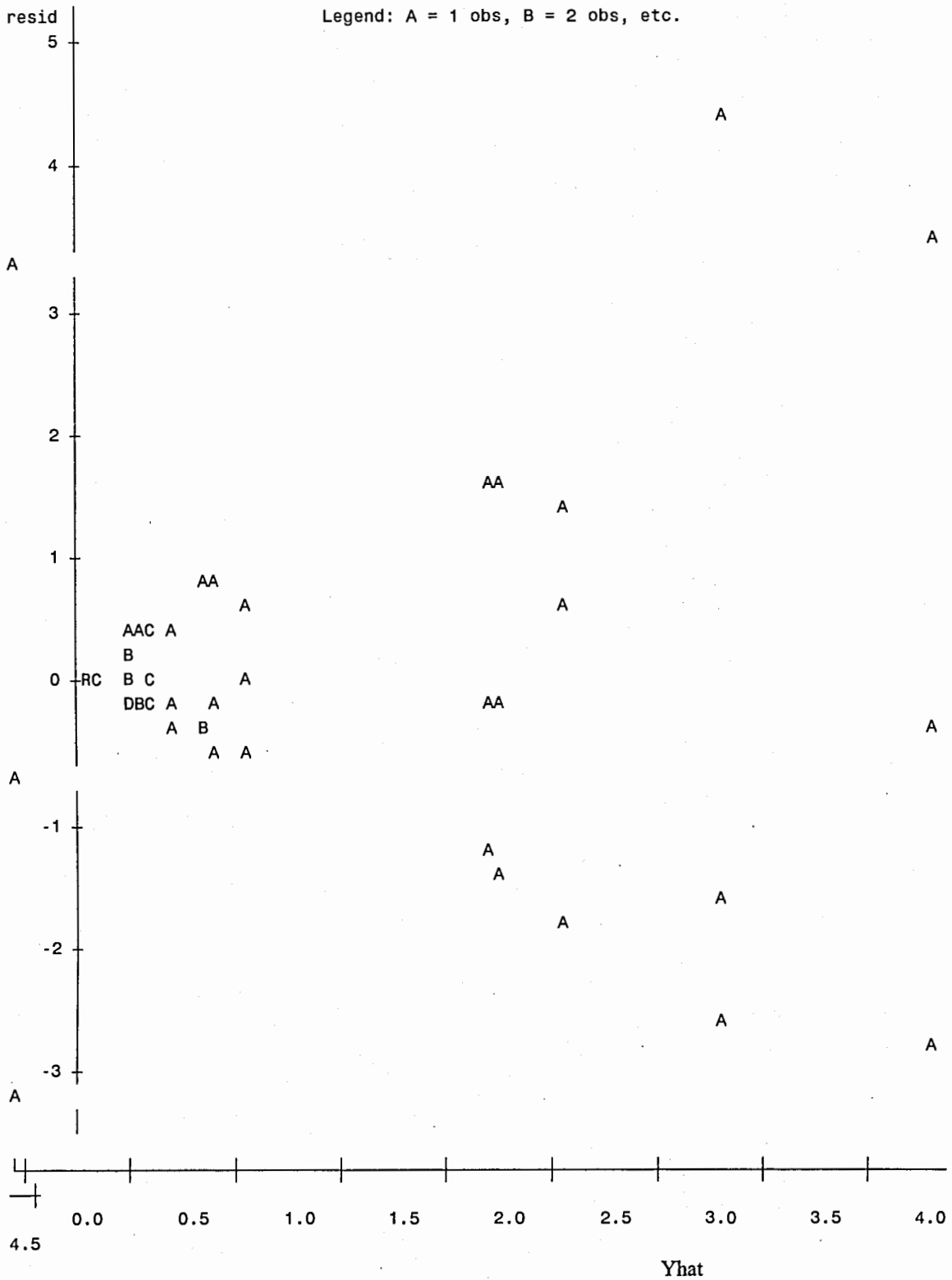

Figure 25. The plot of the residual against the expected absolute means yhat.

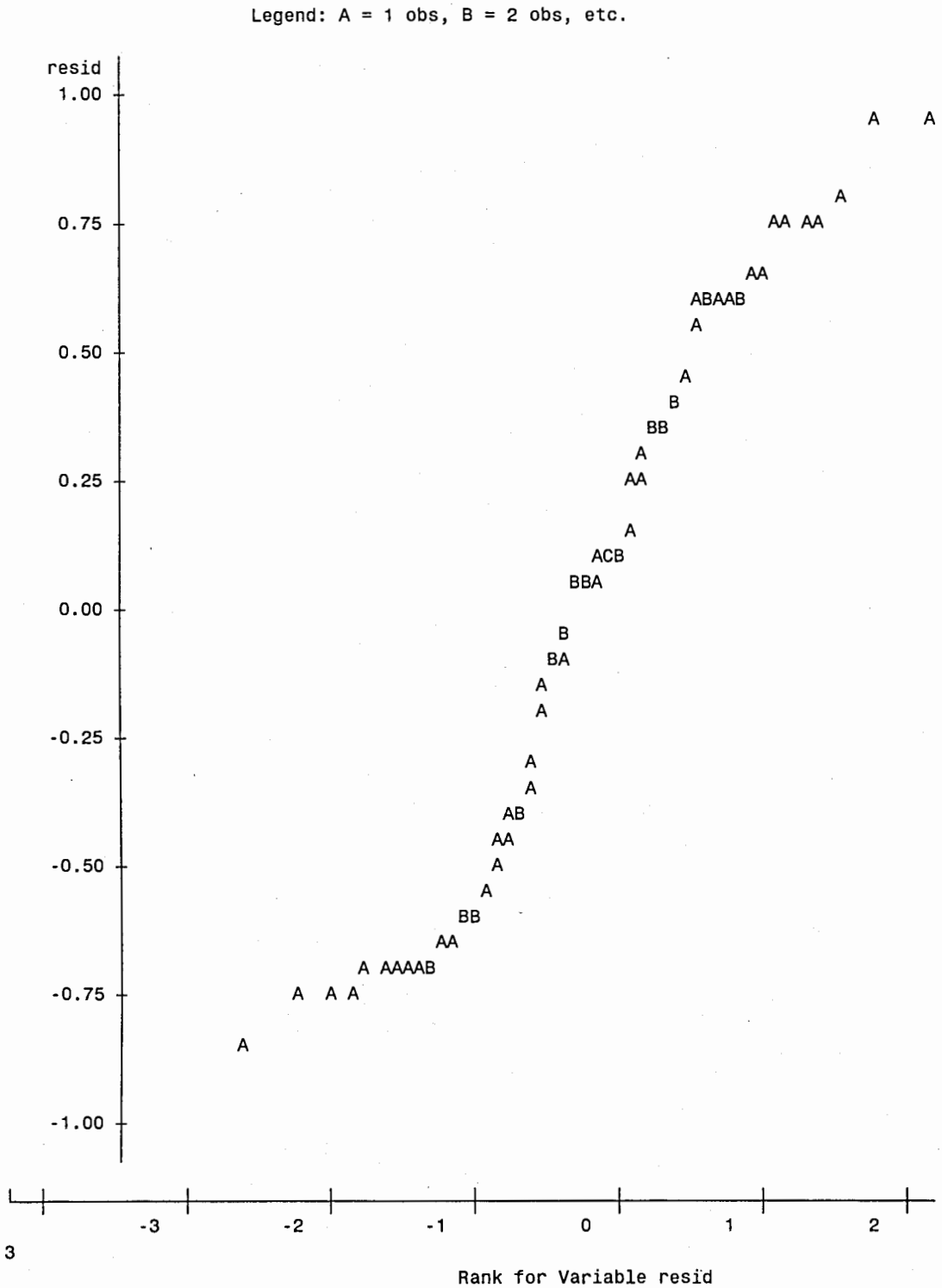

Figure 26. The plot of the logarithmic residual against the normalized score (Plot of resid*nscore).

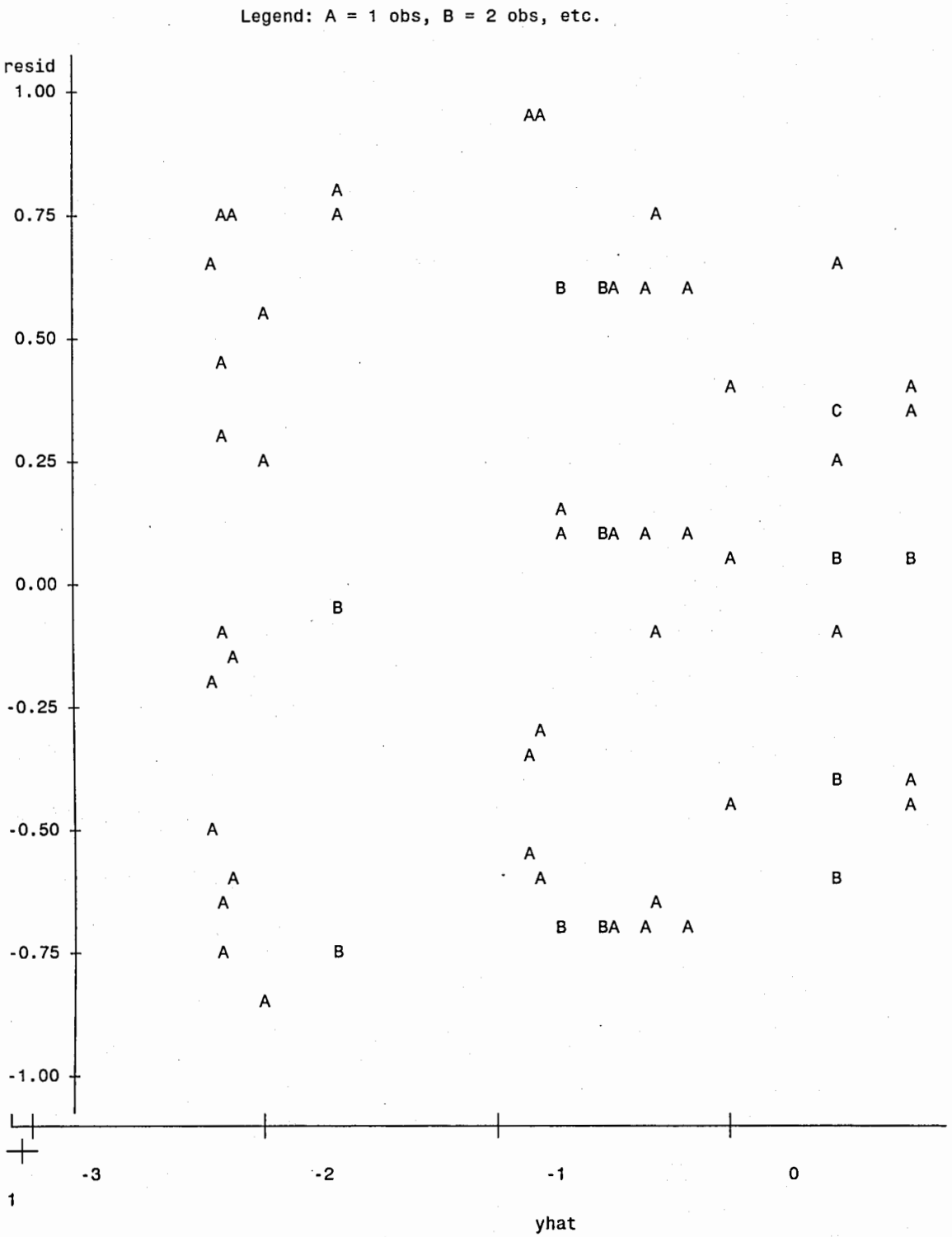

Figure 27. The plot of the logarithmic residual against the expected logarithmic mixing ratio means yhat (Plot of resid*yhat)

CHAPTER 5

SUMMARY, CONCLUSIONS AND RECOMMENDATIONS

Summary

Statement of the Problem

The problem of this study was to investigate the effects of type of static mixer, type of carrier gas (argon and nitrogen gases), carrier gas inlet pressures, and reactor operating temperatures on the mixing ratio of carbon nanotube synthesizing reactors.

Statement of Purpose

The purpose of this study was to improve the design and performance of reactors used for growing carbon nanotubes in order to improve carbon-metal catalyst vapors and carrier gas mixing/concentration ratio to create preliminary conditions for controlled growth (through obtaining uniform distribution of atoms/molecules, and hence forming uniform plume, thereby achieving uniform cooling and uniform nucleation) to increase percentage purity and achieve uniform size and consequently to maximize yield and increase productivity of formed carbon nanotubes.

Statement of Need or Justification

There are five main factors that comprise the need for this study. The first factor is that understanding the role of static mixers together with operating conditions associated with mixing of different carrier gases will help us understand and hopefully help improve carbon-metal catalyst vapors and carrier gas concentration/mixing ratios and consequently improve growth control, yield and productivity of most of the methods employed in carbon nanotubes production (Akos, Bogaerts, Chen & Gijbels, 2003;

Devahastin & Mujumdar, 2001; Devahastin et al., 2004; Fang & Lee, 2001; Flamant et al; Gong et al., 2004).

Secondly, Gaines and Regli (1997) have reported on the introduction of a repository at the National Institute of Standards and Technology (NIST) with the goal of providing a publicly accessible collection of 2-D and 3-D CAD, solid models, assemblies and process planning from industry problems. In addition, the third reason for this study is that, Bowden, Ghosh and Harrell (20003) reported that Fishwick (1997) had proposed that technologies such as the internet or world wide web provide a mechanism for maintaining distributed model repositories on the future of simulation. According to Bowden et al. (2000), when these models are available, they can be shared by many modelers.

The fourth reason for this simulation modeling of static mixers for mixing carrier gases to contribute to understanding the growth of carbon nanotubes is that it illustrates use of simulation as a theoretical data gathering technique. Finally, the fifth reason is that the study is consistent with the NSF frame work for such studies.

From the foregoing, the additional benefits of employing simulation modeling of static mixers with the other known factors to improve design of nanotubes synthesizing reactors and hence growth of carbon nanotubes can be derived from the quote "We no longer have the luxury of time to tune and debug new manufacturing systems on the floor, since the expected economic life of a new system, before revision will be required, has become frighteningly short" (Bowden et al., 2000, p. 275).

Research Questions and Statement of Hypotheses

Research Questions

The following research questions were explored in this study:

Research question one. Will a static mixer in a carbon and metal catalyst vapor zone of a laser vaporization reactor for synthesizing carbon nanotubes improve the mixing or concentration ratio between carbon-metal catalyst vapors and carrier gases?

Research question two. Will the main factors, namely type of static mixer, type of carrier gas, carrier gas inlet pressure, and reactor operating temperature have significant effect on the mixing ratio between carbon-metal catalyst vapors and carrier gas at controlled carrier gas inlet flow rate and inlet temperature?

Statement of Hypotheses

The following hypotheses were tested in this study, with the results indicated in brackets:

Hypothesis one. The null hypothesis 1, H_{01}, was that, there are no strong relationships between independent variables (type of static mixer, type of carrier gas- argon and nitrogen, carrier gas inlet pressures, and reactor operating temperatures) and the dependent variable (mixing ratio) at constant carrier gas inlet flow rate and inlet temperature [rejected: there are strong relationships between independent variables (type of static mixer, type of carrier gas- argon and nitrogen, carrier gas inlet pressures, and reactor operating temperatures) and the dependent variable (mixing ratio) at constant carrier gas inlet flow rate and inlet temperature].

Hypothesis two. The null hypothesis 2, H_{02} was that there are no significant differences between type of carrier gas (Argon and Nitrogen) on the dependent variable (mixing ratio) due to the effects of type of static mixer, carrier gas inlet pressures, and reactor operating temperatures at constant carrier gas inlet flow rate and inlet temperature [retained].

Hypothesis three. The null hypothesis 3, H_{03} was that there are no significant differences between types of static mixer on the dependent variable (mixing ratio) due to the effects of type of carrier gas (Argon and Nitrogen), carrier gas inlet pressures, and reactor operating temperatures at constant carrier gas inlet flow rate and inlet temperature [rejected: these variables in combination did affect mixing ratio].

Hypothesis four. The null hypothesis 4, H_{04} was that there are no significant differences between levels of reactor operating temperature on the dependent variable (mixing ratio) due to the effects of type of static mixer, type of carrier gas (Argon and Nitrogen), and carrier gas inlet pressures, at constant carrier gas inlet flow rate and inlet temperature [rejected: there are significant differences between levels of reactor operating temperatures on the dependent variable (mixing ratio) due to the effects of type of static mixer, type of carrier gas (Argon and Nitrogen), and carrier gas inlet pressures at constant carrier gas inlet flow rate and inlet temperature].

Hypothesis five. The null hypothesis 5, H_{05} was that there are no significant differences between levels of carrier gas inlet pressures on the dependent variable (mixing ratio) due to the effects of type of static mixer, type of carrier gas (Argon and

Nitrogen), and reactor operating temperatures at constant carrier gas inlet flow rate and inlet temperature [retained].

Methodology

The modeling and simulation experiment was limited to three types of static mixer designs. Two proposed static mixer designs, namely the baffle type and single bladed aerodynamic type static mixer design were intended to improve the existing reactor. The third static mixer design was the existing reactor since temperature and pressure manipulation could also lead to improvement in the mixing ratio. Two types of carrier gases were chosen for the study: argon and nitrogen.

Temperature profiles at the exit of the modeled mixing zone of laser type reactors were generated. Three data points were extracted at the center, 50% of from the center and the extreme part of the inner wall of the exit of the reactor with the inserted static mixers. The bulk temperatures were also computer generated and the deviations which are the difference between these bulk temperatures and the three temperatures were obtained. These deviations were then divided by the bulk temperatures to obtain the mixing ratios. These mixing ratios were then multiplied by 100% to obtain the mixing indices. In addition, the stream line for each treatment was also obtained to validate the quantitative mixing indices.

With the sample data obtained based on the sampling plan and treatments, the four-way analysis of variance (4-way ANOVA) was completed using the absolute mixing indices. A diagnostic check on the results showed that the statistical assumptions were not met. As a result, the sample data was transformed using logarithm of 10. Another 4-

way ANOVA was completed using the logarithm of 10. A diagnostic check on this new 4-way ANOVA showed that the statistical assumptions were met. The inferential statistics and conclusions in confirming or disconfirming the original research questions and research hypotheses were then based on this new 4-way ANOVA using the logarithm of 10.

Results, Analysis of Data and Discussions

The simulation results were obtained for a single gas because the simulation of the hydrodynamics of mixtures of gases is very difficult to do and could not be accomplished with the available software platforms in a reasonable time. Following similar procedure used by Devahastin et al. (2004), single-phase results were used as the basis for predicting the mixing ratio for a three-phase system. However, it has been recommended that simulations incorporating three-phase gas mixtures involving carbon, metal-catalyst and carrier gas sources must eventually be performed in order to accurately predict the mixing ratio in a real nanotube production system. The simulation results were validated with the differences in stream line patterns in the static mixers, a similar procedure employed by Devahastin et al. (2004), Devahastin and Mujumdar (2001), and COMSOL AB. (2004b).

Nonetheless, integrating a static mixer in the existing reactor did show improvement in the mixing ratio (mixing index). Specifically, the baffle type of static mixer in the carbon and metal catalyst vapor zone of a laser vaporization reactor for synthesizing carbon nanotubes improved the mixing index significantly as compared to the existing reactor. On the other hand the aerodynamic type static mixer could not

significantly improve mixing ratio as compared to the existing reactor (Research Question # 1).

The main factors, namely type of static mixer, type of carrier gas, level of carrier gas inlet pressure and level of reactor operating temperature showed combined significant differences at .05 significant level in their effect on the mixing ratio of the carrier gases at controlled carrier gas inlet flow rate (0.0045 m/s) and inlet temperature (approx. 25 °C). However, considering individual factors, only types of static mixers and levels of reactor operating temperatures showed most significant effects on the mixing ratio (Research Question # 2).

Specific hypotheses and results have already been discussed in this chapter and are not discussed in detail here. Stated succinctly, a baffle static mixer proved to be more efficient than a no-baffle static mixer, or an aerodynamic type mixer. However, the extent of its superiority depended on reactor temperature (but not pressure or type of gas).

In general, at .05 significant level with the coefficient of determination of $R^2 =$ .78, there is a strong relationship between the types of static mixers, types of carrier gases - argon and nitrogen, carrier gas inlet pressures, and furnace temperatures and the mixing ratio at constant carrier gas inlet flow rate and inlet temperature. Therefore four combined factors can be used to explain the variations in the mixing ratio of carbon nanotube reactors with static mixers. However, to develop mixing ratio predicting model, statistically only type of static mixer and reactor temperature should be considered since they have most significant effect on the mixing index (Alternative Hypothesis #1).

Conclusions

The following conclusions were made as a result of this research based on modeling and simulating single phase carrier gas flow which is generalized to multi-phase flows:

1. The problem of this study is important because the type of static mixer configuration (the baffle type static mixer -concept 1, aerodynamic type of mixer -concept 2, existing reactor - concept 3); type of carrier gas (Argon and Nitrogen); and level of carrier gas inlet pressure (500 and 1000 Torr.); and level of reactor operating temperatures taken together could have a significant effect on the mixing index of carbon nanotubes synthesizing reactors. Optimizing these factors as a precondition for carbon nanotubes growth can improve growth control, uniformity of size, purity and consequently improve yield, productivity, and purification cost of carbon nanotubes.
2. The findings indicate that the mixing ratio between carbon nanotubes synthesizing gases or vapors in all other methods of growing carbon nanotubes such as arc, chemical vapor deposition methods, solar, flame, among others can similarly be improved by integrating a baffle type static mixer and applying the appropriate reactor operating temperatures (1200 and 3500 ^{o}C). In addition, considering the performance of the existing static mixer by appropriate selection of the carrier gas inlet pressures and reactor temperatures the mixing ratio of the gases or vapors of these other methods of growing carbon nanotubes can be improved. Furthermore, the findings indicate that type of carrier gas, and carrier gas inlet flow pressures do not

have significant effects on the mixing ratio of the laser method, and hence may not have significant effect on the other methods of growing carbon nanotubes either.

3 The following link the findings to phenomena that should be understood:

3.1 The significant improvement in the mixing ratio using single phase carrier gas flow exhibited by the baffle type static mixer over existing reactor is an indication that the static mixers can improve the inner configuration of the reactor to facilitate the mixing of carrier gases, carbon vapors, and metal catalyst vapors. This further means that with the improvement in the design of the inner configuration of the reactor one can better approximate uniform atomic distances between carrier gases, carbon and metal catalyst vapors. Consequently, size control and the purity of carbon nanotubes can be improved and this can lead to improve yield and translated into improved productivity of laser vapor method and other methods of growing carbon nanotubes.

3.2 The combination of the baffle type static mixer and the high reactor operating temperatures will facilitate the uniform distribution of atoms/molecules of the carrier gases to achieve the significant improvement in the mixing ratio. Hence, these two factors can improve the uniform distribution of atoms/molecules of carrier gases, carbon vapors and metal catalyst vapors to ensure approximate equal distances between the gaseous or vapor phase of these materials before these gaseous materials become plume in the case of laser or solar method of growing carbon nanotubes. This is applicable to flame combustion, arc, CVD and HiPCO methods of growing carbon nanotubes.

3.3 Since the baffle type static mixer performed better than the existing reactor and the existing reactor in turn performed better than the single bladed aerodynamic type mixer, this means that the type of inner configuration of the reactor is very important for achieving an effective mixing ratio. This further means that the form, shape and characteristic dimensions of the static mixers and consequently, the shape, form and characteristic dimensions of inner configuration of the reactor have an effect on the mixing of gases and hence the control of the growth conditions of carbon nanotubes.

3.4 The physical characteristics of type of carrier gas such as fundamental thermal conductivity and viscosity has no direct impact on the mixing ratio.

3.5 The carrier gas inlet flow pressures do not affect the density and hence level of carrier gas pressure does not affect the mixing ratio.

3.6 The reactor operating temperatures have an effect on the density of the carrier gas. Consequently, the reactor operating temperature can also affect the transport properties such as viscosity and thermal property of carrier gases. Hence, the relation between the reactor operating temperature and these transport properties and the density of carrier gases, carbon vapors and metal catalyst vapors will influence the mixing ratio.

4. The following are the needs for future research findings that should be known in order to forge a link between the findings and the phenomena described in 3:

4.1 The baffle type static mixer has to be installed in the carbon nanotubes growth reactors and the results validated.

4.2 The distribution of atoms/molecules in the existing reactor and the improved reactor with passive mixer have to be determined to confirm the role played by expected improved uniform atomic/molecular distances of the gaseous atoms/molecules of the carbon, carbon vapor and the metal catalyst vapor materials during growth of carbon nanotubes.

4.3 The transport properties of carrier gases, carbon vapors, and metal catalyst vapors such as thermal conductivity and viscosity enhancement at the reactor operating temperatures and their likely effects on the mixing ratio need to be established. The effect of diffusion can also be investigated since the existing reactor without static mixer performed better than the aerodynamic type mixer.

5. Real life physical phenomena that are being explained or modeled by the results are explained as follows:

The significant improvement in the mixing ratio using single phase carrier gas flow exhibited by the baffle static mixer over existing reactor is an indication that static mixers can improve the inner configuration of the reactor to facilitate the mixing of carrier gases, carbon vapors, and metal catalyst vapors. This further means that improving the shape, form, and characteristic dimensions of the inner configuration of the carbon nanotube growth reactors can improve achieving uniform atomic distances between carrier gases, carbon and metal catalyst vapors. In the case of the laser method and the solar method this can then lead to consistent plume formation, steady cooling, homogeneous nucleation, uniform growth, standard diameter and length of carbon nanotubes. Consequently, the

purity of carbon nanotubes can be achieved and lead to higher yield and can be translated into improved productivity of laser vapor method and other methods of growing carbon nanotubes. In addition, since the single aerodynamic blade mixer did not perform well despite its merit of easy cleanliness, it means that it is important that static mixers being considered in reactors should have the ability to generate wakes that facilitate flows. Further, the strong performance of an existing reactor without a static mixer over the single aerodynamic bladed mixer means that besides wakes and vortices, diffusion could also play a significant in the mixing of the gases. Additionally, the fact that there is no significant difference on the mixing ratio due type of carrier gas is a further indication that the choice of carrier gas has no significant effect on the mixing ratio. And hence, in choosing carrier gas for the growth of carbon nanotubes one should rather emphasize other criteria such as availability and cost. Similarly, since there is no significance difference between the carrier gas inlet pressures is another indication that the choice of pressure has no significant effect on the mixing ratio and hence one should rather consider criteria such as costs of pressurizing equipment and operation.

Recommendations

The following recommendations have been made as a result of this study:

1. To reduce cost of purification and to improve the mixing ratio of operating gases and consequently the purity and yield of carbon nanotubes, the only significant factors to be considered are type of static mixer design that will

improve the internal design configuration of reactors for growing carbon nanotubes in addition to selecting the right level of reactor operating temperature.

2. Additionally, to reduce production and operational costs, and consequently reduce the cost of purification and price of carbon nanotubes, since type of carrier gas and carrier gas inlet pressure did not show significant effect on the mixing ratio, then availability and cost of carrier gas, and capital and operational costs of pressure equipment should form additional selection criteria.
3. Improved carbon nanotubes processing methods that integrate a static mixer into existing carbon nanotube growth reactors is an innovation and has to be protected under the USA Intellectual Property Regulations.
4. A three phase gaseous fluid modeling and simulation involving carrier gases, carbon and the metal catalyst vapors should be completed early on in validating the results of this research.
5. A prototype baffle type static mixer has to be built and an existing reactor retrofitted with this static mixer and the results of the proposed improvement validated with experimental data.
6. The number of blades of the aerodynamic type static mixer has to be increased (e.g. to three) and its mixing index determined to establish whether there will be improvement over the single bladed aerodynamic type design.

7. To improve the results of the modeling and simulation and consequently the mixing ratio, the location of the graphite target has to be varied and the size of the graphite holder has to be included in the modeling and simulation.
8. A nozzle-diffuser type static mixer design can be investigated since that can also be easily cleaned.
9. Further, a static mixer design combining the aerodynamic type and the nozzle-diffuser type can be investigated (Since this combination can also be cleaned easily).
10. A simulation based flow rate (velocity) variations could also be investigated.
11. The relation between the reactor operating temperatures on the transport properties such as thermal conductivity and viscosity of the carrier gases on the mixing ratio should be investigated.
12. The mixing index could become an important new performance measure for carbon nanotube growth reactors and require further exploration of the concept.
13. The commercially available FEMLAB™ multi-physics modeling and simulation software platform used proved very useful and efficient. It would be very appropriate if the College of Natural Sciences could adopt the software for the Departments of Industrial Technology, Physics, Chemistry and Biology. The software could also support nanoscience, nanotechnology, and nanomanufacturing education. It could be tailored for both undergraduate and graduate studies. However, before final decision is made for adoption the

user-friendliness, the efficiency and scope of beneficial applications to students have to be evaluated and compared with other available software platforms. Graduate students should be encouraged to study MATLAB™ in addition. At the undergraduate level the software should focus on modeling and simulation of cases that students are likely to encounter in industry. The graduate level should go further to exploit the capabilities of the software in new situations.

14. Production of carbon nanotubes (a new and extraordinary material) has great potential in nanomanufacturing, and hence the Department of Industrial Technology should contribute to the development of this field by concentrating on research and development direction in the area of mass production of carbon nanotubes and automation of the nanotube production processes.
15. A local firm has expressed interest in production of carbon nanotubes. Since there are Federal and State funding for university and private sector collaboration the University of Northern Iowa through the Department of Industrial Technology should pursue the collaboration with this local firm to design and develop prototype equipment based on the proposed improvement for producing carbon nanotubes.

REFERENCES

Achiba, Y, Aoyagi, Y, Kataura, H, Nishide, D, Suzuki, S., & Tsukagoshi, K. (2003). High-yield production of single-wall carbon nanotubes in nitrogen gas. *Chemical Physics Letters, 372* (1-2) 45-50. Retrieved August 28, 2004, from http://www.sciencedirect.com/science?

Akos, V., Bogaerts, A., Chen, Z., & Gijbels, R. (2003, August). Laser ablation for analytical sampling: what we can learn from modeling? *Spectrochimica Act A Part B, 58,* 1867-1893. Retrieved October 14, 2004, from http://www.sciencedirect.com

Alcorn, P. A. (2003). *Social issues in technology: a format for investigation.* New Jersey: Pearson Education, Inc.

Alford, J. M., Diener, M. D., & Nielson, N. (2000). Synthesis of single wall carbon nanotubes in flames. *J. Physics. Chem. B 2000, 104, 9615-9620.*

Allard Jr., L. F., Fan, X., Geohegan, D. B., Lance, M. J., Puretzky, A. A., & Schittenhelm, H. (2002). Investigations of single wall carbon nanotubes growth by time-restricted laser vaporization. *Physical Review B, 65,* 245425. Retrieved September 20, 2002, from http://0-www.sciencedirect.com.unistar.uni.edu/science?

American Psychological Association. (5th ed.). (2001). *Publication Manual of the American Psychological Association.* Washington: American Psychological Association.

Banks, J., & Carson II, J. S. (1984). *Discrete-event system simulation.* New Jersey: Prentice-Hall.

Bauer, A., Bolz, D., Khinast, J. G., & Panarello, A. (2003). Mass-transfer enhancement by static mixers in a wall-coated catalytic reactor. *Chemical Engineering Science.* Retrieved October 25, 2004, from http://www.elsevier.com/locate/ces

Bogaerts, A., Chen, Z., Gijbels, R., & Vertes, A. (2003, August 22). Laser ablation for analytical sampling: what can we learn from modeling? *Spectrochimica ACTA Part B,* 58, 1867-1893. Retrieved September 23, 2004 from http://www.sciencedirect.com.unistar.uni.edu/science?

Borowiak-Palen, E., Fink, J., Graff, A., Knupfer, M., Jost, O., Liu, X., et al. (2002). Reduced diameter distribution of single-wall carbon nanotubes by selective oxidation. *Chemical Physics Letters, 363*(5-6), 567-572. Retrieved February 8, 2003, from http://0-www.sciencedirect.com.unistar.uni.edu/science?

Botton, G. A., Braidy, N., & El Khakani, M. A. (2002). Single-wall carbon nanotubes synthesis by means of UV laser vaporization. *Chemical Physics Letter.* Retrieved April 23, 2003, from http://0-www.sciencedirect.com.unistar.uni.edu/science?

Bowden, R., Ghosh, B. K., & Harrell, R. (2000). *Simulation using ProModel.* Boston: McGrawHill

Brighton, J. A., & Hughes, W. F. (*3rd ed.).* (1999). *Schaum's outlines: fluid dynamics* New York: McGraw-Hill.

Chen, Y., Ding, Y., He, Y., Wu, C., Zhang, H., Zhong, S., et al. (2002). The effect of laser power on the formation of carbon nanotubes prepared in CO_2 continuous wave laser ablation at room temperature. *Physica B: Condensed Matter.* Retrieved April 23, 2003, from http://0-www.sciencedirect.com.unistar.uni.edu/science?

Chiashi, S., Kohno, M., Kojima, R., Maruyama, S., & Miyauchi, Y. (2002). Low-temperature synthesis of high-purity single-walled carbon nanotubes from alcohol. *Chemical Physics Letters, 360*(3-4), 229-234. Retrieved February 8, 2003, from http://0-www.sciencedirect.com.unistar.uni.edu/science?

Chou, T., Thostenson, Erik. T., & Zhifeng, R. (2001). *Recent Advancements in Carbon Nanotubes and Their Composites* (Paper No: EM01-353). Society of Manufacturing Engineers. Retrieved February 8, 2003, from http://www.sme.org/cgi-bin/storefront/build_query/T/GROUP/MEMBNUM/SME.

Coleman, M. P. (2005). *An introduction to partial differential equations with MATLAB.* Boca Raton: CRC Press LLC.

COMSOL AB. (2004a). *FEMLAB 3.0: User's guide.* Stockholm: COMSOL AB.

COMSOL AB. (2004b). *FEMLAB 3.0: Model library.* Stockholm: COMSOL AB.

COMSOL AB. (2004c). *FEMLAB 3.0: Modeling guide.* Stockholm: COMSOL AB.

COMSOL AB. (2004d). *Laminar static mixer.* Stockholm: COMSOL AB. Retrieved March 5, 2005, from http://www.comsol.com/showroom/gallery/245.php

COMSOL AB. (2004e). *Residence time in a 2D and a 3D turbulent reactor.* Stockholm: COMSOL AB. Retrieved March 5, 2005, from http://www.comsol.com/showroom/gallery/

COMSOL AB. (2004f). *Non-isothermal flow.* Stockholm: COMSOL AB. Retrieved March 5, 2005, from http://www.comsol.com/showroom/gallery/

COMSOL AB. (2004g). *Heat transfer through conduction and convection.* Stockholm: COMSOL AB. Retrieved March 5, 2005, from http://www.comsol.com/showroom/gallery/

COMSOL AB. (2004h). *FEMLAB: quick start.* Stockholm: COMSOL AB.

Council on Technology Education (CTE). (1987). *Conducting technical research: 36th year book, 1987.* CA: Glencoe Publishing Company.

Creswell, J. W. *(2nd ed.).* (2003). *Research design: Qualitative, quantitative, and mixed methods approaches* London: Sage Publications.

Cross, M., Markatos, N. C., Rhodes, N., & Tatchell, D. G. (eds.). (1986). *Numerical simulation of fluid and heat/mass transfer processes.* New York: Springer-Verlag.

Devahastin, S., & Mujumdar, A. S. (2001). A numerical study of mixing novel impinging stream in-line mixer. *Chemical Engineering and Processing.* Retrieved September 30, 2004, from http://www.elsevier.com/locate/cep

Devahastin, S., Mujumdar, A. S., & Wang, S. J. (2004, June). A numerical investigation of some approaches to improve mixing in laminar confined impinging streams. *Applied Thermal Science.* Retrieved September 24, 2004, from http://www.sciencedirect.com.unistar.uni.edu/science?

Dubson, M. A., Taylor, J. R., & Zafiratos, C. D. (2004). *Modern physics for scientists and engineers (2nd ed.).* New Jersey: Prentice Hall.

Dunn, G., & Everitt, B. S. (1983). *Advanced methods of data exploration and modeling.* London: Heinemann Educational Books.

Elliot, R. J. *(2nd ed.).* (2000). *Learning SAS in the Computer lab.* Canada: Duxbury Thompson Learning.

Environmental Chemistry.Com (n.d). *Chemistry & environmental chemistry dictionary.* Retrieved February 6, 2005, from http://environmentalchemistry.com/yogi/chemistry/dictionary/H01.html#Heat%20of%20Vaporization

Fabian, C. M. (2001). *Carbon nanotubes fabrication.* Retrieved March 20, 2003, from http://www.ee.virginia.edu/~cmf6p/research_docs/nanotubes.pdf

Fan, X., Geohegan, D. B., Pennycook, S. J., & Puretzky, A. A.(January, 2000). In situ imaging and spectroscopy of single-wall carbon nanotube synthesis by laser vaporization. *Applied Physics Letters, 76* (2), 182-184.

Fan, X., Geohegan, D. B., Pennycook, S. J., & Puretzky, A. A.(February, 2002). Dynamics of single-wall carbon nanotube synthesis by laser vaporization. *Applied Physics A: Materials Science & Processing.* Retrieved February 1, 2005, from http://www.springerlink.com/app/home/contribution.asp?

Fan, X., Geohegan, D. B., Guillorn, M. A., Puretzky, A. A., & Schittenhelm, H. (September 30, 2002). Time resolved diagnostics of single wall carbon nanotubes synthesis by laser vaporization. *Applied Surface Science, 197-198*(2002), 552-562. Retrieved April 4, 2004, from http://0-www.sciencedirect.com.unistar.uni.edu/science?

Fang, J. Z., & Lee, D. J. (2001, February). Micromixing efficiency of static mixers. *Chemical Engineering Science, 56*(2001), 3797-3802. Retrieved September 25, 2004, from http://www.elsevier.nl/locate/ces.

Flamant, G., Giral, J., Guillard, T., Laplaze, D., Rivoire, B., & Robert, J. (2001). Towards the large scale production of fullerenes and nanotubes by solar energy. *Proceedings of Solar Forum 2001: Solar Energy the Power to Choose,* April 21-25, 2001, Washington, DC. Retrieved on November 25, 2003, from http://www.imp.cnrs.fr/groupe3/publiSolarForum.pdf

Fraenkel, J. R., & Wallen, N. E. (2003). *How to design and evaluate research in education.* New York: McGraw-Hill.

Gaines, D. M., & Regli, W. C. (n.d.). A research report-a repository for design, process planning and assembly. *Computer-Aided-Design, 29*(12), 895-905. Great Britain: Elsevier Science Ltd.

Gong, M. Q., Luo, E. C., & Wu, J. F. (2004, April). The mixing effects for real gases and their mixtures. *Cryogenics, 44* (2004) 741-753. Retrieved November 25, 2004, from http://www.elsevier.com/locate/cryogenics

Hester, J. R., & Louchev, O. A. (2003, May). Kinetic pathways of carbon nanotube nucleation from graphitic nanofragments. *Journal of Applied Physics, 94*(4).

Ichihashi, T., Iijima, S., Kokai, F., Takahashi, K., Yamada, R., Yudasaka, M.(1999). Growth Dynamics of Single-Wall Carbon Nanotubes Synthesized by CO_2 Laser Vaporization . *Phys. Chem. B, 103* (21), 4346 -4351. Retrieved September 3, 2004 from http://pubs.acs.org/cgi-bin/archive.cgi/jpcbfk/1999/103/i21/html/jp990065s.html

Kamat, P. V., & Liz-Marzan, L. M. (2003). *Nanoscale materials*. Boston: Kluwer Academic Publishers.

Kannangara, K., Raguse, B., Simmons, M., Smith, G., & Wilson, M. (2002). *Nanotechnology: basic science and emerging technologies*. New York: Chapman & Hall/CRC.

Kasuya, M., Kokai, F., Iijima, S., Takahashi, K, & Yudsaka, M. (2002, May). Growth dynamics of single- wall carbon nanotubes and nanohorn aggregates by CO_2 laser vaporization at room temperature. *Applied Surface Science*. Retrieved April 23, 2003, from http://0-www.sciencedirect.com.unistar.uni.edu/science?.

Kim, B. J., Liu, Y. Z., & Sung, H. J. (in press). Two-fluid mixing in a microchannel *International Journal of Heat and Fluid Flow*. Retrieved October 30, 2004, from http://www.sciencedirect.com

Kittel, C., & Kroemer, H. (1980). *Thermal Physics*. New York: W. H. Freeman and Company.

Lai, H. J., Li, A. K., Lin, M. C. C., & Yang, M. H. (2001, October). Synthesis of carbon nanotubes using polyclic aromatic hydrocarbons as carbon sources in an arc discharge. *Materials Science and Engineering,* 16(1-2), 23-26. Retrieved February 13, 2003, from http://0-www.sciencedirect.com.unistar.uni.edu/science?.

Li, X., Xu, C., Wu, D., & Zhu, H. (2002, January). Co-synthesis of single-walled carbon nanotubes and carbon fibers. *Materials Research Bulletin, 37*(1), 177-183. Retrieved February 8, 2003, from http://0-www.sciencedirect.com.unistar.uni.edu/science?

Lide, D. R. (83rd ed.). (2002). *Handbook of chemistry and physics*. United States of America: CRC Press LLC.

Longnecker, M. L., & Ott, R. L. *(5th ed.).* (2001). *An introduction to statistical methods and data analysis.* United States: Duxbury Thomson Learning.

Los Alamos National Laboratory Chemistry Division [LANLCD],(n.d). *Periodic table: Argon*. Retrieved February 6, 2005, from http://pearl1.lanl.gov/periodic/default.htm

Mitsui to build carbon nanotubes mass output plant (2001, Dec.) Retrieved February 11, 2003, from http://www.planetark.org/dailynews&story

National Science Foundation (n.d). Division of Design Manufacture and Industrial Innovation: Nanomanufacturing. Retrieved February 1, 2005, from http://www.nsf.gov/funding/pgm_summ.jsp?pims_id=13347

Nicolini, C. (Ed.). (1996). *Molecular manufacturing (Vol. 2).* New York: Plenum Press.

Nieto de Castro, C. A., Dymod, J. H., & Millat, J. (1996). *Transport properties of fluids: their correlation, prediction and estimation.* United States of America: The International Union of Pure and Applied Chemistry.

NIST/SEMATECH. (2003). *E-Engineering statistics handbook.* Retrieved October 10, 2003, from http://www.itl.nist.gov/div898/handbook/

Nonlinear Engineering (NE). (February 2005). Simulation process. *Mechanical Engineering, 127 (2).* Retrieved February 4, 2005, from http://www.nleng.com/sim_process/

Papadopoulos, C. (2000). Nanotube engineering and science: synthesis and properties of highly ordered carbon nanotube arrays and Y-junction carbon nanotubes (Masters thesis, University of Toronto, 2000). *Digital Dissertations*. Retrieved February 9, 2003, from http://0-wwwlib.umi.unistar.uni.edu/dissertations/ (Pub. No. AATMQ53443).

Parkes, G. D. (1961). *Mellor's Modern Inorganic Chemistry*(Rev. ed.). London: Green and Co. Ltd.

Popov, V. N. (2003). Carbon nanotubes: properties and application. *Materials Science and Engineering, R 43*(2004), 61-102. Retrieved September 16, 2004, from http://0-www.sciencedirect.com.unistar.uni.edu.

Povitsky, A. (2002). Improving jet reactor configuration for production of carbon nanotubes.*Computers & Fluids,* 31, 957-976. Retrieved December 15, 2004, from http://www.elsevier.com/locate/ces

Ratner, D., & Ratner, M. (2003). *Nanotechnology: a gentle introduction to the next big idea.* New Jersey: Pearson Education, Inc.

Salzman, W. R. (2004). *Entropy of mixing, what does entropy measure*? Retrieved August 28, 2004, from http://www.chem.arizona.edu/~salzmanr/480a/480ants/mixing/mixing.html

Smith, B. W. (2001). Carbon nanotube supramolecular assemblies: discovery, characterization, and high-yield synthesis of carbon-60 SWNT (Doctoral dissertation, University of Pennsylvania, 2001). *Digital Dissertations*. Retrieved February 9, 2003, from http://0-wwwlib.umi.unistar.uni.edu/dissertations/(Pub. No. AAT3015374).

SPSS Inc. (1999). *SPSS base 9.0: applications guide*. United States: SPSS Inc.

Universal Industrial Gases, Inc. (n.d.). *Nitrogen (N_2) gases and uses*. Retrieved November 20, 2004, from http://www.uigi.com/nitrogen.html. 2200 Northwood Ave. Suite 3, Easton, Pennsylvania 18045-2239 USA.

Zhang, J. (1995). Production, properties and purification of carbon nanotubes (Masters thesis, Rice University, 1995). *Digital Dissertations*. Retrieved February 9, 2003, from http://0-wwwlib.umi.unistar.uni.edu/dissertations/(Pub. No. AAT1377075).

APPENDIX A

CHARACTERISTIC PROPERTIES OF CARBON

Characteristic Properties of Carbon (Graphite)

Properties/Parameters	Units	Values
Atomic (Z)		6
Chemical atomic mass (M)	au	12.011
Mass number (A)		12
Mass of neutral atom (m)	au	12
Quantum number for total angular momentum of nucleus (j)		0
Maximum percentage abundance	%	98.9
Atomic radius	(angstrom) A°	0.91
Atomic volume	cm3/mol	4.58
Covalent radius	(angstrom) A°	0.77
Electrons in various quantum levels		
1st		2
2nd		4
Ionization potentials	V	
1st electron	V	11.2
2 nd electron	V	24.3
3 rd electron	V	47.6
4 th electron	V	64.2
Molar volume	cm^3/mole	5.34
Electron work function	eV	
Specific gravity		1.9-2.3
Density	g/cc (at 300K)	2.25
Melting point	°C	3500
Boiling point	°C	4830
Thermal conductivity	W/mK (at 293K)	160 (natural)
	W/cmK (at 293K)	1.29
Linear thermal expansion coeffiecient (overall)	$10^{-6}K^{-1}$	7.8 (at 293 K)
		8.9 (at 293 K)
	cm/cm/°C(at 0 °C)	0.0000021
Heat of fusion	kj/mol	17.47
Heat of sublimation	kcal	170.4
Heat of vaporization	kJ/mole	355.8
Enthalpy of fusion	kJ/mol at 25 °C	104.6
Enthalpy of vaporization	kJ/mol at 25 °C	716.7
Specific heat	J/gK	0.71
Vapor pressure	mmHg at 20 °C	0
Optical Refractive Index		2.417 (diamond)
Optical Reflectivity	%	27

Note: Values were retrieved from
http://www.environmentalchemistry.com/yogi/periodic/Ni.html?new=periodic/Ni.html

APPENDIX B

CHARACTERISTIC PROPERTIES OF NITROGEN CARRIER GAS

Propertiesof Nitrogen Carrier Gas

Properties	Units	Values	References
Atomic (Z)		7	Dubson, Taylor & Zafiratos, 2004.
Chemical atomic mass (M)	au	14.007	Dubson, Taylor & Zafiratos, 2004.
Mass number (A)		14	Dubson, Taylor & Zafiratos, 2004.
Mass of neutral atom (m)	au	14.003074	Dubson, Taylor & Zafiratos, 2004.
Quantum number for total angular momentum of nucleus (j)		1	Dubson, Taylor & Zafiratos, 2004.
Maximum percentage abundance	%	99.634	
Atomic radius	(angstrom) A°	0.75	
Atomic volume	cm3/mol	17.3	
Covalent radius	(angstrom) A°	0.75	
Cross section	barns (1barn = E^{-24} cm^2)		
Crystal structure			
Chemical			
Molecular Weight		28.01	Universal Industrial Gases, Inc.(n.d)
Electrons in various quantum levels			
1st		2	
2nd		5	
Ionization potentials	V		
1st electron		14.48	
2 nd electron		29.47	
3 rd electron		47.4	
4 th electron		77	
5th electron		97	
Radius of M^{++} in solids	cm x 10^{8}		
Radius of M^{-3} ion	cm x 10^{8}	1.71	
Ionic radius	(angstrom) A°	0.13	
Molar volume	cm3/mole	17.3	
Electron work function	eV		
Specific gravity	air=1 and water=1	0.9737 (@ 0° C & @ 101.325 kPa)	Universal Industrial Gases, Inc.(n.d)

Density	Kg/m^3	1.2506 (@ 0° C or 274K & @ 101.325 kPa or 1 atm)	Universal Industrial Gases, Inc.(n.d)
Melting point	°C	-210.01	
Boiling point (Temperature)	°C (Boiling point @ 101.32kPa)	-195.8	Universal Industrial Gases, Inc.(n.d)
Thermal conductivity (k)	W/cmK (at 293K)	0.0002598	
Thermal conductivity (k)	mW/mK at 300K (approx. 25°C) and 0.1MPa(1bar)	25.8	Lide, D. R. (83rd ed.). (2002).
Thermal conductivity (k)	mW/mK at 600K and 0.1MPa(1bar)	44	Lide, D. R. (83rd ed.). (2002).
Thermal conductivity (k)	mW/mK at 300K (approx. 25°C) and 10MPa	31.9	Lide, D. R. (83rd ed.). (2002).
Thermal conductivity (k)	mW/mK at 1000K (approx. 727°C) and 0.1MPa (1bar)	67.7	Lide, D. R. (83rd ed.). (2002).
Thermal conductivity (k)	mW/mK at 1000K (approx. 727°C) and 10MPa	69.6	Lide, D. R. (83rd ed.). (2002).
Thermal conductivity (k)	mW/mK at 1500K (approx. 1227°C) and 10MPa	94.7	Lide, D. R. (83rd ed.). (2002).
Triple Point			
Temperature	oC	-210	Universal Industrial Gases, Inc.(n.d)
Pressure	kPa abs	12.5	Universal Industrial Gases, Inc.(n.d)
Critical Point			
Temperature	oC	-146.9	Universal Industrial Gases, Inc.(n.d)
Pressure	kPa abs	3399	Universal Industrial Gases, Inc.(n.d)
Density	Kg/m^3	314.9	Universal Industrial Gases, Inc.(n.d)
Heat of fusion	kj/mol	0.3604	
Heat of vaporization	cal/mole	1,350	
	kJ/mole	2.7928	
Heat of dissociation	kcal/mole	226	
Enthalpy of atomization	kj/mol at 25 oC	472.8	
Enthalpy of fusion	kj/mol at 25 oC	0.36	
Enthalpy of vaporization	kj/mol at 25 oC	2.79	
Latent of vaporization Boiling Point	kJ/Kg (boiling point @ 101.325 kPa)	199.1	Universal Industrial Gases, Inc.(n.d)

Specific heat (Cp)	J/Kg °C	1.04 (@ 0° C & @ 101.325 kPa)	Universal Industrial Gases, Inc.(n.d)
Vapor pressure	Pa mmHg at 20 °C		
Viscosity (eta)	centi-poise(cP) at 20°C		
Viscosity (eta)	uPa s at 300K (approx. 25°C) and 0.1MPa(1bar)	18	Lide, D. R. (83rd ed.). (2002).
Viscosity (eta)	uPa s at 300K (approx. 25°C) and 10MPa	20.1	Lide, D. R. (83rd ed.). (2002).
Viscosity (eta)	uPa s at 1000K (approx. 727°C) and 0.1MPa (1bar)	41.5	Lide, D. R. (83rd ed.). (2002).
Viscosity (eta)	uPa s at 1000K (approx. 727°C) and 10MPa	42	Lide, D. R. (83rd ed.). (2002).
Viscosity (eta)	uPa s at 1500K (approx. 1227°C) and 10MPa	54.3	Lide, D. R. (83rd ed.). (2002).
Optical Refractive Index		1.000298	
Optical Reflectivity	%		

Note: References not shown were retrieved from http://www.environmentalchemistry.com/yogi/periodic/Ni.html?new=periodic/Ni.html

APPENDIX C

CHARACTERISTIC PROPERTIES OF ARGON CARRIER GAS

Characteristic Properties of Argon Carrier Gas

Properties	Units	Values	References
Atomic (Z)		18	Dubson, Taylor & Zafiratos, 2004.
Mass number (A)		40	Dubson, Taylor & Zafiratos, 2004.
Mass of neutral atom (m)	au	39.962 384	Dubson, Taylor & Zafiratos, 2004.
Quantum number for total angular momentum of nucleus (j)		0	Dubson, Taylor & Zafiratos, 2004.
Maximum percentage abundance	%	99.6	Dubson, Taylor & Zafiratos, 2004.
Atomic radius	(angstrom) A°	0.88	http://environmentalchemistry.com/yogi/periodic/Ar.html
Atomic volume	cm^3/mol	28.5	http://environmentalchemistry.com/yogi/periodic/Ar.html
Covalent radius	(angstrom) A°	0.98	http://environmentalchemistry.com/yogi/periodic/Ar.html
Cross section	barns (1barn = E^{-24} cm^2)	0.66	http://environmentalchemistry.com/yogi/periodic/Ar.html
Crystal structure		Cube face centered	http://environmentalchemistry.com/yogi/periodic/Ar.html
Electron configuration		$1s^2\ 2s^2p^6\ 3s^2p^6$	http://environmentalchemistry.com/yogi/periodic/Ar.html
Electrons per energy level		2, 8, 8	
Filling orbital		$3p^6$	http://environmentalchemistry.com/yogi/periodic/Ar.html
Number electrons	(with no charge)	18	http://environmentalchemistry.com/yogi/periodic/Ar.html
Number neutrons	most stable	22	http://environmentalchemistry.com/yogi/periodic/Ar.html
Number of protons		18	http://environmentalchemistry.com/yogi/periodic/Ar.html
Oxidation states		0	http://environmentalchemistry.com/yogi/periodic/Ar.html
Valence electrons		$3s^2p^6$	http://environmentalchemistry.com/yogi/periodic/Ar.ht

			ml
Ionization potentials	eV		
1st electron		15.759	http://environmentalchemistry.com/yogi/periodic/Ar.html
2 nd electron		27.629	http://environmentalchemistry.com/yogi/periodic/Ar.html
3 rd electron		40.74	http://environmentalchemistry.com/yogi/periodic/Ar.html
Chemical atomic mass (M)	au	39.948	Dubson, Taylor & Zafiratos, 2004.
Boiling point (Temperature)	°C (Boiling point @ 20°C and 1atm)	-185.7 or (85.7K) or ('-302.3oF)	http://environmentalchemistry.com/yogi/periodic/Ar.html
Thermal conductivity (k)	W/cmK (at 293K)	0.0001772	http://environmentalchemistry.com/yogi/periodic/Ar.html
Thermal conductivity (k)	mW/mK at 300K (approx. 25°C) and 0.1MPa(1bar)	17.9	Lide, D. R. (83rd ed.). (2002).
Thermal conductivity (k)	mW/mK at 380K (approx.25°C) and 0.1MPa (1bar)	21.7	Lide, D. R. (83rd ed.). (2002).
Thermal conductivity (k)	mW/mK at 600K and 0.1MPa (1bar)	30.6	Lide, D. R. (83rd ed.). (2002).
Thermal conductivity (k)	mW/mK at 300K (approx. 25°C) and 10MPa(1bar)	22.3	Lide, D. R. (83rd ed.). (2002).
Thermal conductivity (k)	mW/mK at 380K (approx.107°C) and 10MPa	24.9	Lide, D. R. (83rd ed.). (2002).
Thermal conductivity (k)	mW/mK at 1000K (approx. 727°C) and 10MPa		
Density	Kg/m^3 =g/L		Universal Industrial Gases, Inc.(n.d)
	g/L (at 273K and 1atm)	1.7824	http://environmentalchemistry.com/yogi/periodic/Ar.html
Molar volume	cm3/mole	24.2	http://environmentalchemistry.com/yogi/periodic/Ar.html
Specific gravity	air=1 and water=1		Universal Industrial Gases, Inc.(n.d)
Melting point	°C (Boiling point @ 20°C and 1atm)	-189.19	http://environmentalchemistry.com/yogi/periodic/Ar.html

	K	83.81	http://environmentalchemistry.com/yogi/periodic/Ar.html
	°F	-308.54	http://environmentalchemistry.com/yogi/periodic/Ar.html
Triple Point			
Temperature	oC		Universal Industrial Gases, Inc.(n.d)
Pressure	kPa abs		Universal Industrial Gases, Inc.(n.d)
Critical Point			
Temperature	oC		Universal Industrial Gases, Inc.(n.d)
Pressure	kPa abs		Universal Industrial Gases, Inc.(n.d)
Density	Kg/m^3		Universal Industrial Gases, Inc.(n.d)
Heat of fusion	kJ/mole	1.88	http://environmentalchemistry.com/yogi/periodic/Ar.html
Heat of sublimation	kcal		
Heat of vaporization	cal/mole		
	kJ/mole	6.447	http://environmentalchemistry.com/yogi/periodic/Ar.html
Enthalpy of fusion	kJ/mole at 25 oC and 1 atm	1.18	http://environmentalchemistry.com/yogi/periodic/Ar.html
Enthalpy of vaporization	kJ/mol at 25 oC and 1atm	6.43	http://environmentalchemistry.com/yogi/periodic/Ar.html
Latent of vaporization Boiling Point	kJ/Kg (boiling point @ 101.325 kPa)		Universal Industrial Gases, Inc.(n.d)
Specific heat (Cp)	J/Kg °C		Universal Industrial Gases, Inc.(n.d)
	j/gK	0.52	http://environmentalchemistry.com/yogi/periodic/Ar.html
Viscosity (eta)	centi-poise(cP) at 20°C	0.0227	
Viscosity (eta)	uPa s at 300K (approx. 25°C) and 0.1MPa(1bar)	22.9	Lide, D. R. (83rd ed.). (2002).
Viscosity (eta)	uPa s at 380K (approx.25°C) and 0.1MPa	27.8	Lide, D. R. (83rd ed.). (2002).
Viscosity (eta)	uPa s at 300K (approx. 25°C) and 10MPa(1bar)	26.7	Lide, D. R. (83rd ed.). (2002).

Viscosity (eta)	uPa s at 380K (approx.107°C) and 10MPa	29.7	Lide, D. R. (83rd ed.). (2002).
Viscosity (eta)	uPa s at 600K (approx.107°C) and 100kPa=0.1Mpa)(1bar)	39	Lide, D. R. (83rd ed.). (2002).
Optical Refractive Index		1.000281	http://environmentalchemistry.com/yogi/periodic/Ar.html

APPENDIX D

STATISTICAL PROGRAM FOR 4-WAY ANOVA USING ABSOLUTE MIXING INDEX (PERCENTAGE MIXING RATIO) RAW DATA

```
data percentagemixingratio;
input mixer gas pressure temperature mixingratio;
mixingratio  = mixingratio;
cards;
1 1 500 1200 0.001
1 1 500 1200 0.003
1 1 500 1200 0.022
1 1 500 3500 0.001
1 1 500 3500 0.002
1 1 500 3500 0.014
1 1 1000 1200 0.002
1 1 1000 1200 0.010
1 1 1000 1200 0.062
1 1 1000 3500 0.0008
1 1 1000 3500 0.003
1 1 1000 3500 0.02
1 2 500 1200 0.04
1 2 500 1200 0.70
1 2 500 1200 0.02
1 2 500 3500 0.0006
1 2 500 3500 0.007
1 2 500 3500 0.01
1 2 1000 1200 0.002
1 2 1000 1200 0.01
1 2 1000 1200 0.07
1 2 1000 3500 0.0008
1 2 1000 3500 0.01
1 2 1000 3500 0.02
2 1 500 1200 1.6
2 1 500 1200 0.6
2 1 500 1200 3.5
2 1 500 3500 0.63
2 1 500 3500 0.2
2 1 500 3500 1.35
2 1 1000 1200 3.5
2 1 1000 1200 1.2
2 1 1000 1200 7.3
2 1 1000 3500 1.3
2 1 1000 3500 0.4
2 1 1000 3500 7.3
2 2 500 1200 1.7
2 2 500 1200 0.6
2 2 500 1200 3.6
2 2 500 3500 0.06
2 2 500 3500 0.2
2 2 500 3500 1.4
2 2 1000 1200 3.6
2 2 1000 1200 1.2
2 2 1000 1200 7.6
2 2 1000 3500 3.6
2 2 1000 3500 0.4
2 2 1000 3500 2.8
3 1 500 1200 0.2
3 1 500 1200 0.03
```

```
3 1 500 1200 0.61
3 1 500 3500 0.13
3 1 500 3500 0.02
3 1 500 3500 0.44
3 1 1000 1200 0.42
3 1 1000 1200 0.07
3 1 1000 1200 1.30
3 1 1000 3500 0.198
3 1 1000 3500 0.03
3 1 1000 3500 0.618
3 2 500 1200 0.199
3 2 500 1200 0.034
3 2 500 1200 0.621
3 2 500 3500 0.14
3 2 500 3500 0.02
3 2 500 3500 0.4
3 2 1000 1200 0.3
3 2 1000 1200 0.05
3 2 1000 1200 0.9
3 2 1000 3500 0.020
3 2 1000 3500 0.03
3 2 1000 3500 0.6
;
run;
* Note: mixer variable;
*      1=baffle type mixer, 2=aerodynamic type mixer, 3=existing reactor
mixer;
* Note: gas variable;
*      1=nitrogen, 2=argon;

proc glm data=percentagemixingratio;
class mixer gas pressure temperature;
      model mixingratio= mixer gas pressure temperature mixer*gas
mixer*pressure mixer*temperature gas*pressure gas*temperature
pressure*temperature mixer*gas*pressure mixer*gas*temperature
mixer*gas*pressure*temperature;
title1 Four-Way ANOVA Model for Mixing Ratio of Reactor Mixing Chamber
Based on Only Positive Absolute Percentage Mixing Ratio Data;
run;

means mixer /tukey lsd;
means gas /tukey lsd;
means pressure/tukey lsd;
means temperature/ tukey lsd;
title2 'Comparison of Means of the Main Factors';
run;

output out=next r=resid p=yhat;
proc print data=next;

proc rank normal=blom;
      var resid;
      ranks nscore;
```

```
proc plot;
      plot resid*nscore;
      plot resid*yhat;
run;

proc corr data=percentagemixingratio;
      var mixer gas pressure temperature;
title 'Correlations of Mixing Ratio for Reactor';
run;

proc corr data=percentagemixingratio;
      var mixer gas pressure temperature;
      with mixingratio;
title 'Correlations of Mixing Ratio for Reactor';
run;

proc plot data percentagemixingratio;
proc plot;
      plot mixingratio*mixer='m';
      plot mixingratio*gas='g';
      plot mixingratio*pressure='p';
      plot mixingratio*temperature='t';
      Title 'Scatter Diagram - Mixing Ratio Vs Main Factors'
run;

proc chart data percentagemixingratio;
proc chart;
      vbar mixingratio/subgroup=mixer;
      vbar mixingratio/subgroup=gas;
      vbar mixingratio/subgroup=pressure;
      vbar mixingratio/subgroup=temperature;
Title 'Histogram of Mixing Ratio vs Main Factors';
run;

proc univariate plot;
      by mixer;
      var mixingratio;
Title 'Mixing Ratio Due to Mixer Effect';
run;
proc univariate plot;
      by gas;
      var mixingratio;
Title 'Mixing Ratio Due to Gas Effect';
run;
proc univariate plot;
      by pressure;
      var mixingratio;
Title 'Mixing Ratio Due to Pressure Effect';
run;
proc univariate plot;
      by temperature;
      var mixingratio;
Title 'Mixing Ratio Due to Temperature Effect';
run;
```

APPENDIX E

STATISTICAL PROGRAM FOR 4-WAY ANOVA USING TRANSFORMED ABSOLUTE MIXING INDEX RAW DATA IN LOGARITHM OF 10

```
data percentagemixingratio;
input mixer gas pressure temperature mixingratio;
mixingratio  = log10(mixingratio);
cards;
1 1 500 1200 0.001
1 1 500 1200 0.003
1 1 500 1200 0.022
1 1 500 3500 0.001
1 1 500 3500 0.002
1 1 500 3500 0.014
1 1 1000 1200 0.002
1 1 1000 1200 0.010
1 1 1000 1200 0.062
1 1 1000 3500 0.0008
1 1 1000 3500 0.003
1 1 1000 3500 0.02
1 2 500 1200 0.04
1 2 500 1200 0.70
1 2 500 1200 0.02
1 2 500 3500 0.0006
1 2 500 3500 0.007
1 2 500 3500 0.01
1 2 1000 1200 0.002
1 2 1000 1200 0.01
1 2 1000 1200 0.07
1 2 1000 3500 0.0008
1 2 1000 3500 0.01
1 2 1000 3500 0.02
2 1 500 1200 1.6
2 1 500 1200 0.6
2 1 500 1200 3.5
2 1 500 3500 0.63
2 1 500 3500 0.2
2 1 500 3500 1.35
2 1 1000 1200 3.5
2 1 1000 1200 1.2
2 1 1000 1200 7.3
2 1 1000 3500 1.3
2 1 1000 3500 0.4
2 1 1000 3500 7.3
2 2 500 1200 1.7
2 2 500 1200 0.6
2 2 500 1200 3.6
2 2 500 3500 0.06
2 2 500 3500 0.2
2 2 500 3500 1.4
2 2 1000 1200 3.6
2 2 1000 1200 1.2
2 2 1000 1200 7.6
2 2 1000 3500 3.6
2 2 1000 3500 0.4
2 2 1000 3500 2.8
3 1 500 1200 0.2
3 1 500 1200 0.03
```

```
3 1 500 1200 0.61
3 1 500 3500 0.13
3 1 500 3500 0.02
3 1 500 3500 0.44
3 1 1000 1200 0.42
3 1 1000 1200 0.07
3 1 1000 1200 1.30
3 1 1000 3500 0.198
3 1 1000 3500 0.03
3 1 1000 3500 0.618
3 2 500 1200 0.199
3 2 500 1200 0.034
3 2 500 1200 0.621
3 2 500 3500 0.14
3 2 500 3500 0.02
3 2 500 3500 0.4
3 2 1000 1200 0.3
3 2 1000 1200 0.05
3 2 1000 1200 0.9
3 2 1000 3500 0.020
3 2 1000 3500 0.03
3 2 1000 3500 0.6
;
run;
* Note: mixer variable;
*     1=baffle type mixer, 2=aerodynamic type mixer, 3=existing reactor
mixer;
* Note: gas variable;
*     1=nitrogen, 2=argon;

proc glm data=percentagemixingratio;
class mixer gas pressure temperature;
      model mixingratio= mixer gas pressure temperature mixer*gas
mixer*pressure mixer*temperature gas*pressure gas*temperature
pressure*temperature mixer*gas*pressure mixer*gas*temperature
mixer*gas*pressure*temperature;
title1 Four-Way ANOVA Model for Mixing Ratio of Reactor Mixing Chamber
Based on Log10(Positive Absolute Mixing Ratio Data);
run;

means mixer /tukey lsd;
means gas /tukey lsd;
means pressure/tukey lsd;
means temperature/ tukey lsd;
title2 'Comparison of Means of the Main Factors';
run;

output out=next r=resid p=yhat;
proc print data=next;

proc rank normal=blom;
      var resid;
      ranks nscore;
```

```
proc plot;
      plot resid*nscore;
      plot resid*yhat;
run;

proc corr data=percentagemixingratio;
      var mixer gas pressure temperature;
title 'Correlations of Mixing Ratio for Reactor';
run;

proc corr data=percentagemixingratio;
      var mixer gas pressure temperature;
      with mixingratio;
title 'Correlations of Mixing Ratio for Reactor';
run;

proc plot data percentagemixingratio;
proc plot;
      plot mixingratio*mixer='m';
      plot mixingratio*gas='g';
      plot mixingratio*pressure='p';
      plot mixingratio*temperature='t';
      Title 'Scatter Diagram - Mixing Ratio Vs Main Factors'
run;

proc chart data percentagemixingratio;
proc chart;
      vbar mixingratio/subgroup=mixer;
      vbar mixingratio/subgroup=gas;
      vbar mixingratio/subgroup=pressure;
      vbar mixingratio/subgroup=temperature;
Title 'Histogram of Mixing Ratio vs Main Factors';
run;

proc univariate plot;
      by mixer;
      var mixingratio;
Title 'Mixing Ratio Due to Mixer Effect';
run;
proc univariate plot;
      by gas;
      var mixingratio;
Title 'Mixing Ratio Due to Gas Effect';
run;
proc univariate plot;
      by pressure;
      var mixingratio;
Title 'Mixing Ratio Due to Pressure Effect';
run;
proc univariate plot;
      by temperature;
      var mixingratio;
Title 'Mixing Ratio Due to Temperature Effect';
run;
```

APPENDIX F

STATISTICAL PROGRAM FOR MULTIPLE REGRESSION MODEL USING TRANSFORMED ABSOLUTE MIXING INDEX RAW DATA IN LOGARITHM OF 10

```
data percentagemixingratio;
input mixer gas pressure temperature mixingratio;
mixingratio  = Log10(mixingratio);
cards;
1 1 500 1200 0.001
1 1 500 1200 0.003
1 1 500 1200 0.022
1 1 500 3500 0.001
1 1 500 3500 0.002
1 1 500 3500 0.014
1 1 1000 1200 0.002
1 1 1000 1200 0.010
1 1 1000 1200 0.062
1 1 1000 3500 0.0008
1 1 1000 3500 0.003
1 1 1000 3500 0.02
1 2 500 1200 0.04
1 2 500 1200 0.70
1 2 500 1200 0.02
1 2 500 3500 0.0006
1 2 500 3500 0.007
1 2 500 3500 0.01
1 2 1000 1200 0.002
1 2 1000 1200 0.01
1 2 1000 1200 0.07
1 2 1000 3500 0.0008
1 2 1000 3500 0.01
1 2 1000 3500 0.02
2 1 500 1200 1.6
2 1 500 1200 0.6
2 1 500 1200 3.5
2 1 500 3500 0.63
2 1 500 3500 0.2
2 1 500 3500 1.35
2 1 1000 1200 3.5
2 1 1000 1200 1.2
2 1 1000 1200 7.3
2 1 1000 3500 1.3
2 1 1000 3500 0.4
2 1 1000 3500 7.3
2 2 500 1200 1.7
2 2 500 1200 0.6
2 2 500 1200 3.6
2 2 500 3500 0.06
2 2 500 3500 0.2
2 2 500 3500 1.4
2 2 1000 1200 3.6
2 2 1000 1200 1.2
2 2 1000 1200 7.6
2 2 1000 3500 3.6
2 2 1000 3500 0.4
2 2 1000 3500 2.8
3 1 500 1200 0.2
3 1 500 1200 0.03
```

```
3 1 500 1200 0.61
3 1 500 3500 0.13
3 1 500 3500 0.02
3 1 500 3500 0.44
3 1 1000 1200 0.42
3 1 1000 1200 0.07
3 1 1000 1200 1.30
3 1 1000 3500 0.198
3 1 1000 3500 0.03
3 1 1000 3500 0.618
3 2 500 1200 0.199
3 2 500 1200 0.034
3 2 500 1200 0.621
3 2 500 3500 0.14
3 2 500 3500 0.02
3 2 500 3500 0.4
3 2 1000 1200 0.3
3 2 1000 1200 0.05
3 2 1000 1200 0.9
3 2 1000 3500 0.020
3 2 1000 3500 0.03
3 2 1000 3500 0.6
;
run;
* Note: mixer variable;
*     1=baffle type mixer, 2=aerodynamic type mixer, 3=existing reactor
mixer;
* Note: gas variable;
*     1=nitrogen, 2=argon;

proc reg data=percentagemixingratio;
      model mixingratio=mixer gas pressure temperature / clm cli r p
influence;

run;
```

APPENDIX G

TEMPERATURE PROFILES AT THE EXIT OF THE REACTOR MIXING ZONE BASED ON NITROGEN AND ARGON CARRIER GASES FLOWING THROUGH THE BAFFLE TYPE STATIC MIXER (CONCEPT 1)

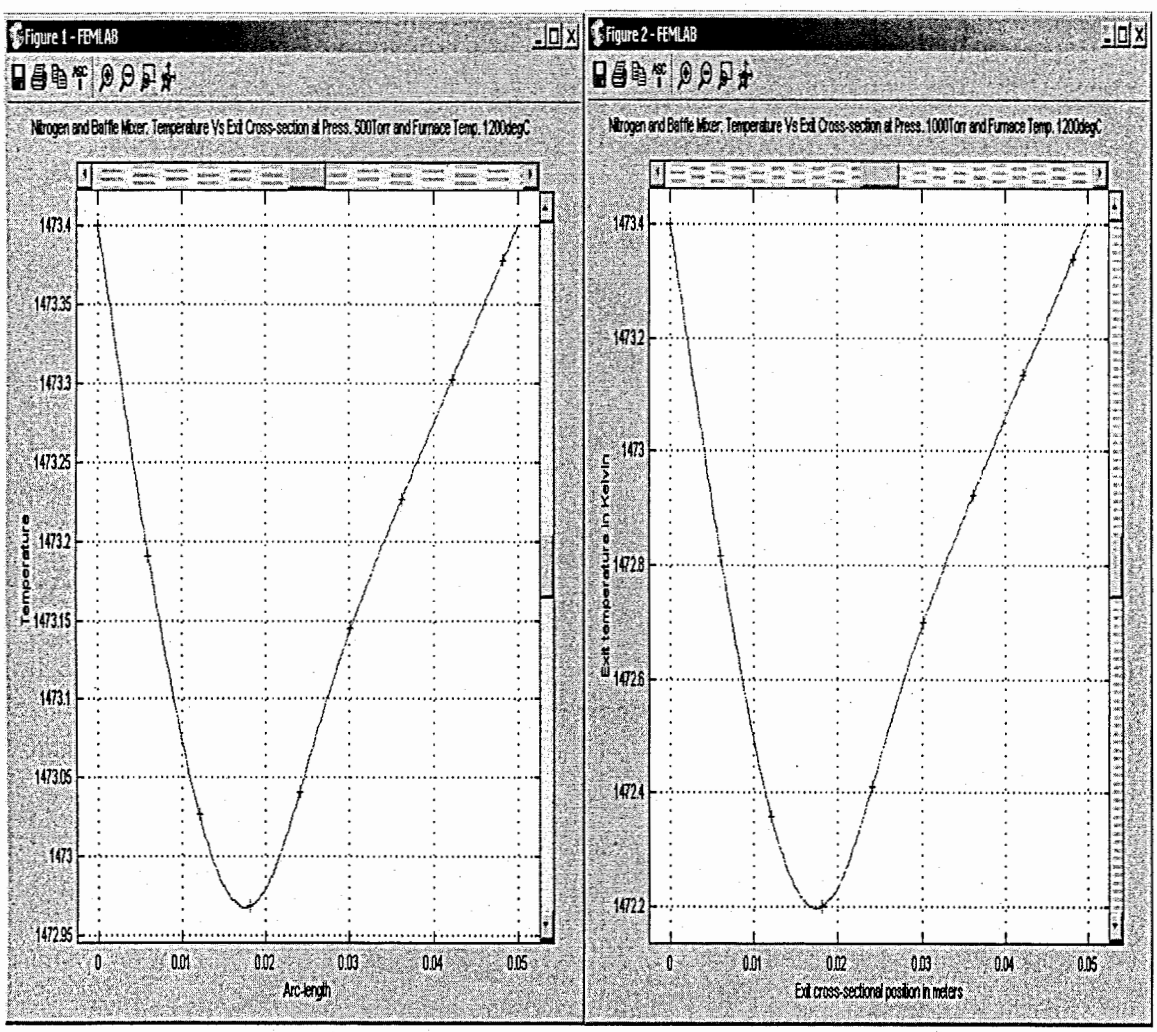

Figure G1. Plot of exit temperatures vs. vertical positions at the exit for nitrogen flowing through baffle type static mixer at 1200 °C (1473.4 K). The left figure shows plot at pressure of 500 Torr. (66650 Pa) and temperature of 1200 °C (1473.4 K). The right figure shows similar plot results but at a pressure of 1000 Torr. (133300 Pa).

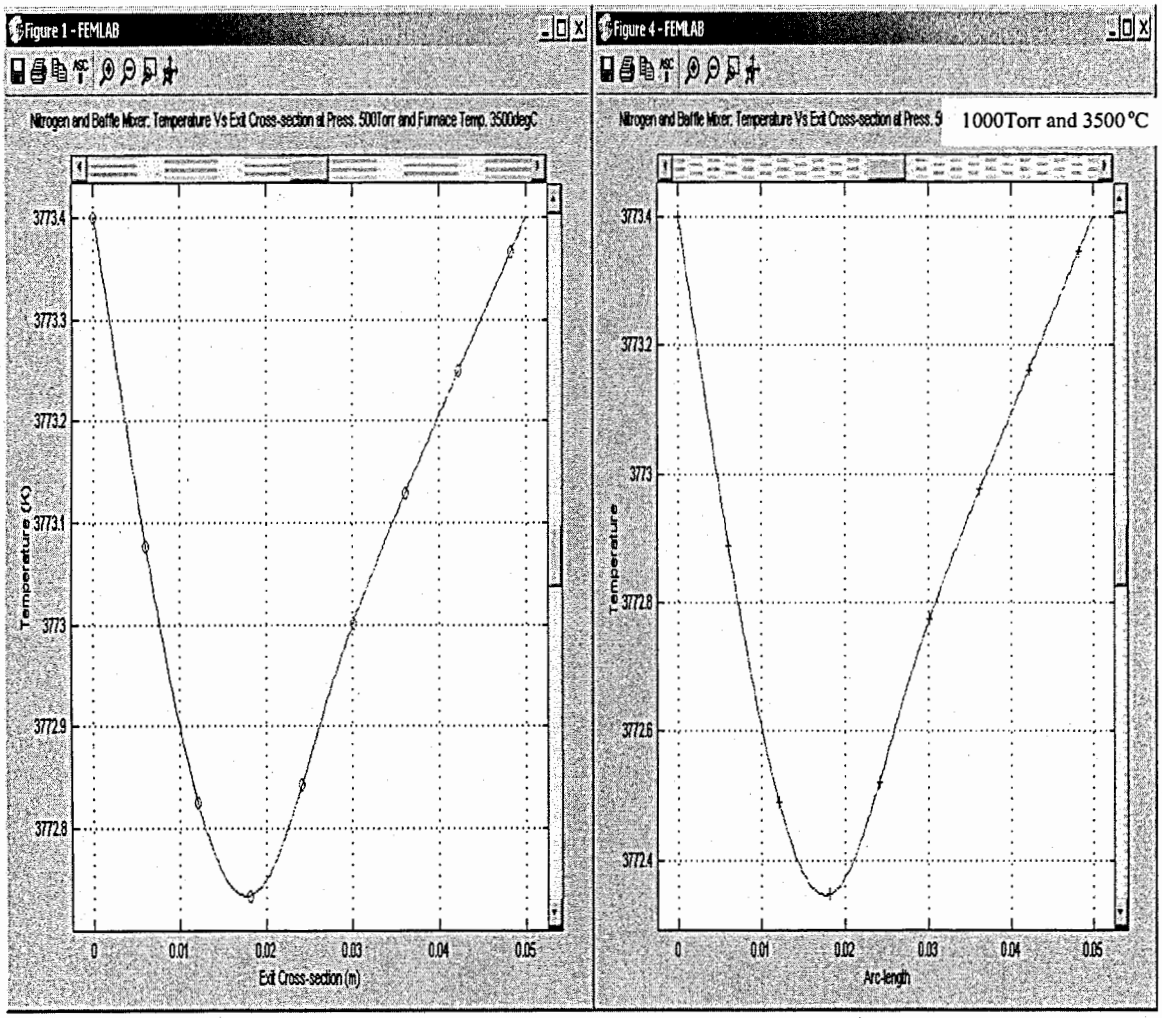

Figure G2. Plot of exit temperatures vs. vertical positions at the exit for nitrogen flowing through baffle type static mixer at 3500 °C (3773.4 K). The left figure shows plot at pressure of 500 Torr (66650 Pa) and temperature of 3500 °C (3773.4 K). The right figure shows similar plot results but at a pressure of 1000 Torr (133300 Pa).

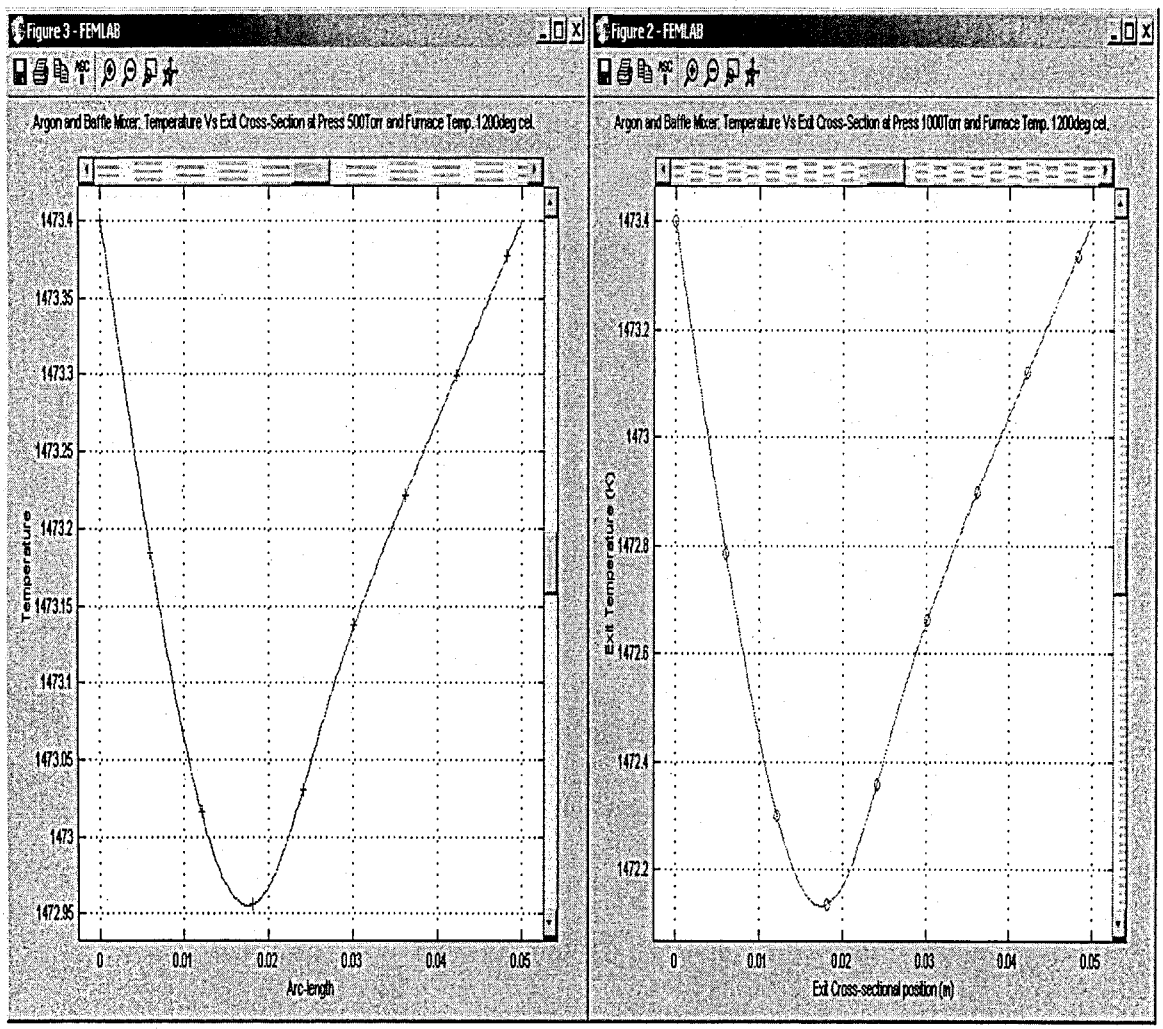

Figure G3. Plot of exit temperatures vs. vertical positions at the exit for argon flowing through baffle type static mixer at 1200 °C (1473.4 K). The left figure shows plot at pressure of 500 Torr. (66650 Pa) and temperature of 1200 °C (1473.4 K). The right figure shows similar plot results but at a pressure of 1000 Torr. (133300 Pa).

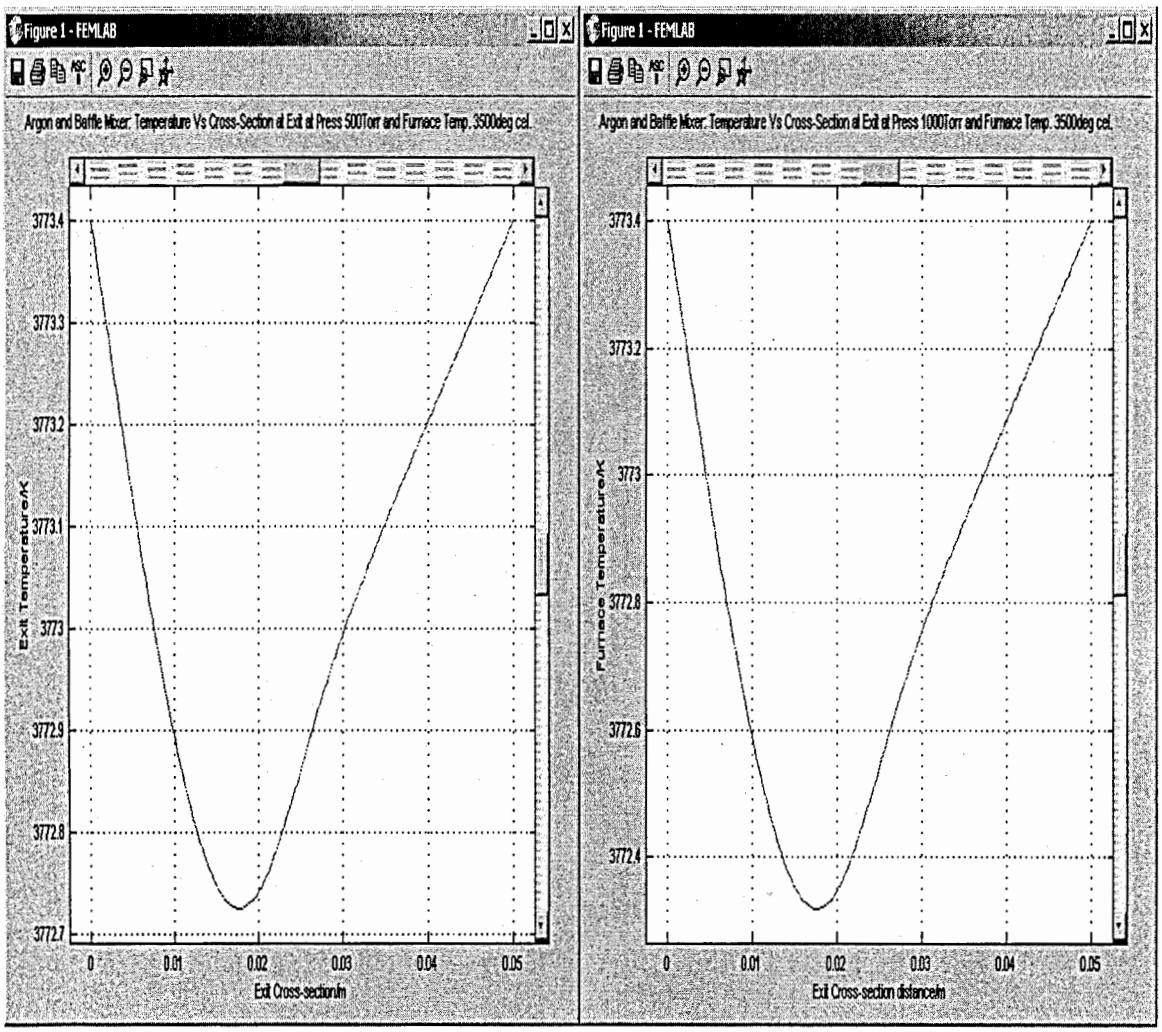

Figure G4. Plot of exit temperatures vs. vertical positions at the exit for argon flowing through baffle type static mixer at 3500 °C (3773.4 K). The left figure shows plot at pressure of 500 Torr (66650 Pa) and temperature of 3500 °C. (3773.4 K). The right figure shows similar plot results but at a pressure of 1000 Torr (133300 Pa).

APPENDIX H

TEMPERATURE PROFILES AT THE EXIT OF THE REACTOR MIXING ZONE BASED ON NITROGEN AND ARGON CARRIER GASES FLOWING THROUGH THE AERODYNAMIC TYPE STATIC MIXER (CONCEPT 2)

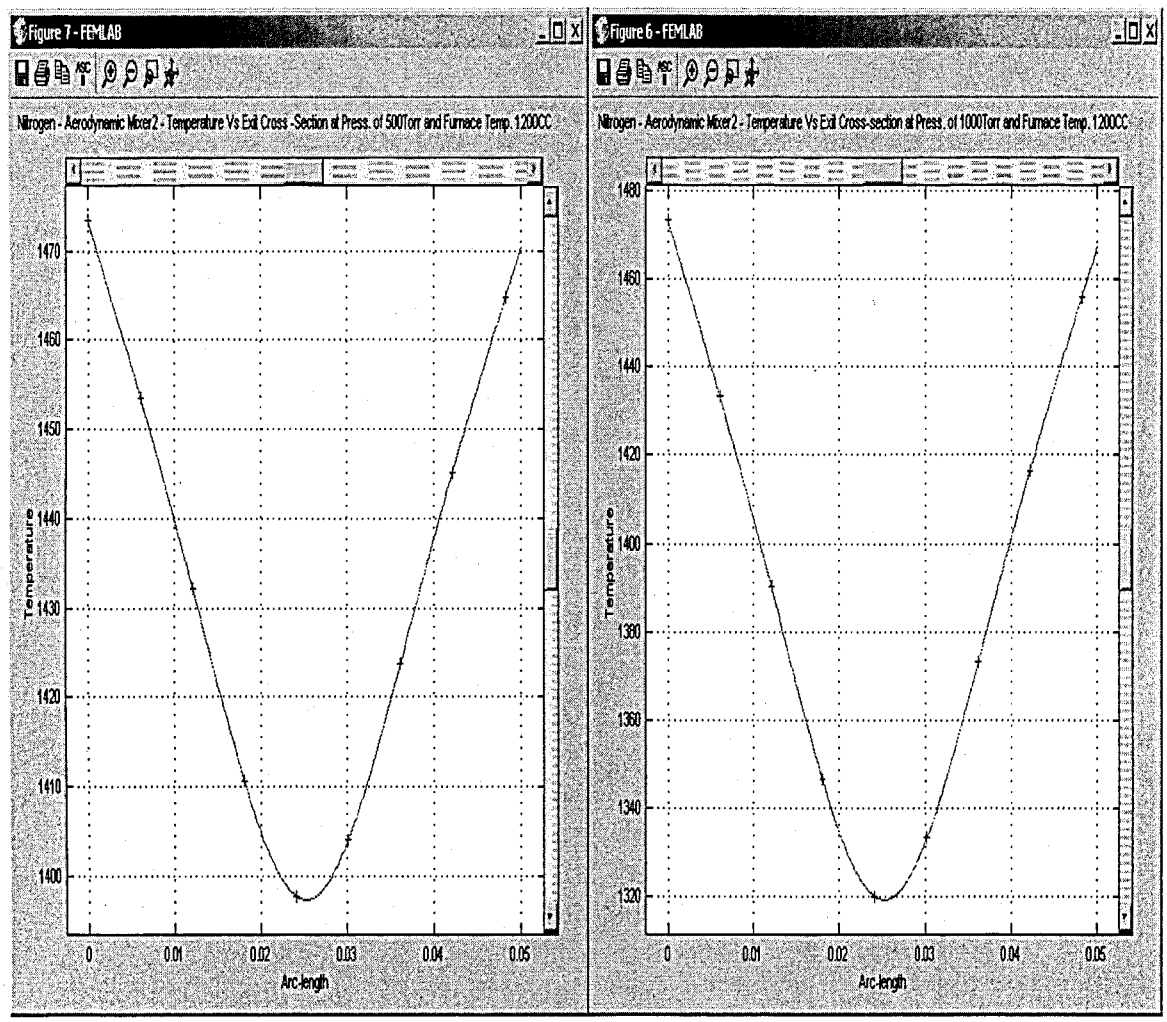

Figure H1. Plot of exit temperatures vs. vertical positions at the exit for nitrogen flowing through aerodynamic type static mixer at 1200 °C (1473.4 K). The left figure shows plot at pressure of 500 Torr. (66650 Pa) and temperature of 1200 °C (1473.4 K). The right figure shows similar plot results but at a pressure of 1000 Torr. (133300 Pa).

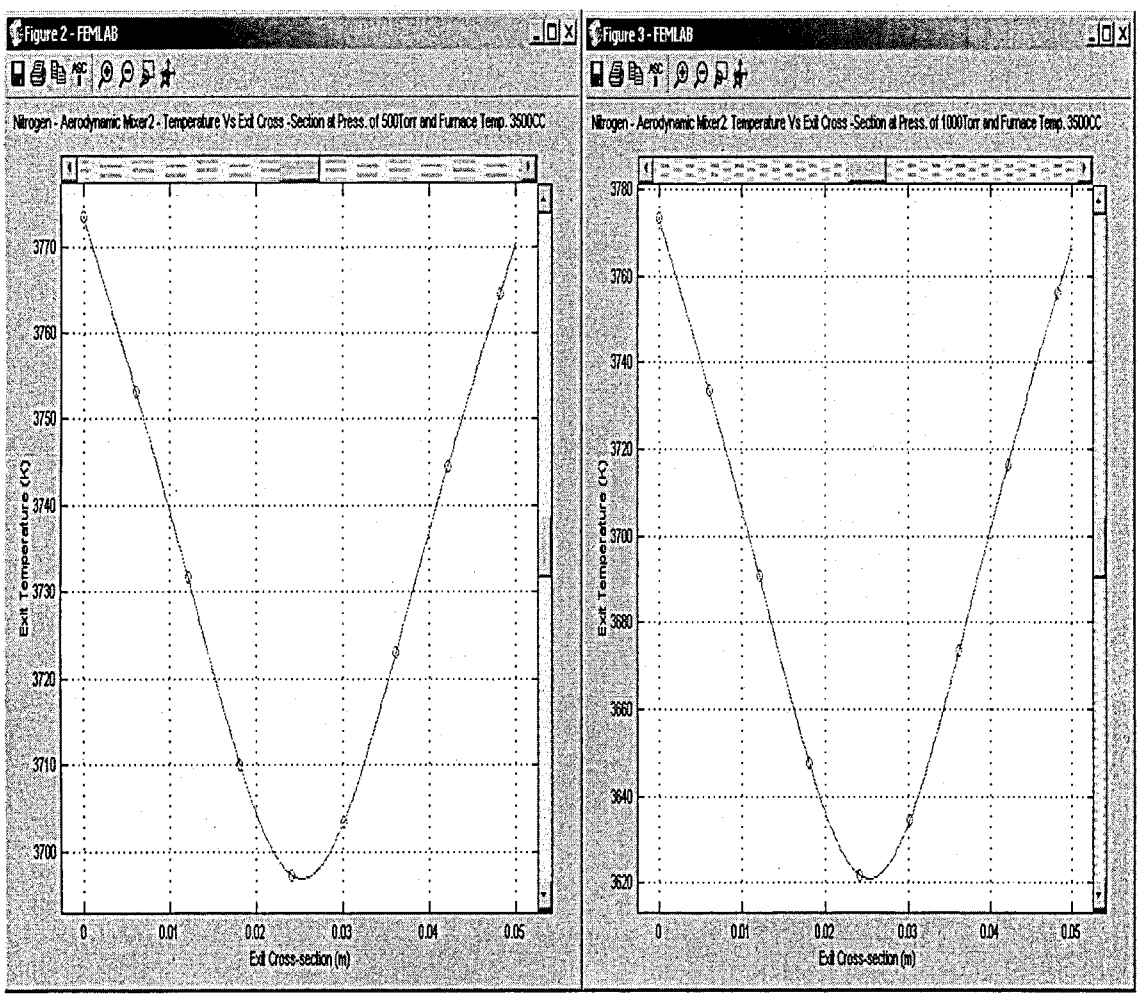

Figure H2. Plot of exit temperatures vs. vertical positions at the exit for nitrogen flowing through aerodynamic type static mixer at 3500 °C (3773.4 K). The left figure shows plot at pressure of 500 Torr (66650 Pa) and temperature of 3500 °C (3773.4 K). The right figure shows similar plot results but at a pressure of 1000 Torr (133300 Pa).

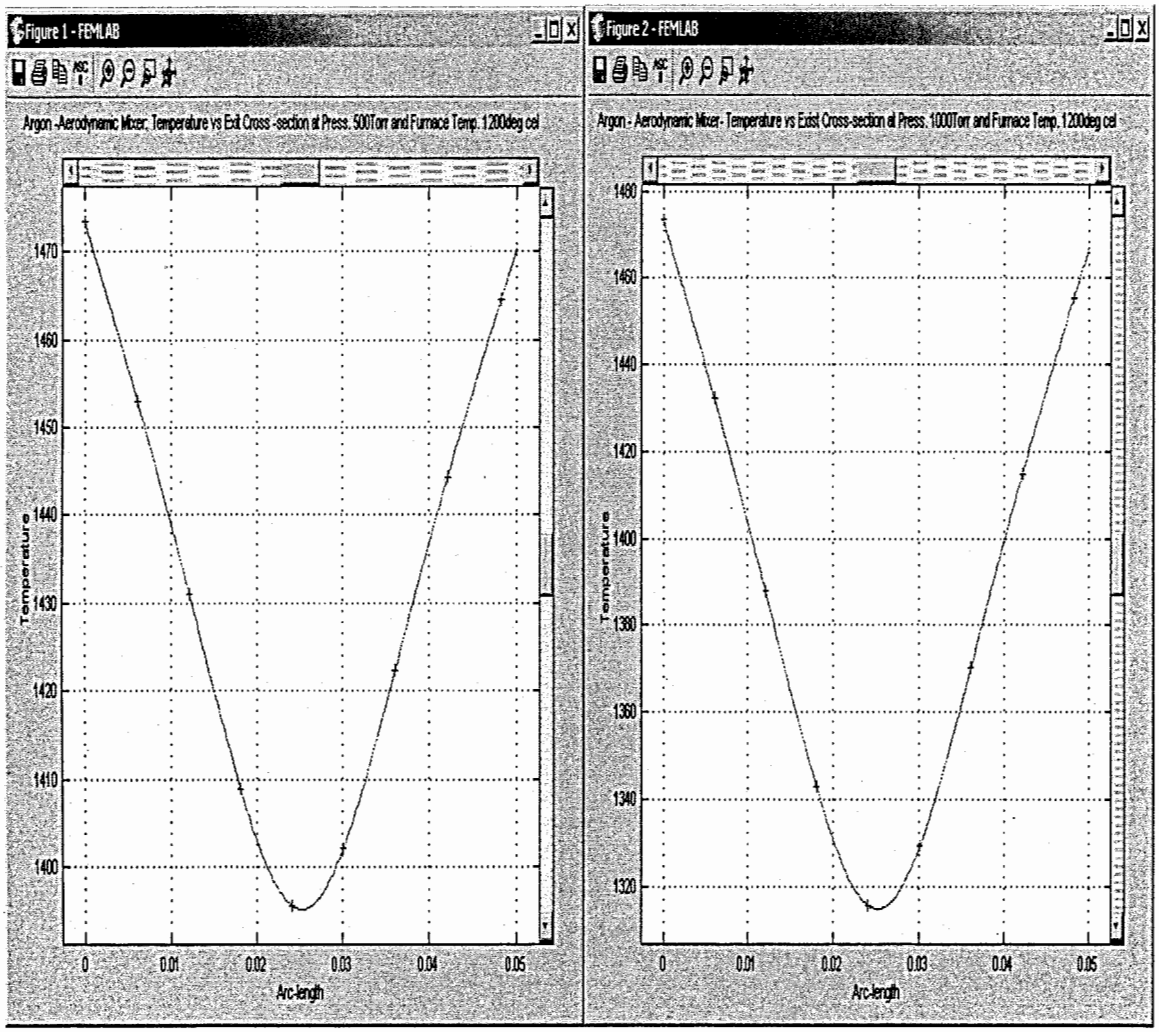

Figure H3. Plot of exit temperatures vs. vertical positions at the exit for argon flowing through aerodynamic type static mixer at 1200 °C (1473.4 K). The left figure shows plot at pressure of 500 Torr. (66650 Pa) and temperature of 1200 °C (1473.4 K). The right figure shows similar plot results but at a pressure of 1000 Torr. (133300 Pa).

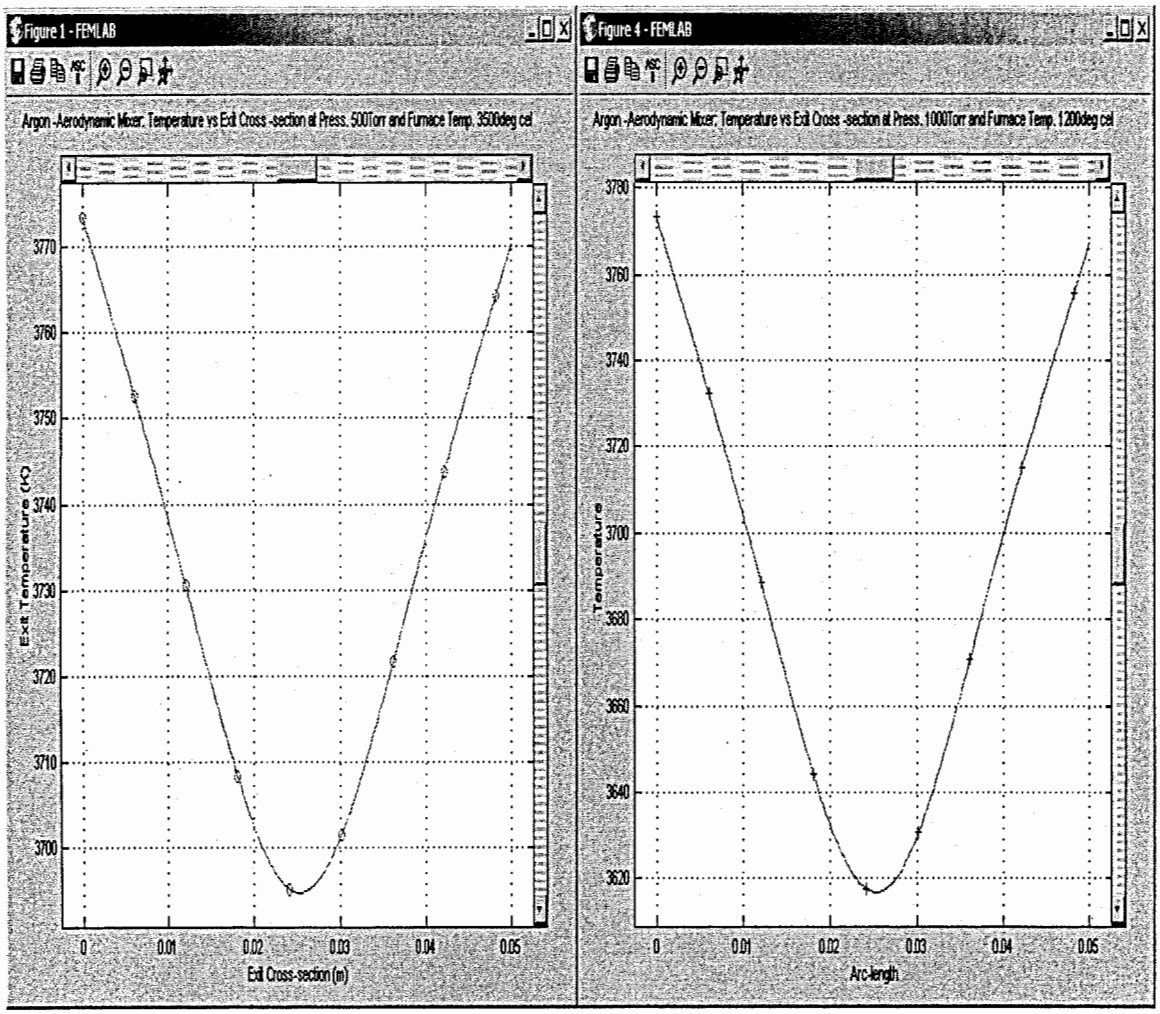

Figure H4. Plot of exit temperatures vs. vertical positions at the exit for argon flowing through aerodynamic type static mixer at 3500 °C (3773.4 K). The left figure shows plot at pressure of 500 Torr (66650 Pa) and temperature of 3500 °C. (3773.4 K). The right figure shows similar plot results but at a pressure of 1000 Torr (133300 Pa).

APPENDIX I

TEMPERATURE PROFILES AT THE EXIT OF THE REACTOR MIXING ZONE BASED ON NITROGEN AND ARGON CARRIER GASES FLOWING THROUGH THE EXISTING REACTOR WITHOUT STATIC MIXER (CONCEPT 3)

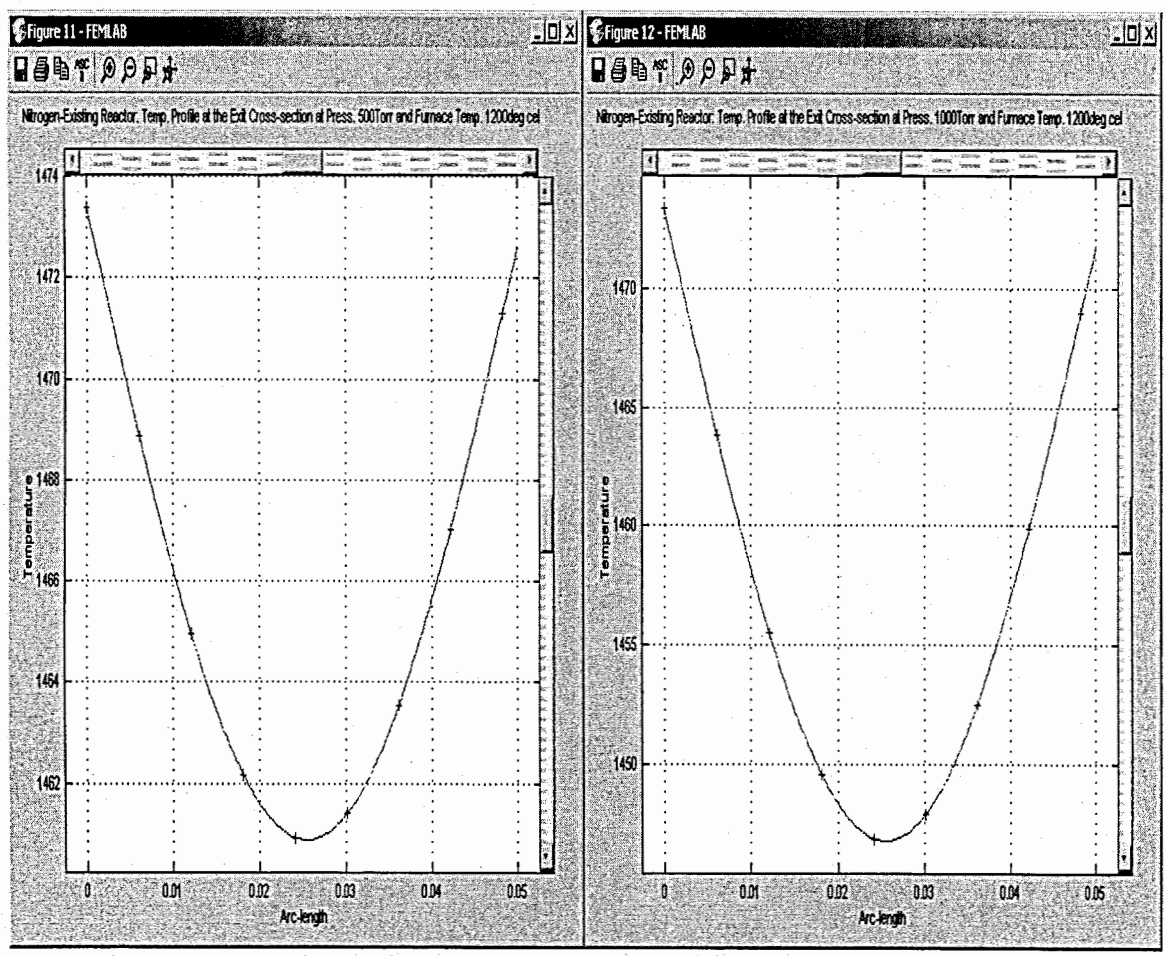

Figure I1. Plot of exit temperatures vs. vertical positions at the exit for nitrogen flowing through an existing reactor at 1200 °C (1473.4 K). The left figure shows plot at pressure of 500 Torr. (66650 Pa) and temperature of 1200 °C (1473.4 K). The right figure shows similar plot results but at a pressure of 1000 Torr. (133300 Pa).

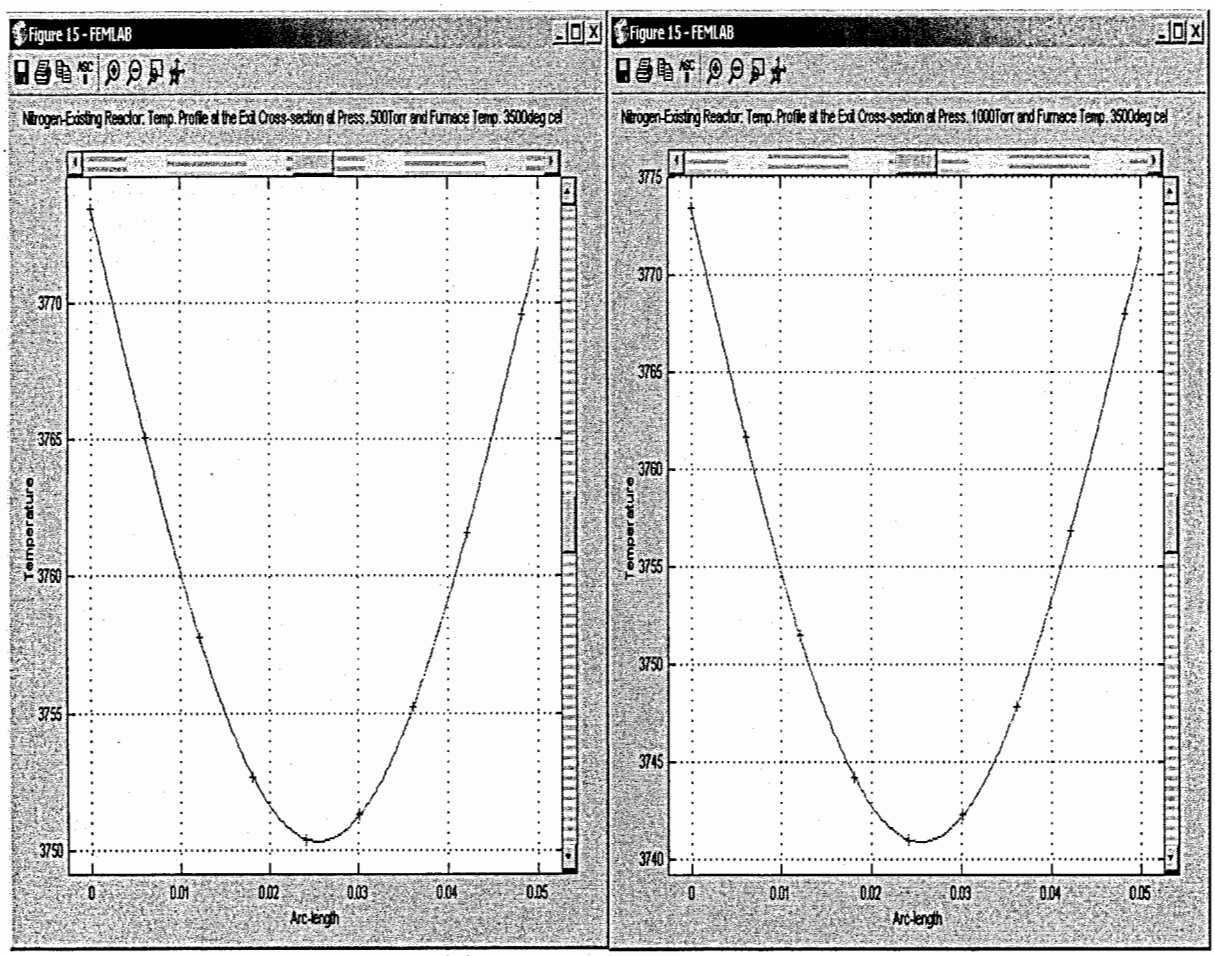

Figure I2. Plot of exit temperatures vs. vertical positions at the exit for nitrogen flowing through existing reactor without a mixer at 3500 °C (3773.4 K). The left figure shows plot at pressure of 500 Torr (66650 Pa) and temperature of 3500 °C. (3773.4 K). The right figure shows similar plot results but at a pressure of 1000 Torr (133300 Pa).

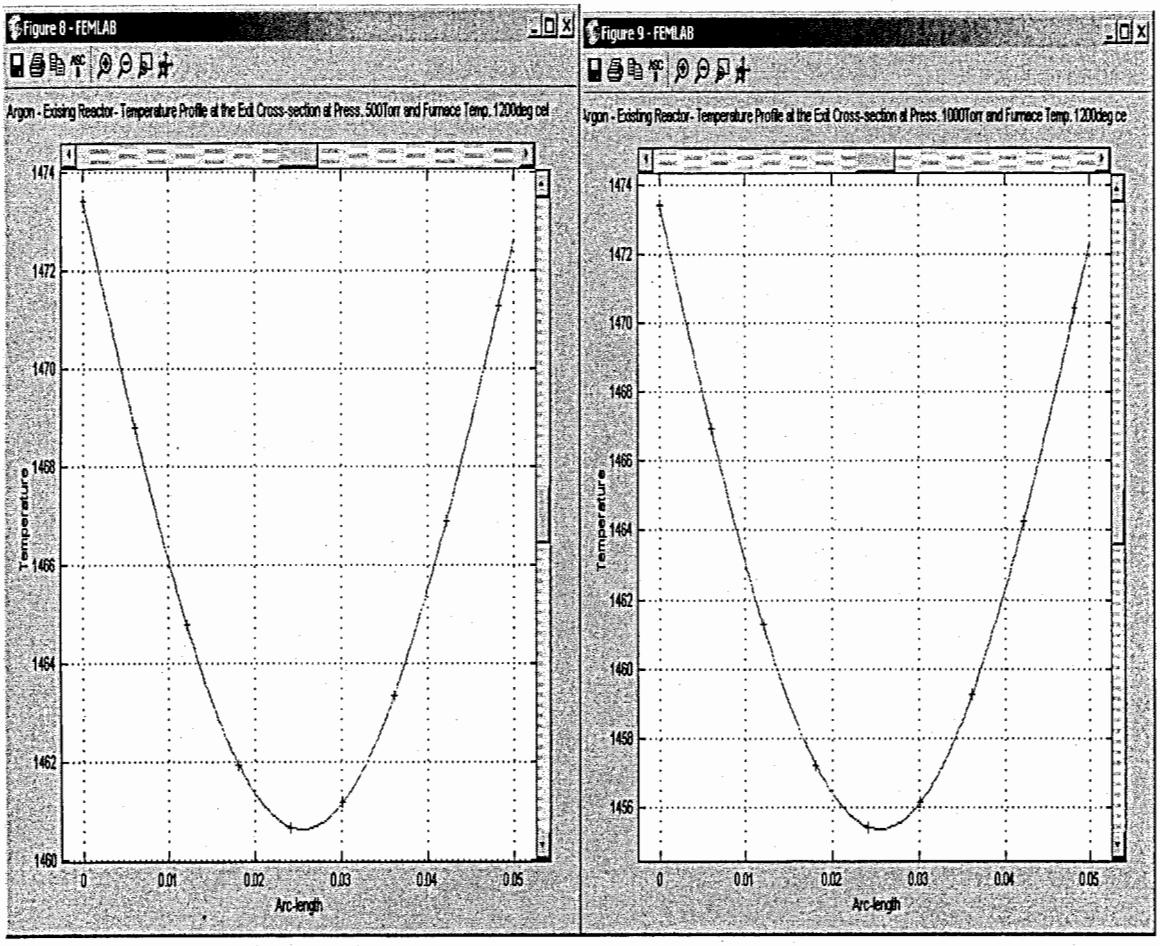

Figure I3. Plot of exit temperatures vs. vertical positions at the exit for argon gas flowing through an existing reactor at 1200 °C (1473.4 K). The left figure shows plot at pressure of 500 Torr. (66650 Pa) and temperature of 1200 °C (1473.4 K). The right figure shows similar plot results but at a pressure of 1000 Torr. (133300 Pa).

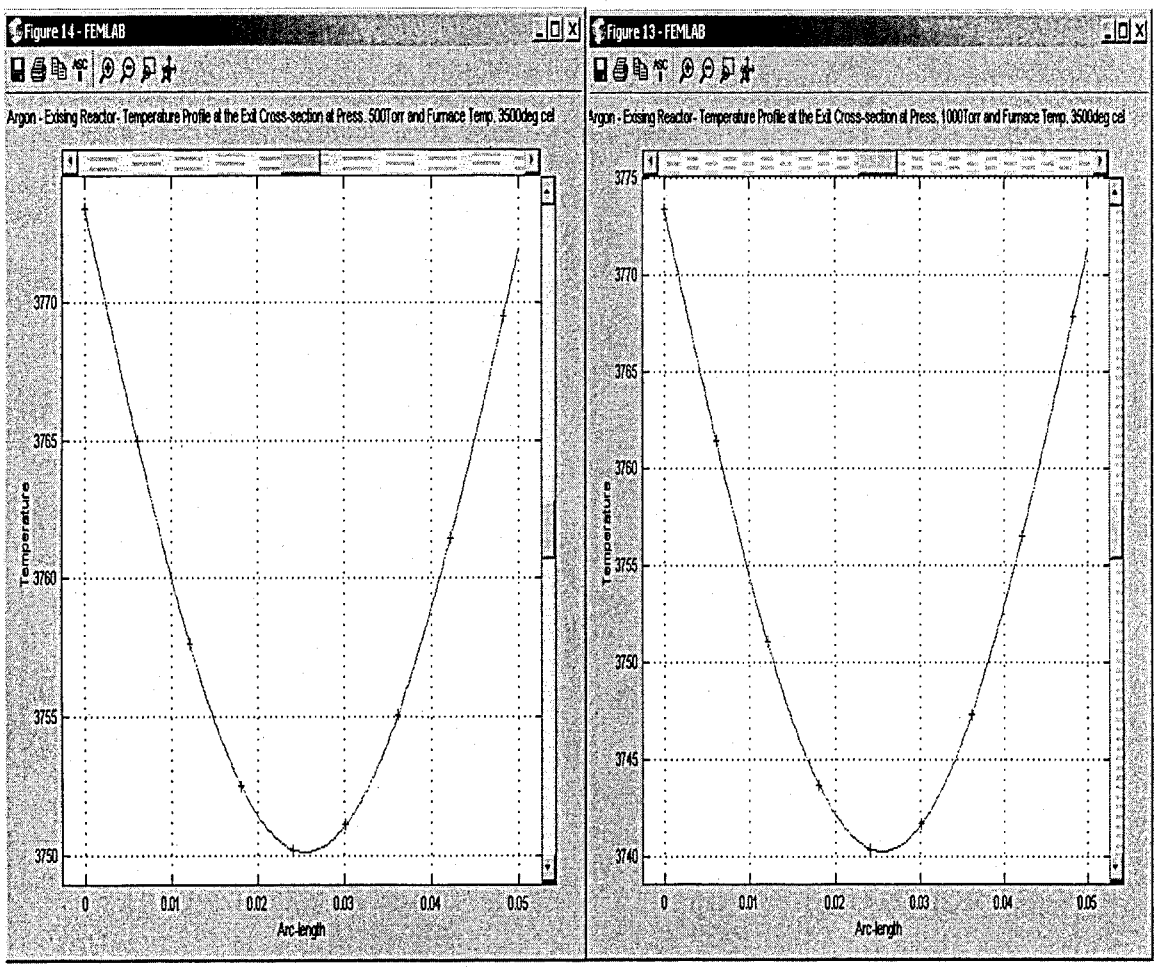

Figure I4. Plot of exit temperatures vs. vertical positions at the exit for argon flowing through existing reactor without a mixer at 3500 °C (3773.4 K). The left figure shows plot at pressure of 500 Torr (66650 Pa) and temperature of 3500 °C. (3773.4 K). The right figure shows similar plot results but at a pressure of 1000 Torr (133300 Pa).

APPENDIX J

STREAM LINES IN THE MODEL REACTOR MIXING ZONE BASED ON NITROGEN AND ARGON CARRIER GASES FLOWING THROUGH THE BAFFLE TYPE STATIC MIXER (CONCEPT 1)

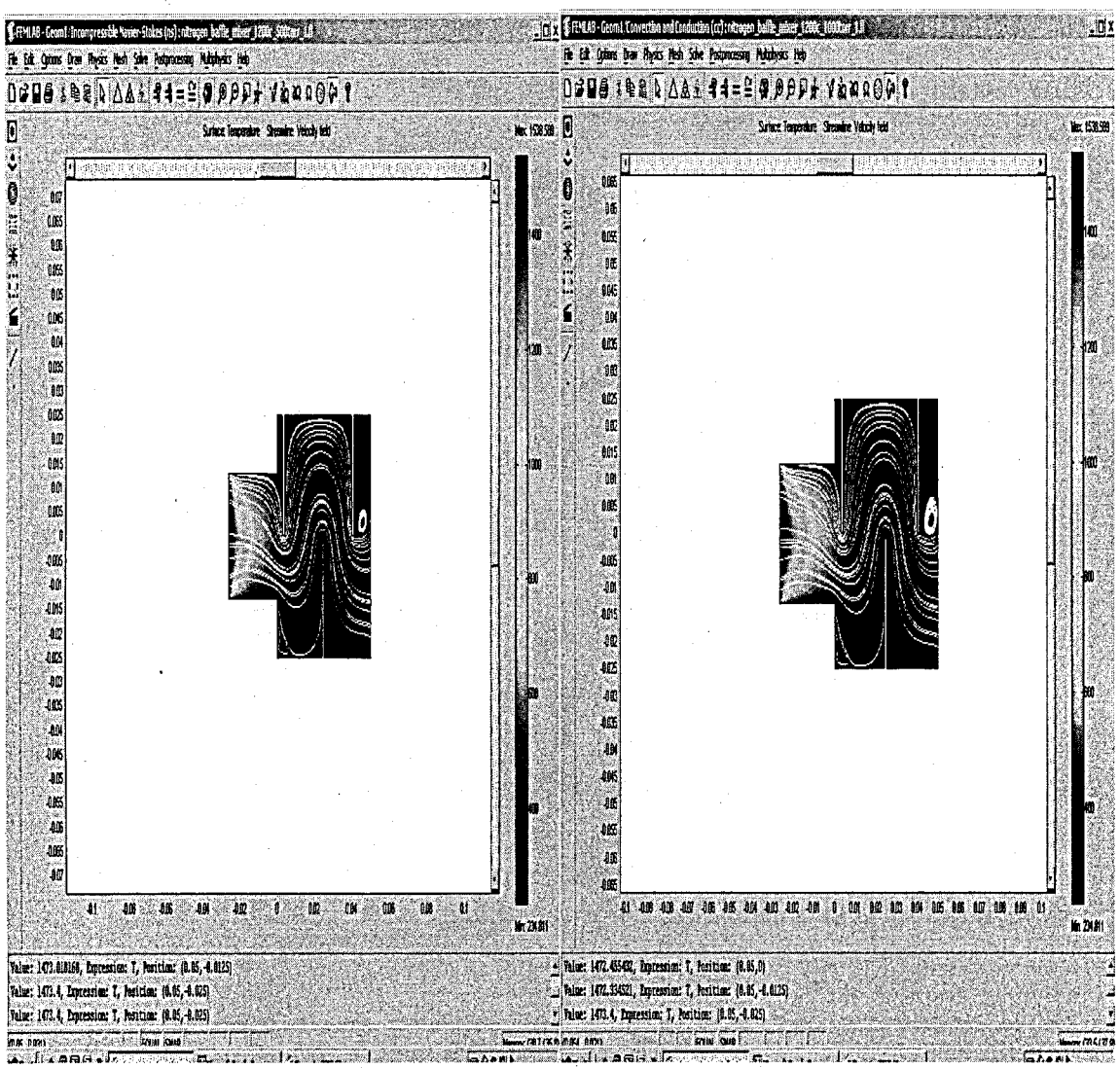

Figure J1. Streamlines in the model reactor due to nitrogen flowing through the baffle type static mixer at 1200 °C (1473.4 K). The left figure shows streamlines at pressure of 500 Torr (66650 Pa) and temperature of 1200 °C (1473.4 K). The right figure shows similar streamlines but at a pressure of 1000 Torr (133300 Pa).

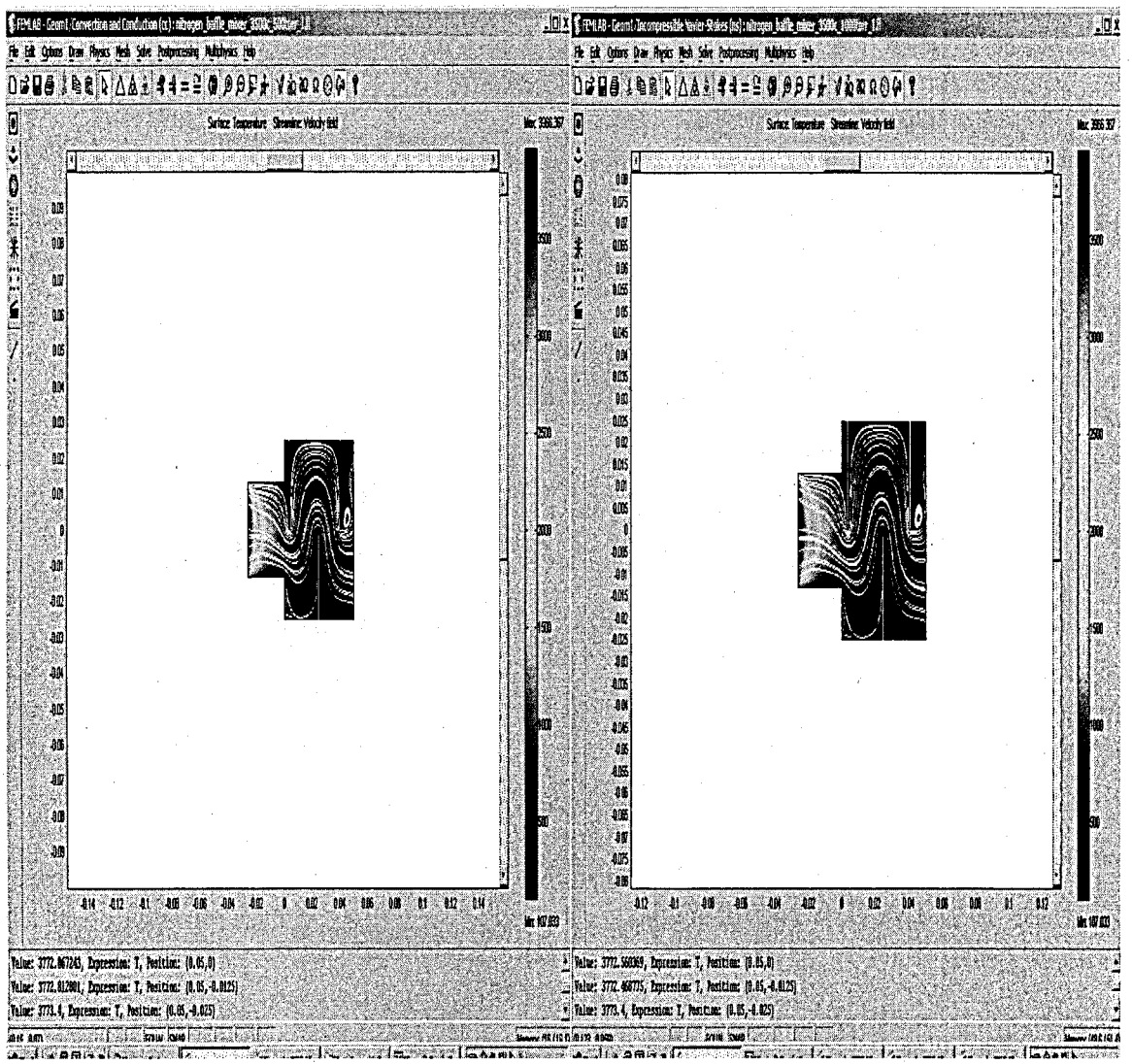

Figure J2. Streamlines in the model reactor due to nitrogen flowing through the baffle type static mixer at 3500 °C (3773.4 K). The left figure shows streamlines at pressure of 500 Torr (66650 Pa) and temperature of 3500 °C (3773.4 K). The right figure shows similar streamlines but at a pressure of 1000 Torr (133300 Pa).

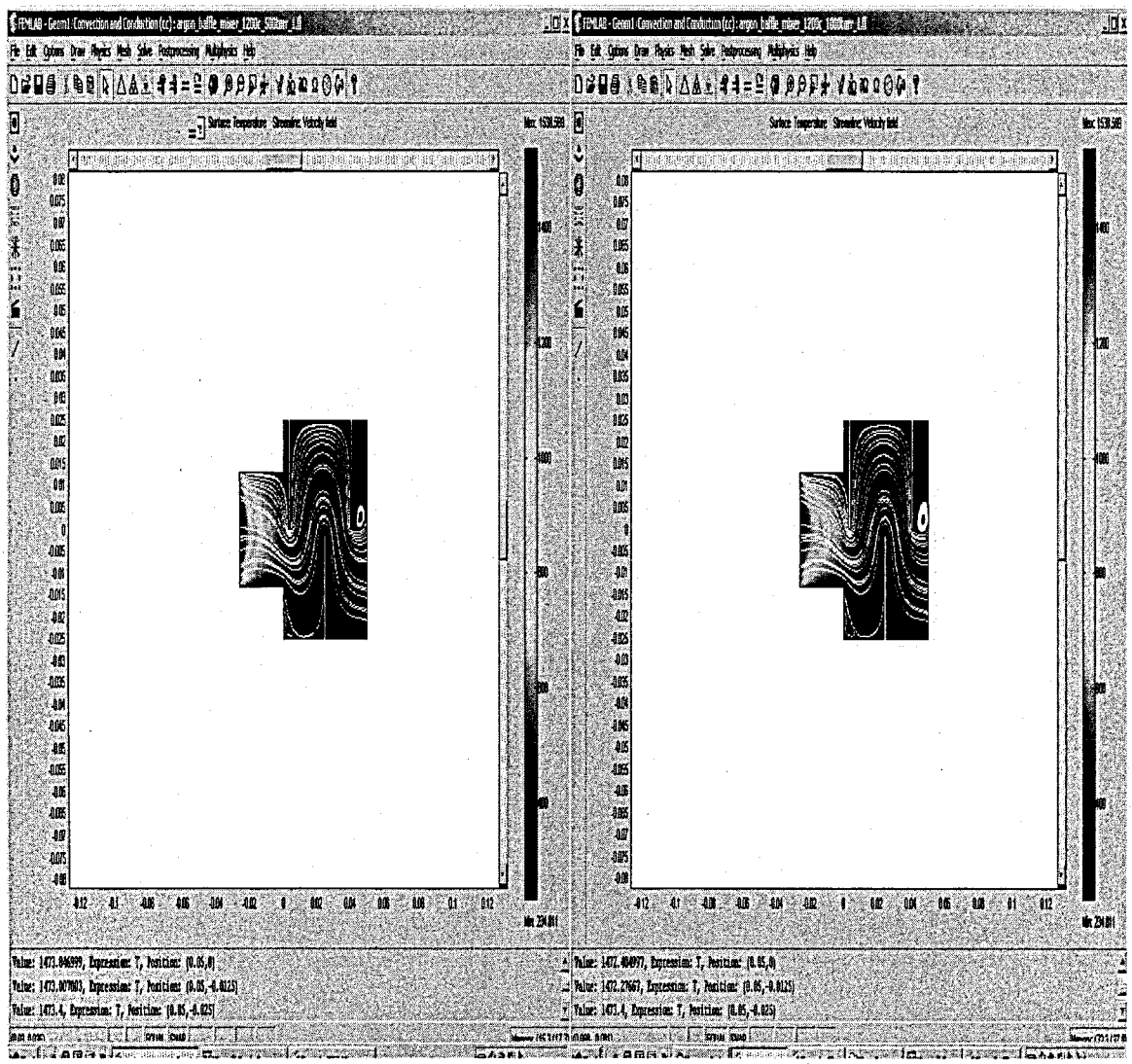

Figure J3. Streamlines in the model reactor due to argon flowing through the baffle type static mixer at 1200 °C (1473.4 K). The left figure shows streamlines at pressure of 500 Torr (66650 Pa) and temperature of 1200 °C (1473.4 K). The right figure shows similar streamlines but at a pressure of 1000 Torr (133300 Pa).

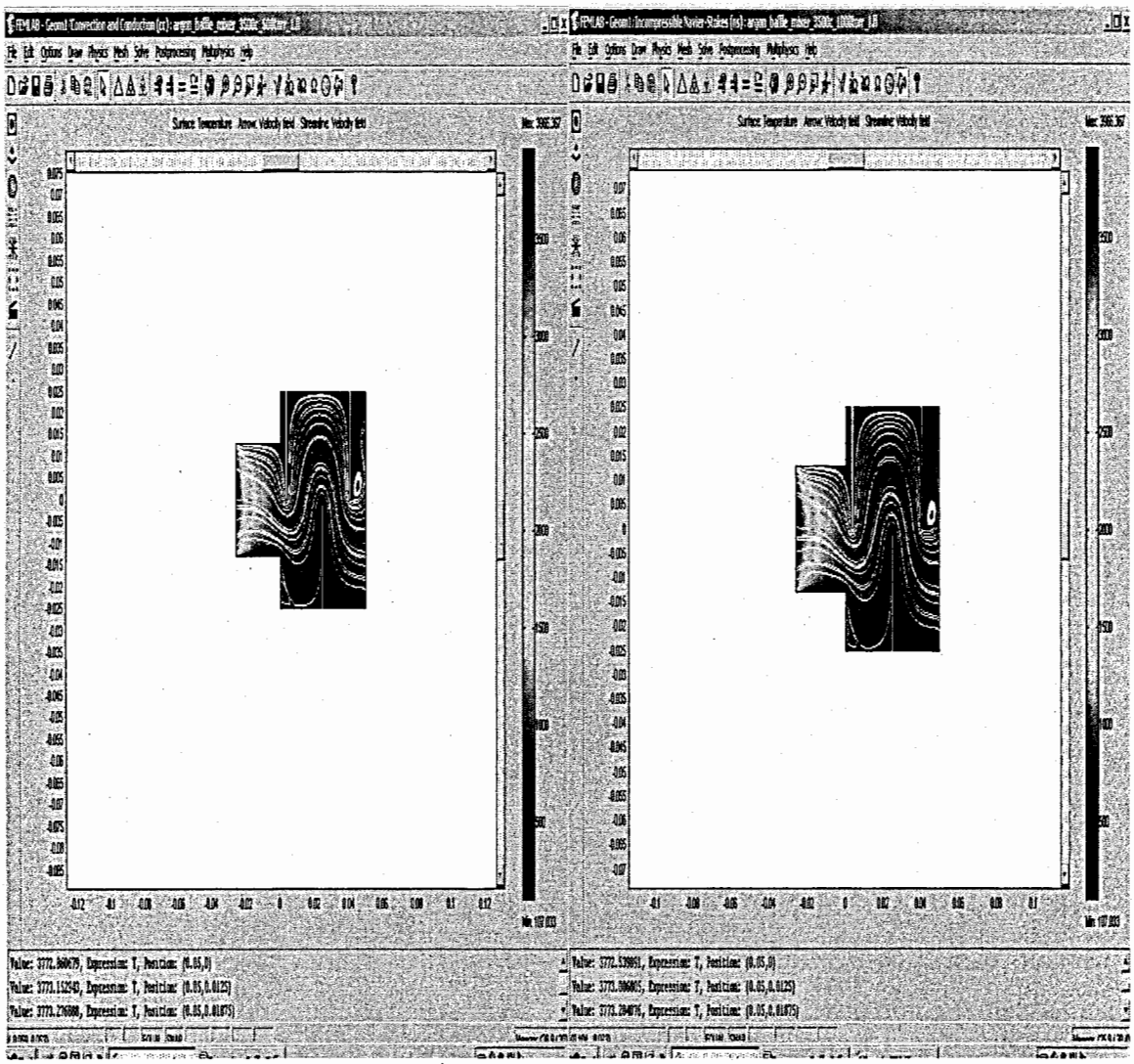

Figure J4. Streamlines in the model reactor due to argon flowing through the baffle type static mixer at 3500 °C (3773.4 K). The left figure shows streamlines at pressure of 500 Torr (66650 Pa) and temperature of 3500 °C (3773.4 K). The right figure shows similar streamlines but at a pressure of 1000 Torr (133300 Pa).

APPENDIX K

STREAM LINES IN THE MODELED REACTOR MIXING ZONE BASED ON NITROGEN AND ARGON CARRIER GASES FLOWING THROUGH THE AERODYNAMIC TYPE STATIC MIXER (CONCEPT 2)

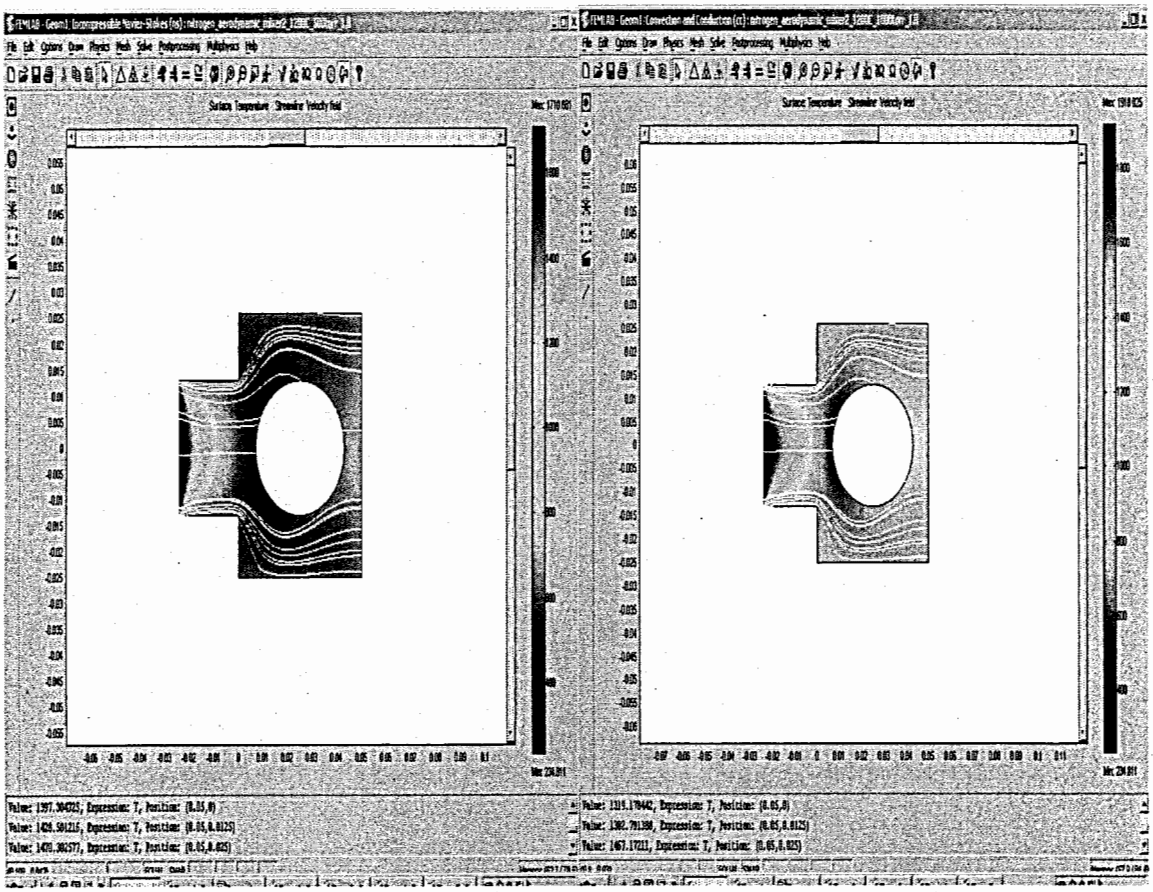

Figure K1. Streamlines in the model reactor due to nitrogen flowing through the aerodynamic type static mixer at 1200 °C (1473.4 K). The left figure shows streamlines at pressure of 500 Torr (66650 Pa) and temperature of 1200 °C (1473.4 K). The right figure shows similar streamlines but at a pressure of 1000 Torr (133300 Pa).

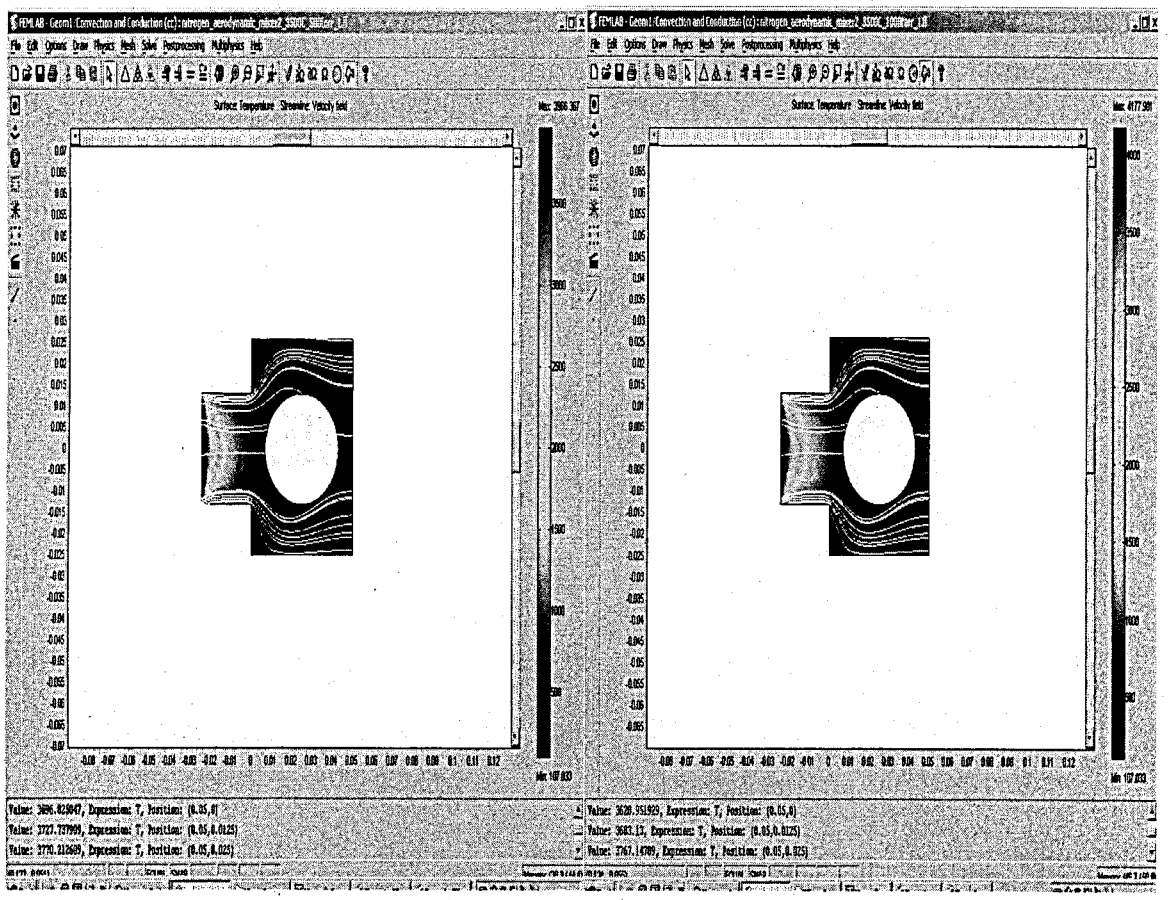

Figure K2. Streamlines in the model reactor due to nitrogen flowing through the aerodynamic type static mixer at 3500 °C (3773.4 K). The left figure shows streamlines at pressure of 500 Torr (66650 Pa) and temperature of 3500 °C (3773.4 K). The right figure shows similar streamlines but at a pressure of 1000 Torr (133300 Pa).

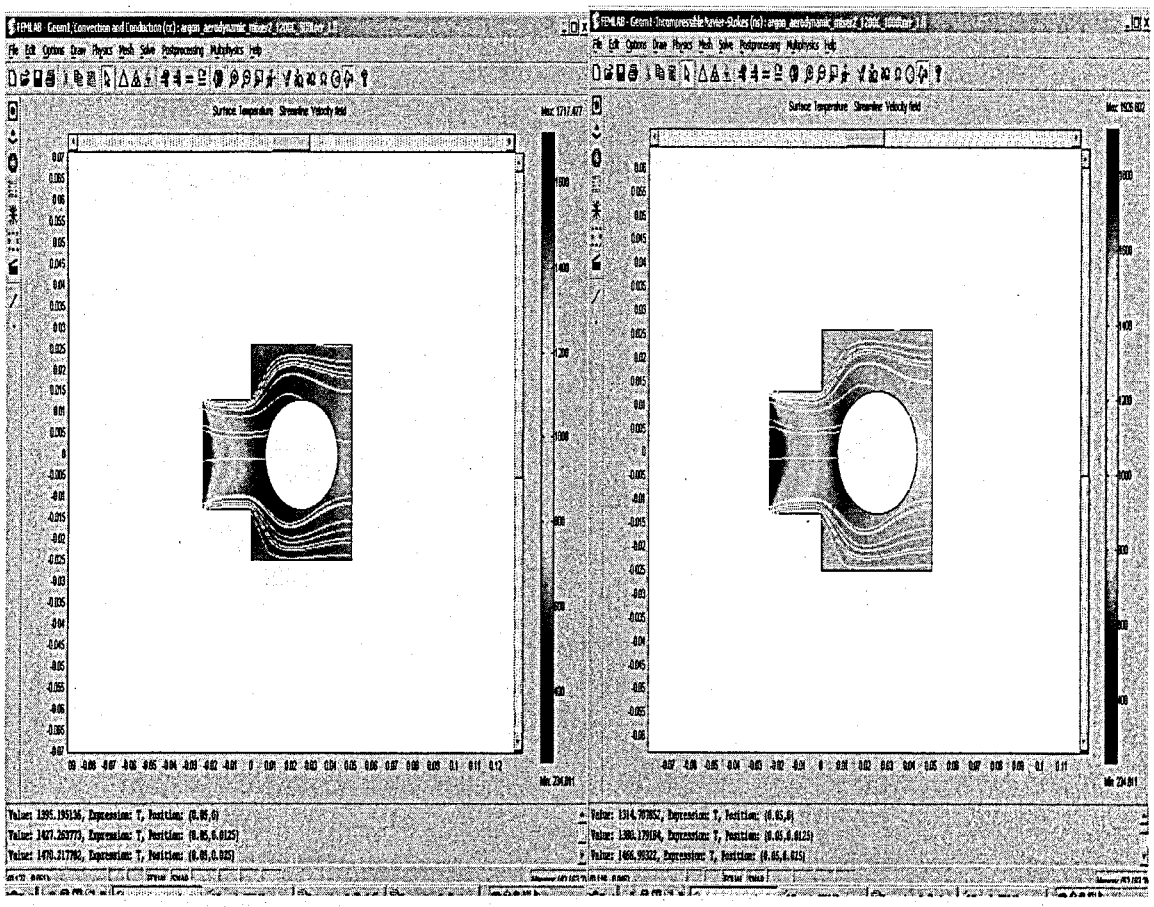

Figure K3. Streamlines in the model reactor due to argon flowing through the aerodynamic type static mixer at 1200 °C (1473.4 K). The left figure shows streamlines at pressure of 500 Torr (66650 Pa) and temperature of 1200 °C (1473.4 K). The right figure shows similar streamlines but at a pressure of 1000 Torr (133300 Pa). The argon carrier gas flow rate is 0.0045 m/s and the inlet temperature is 300 K.

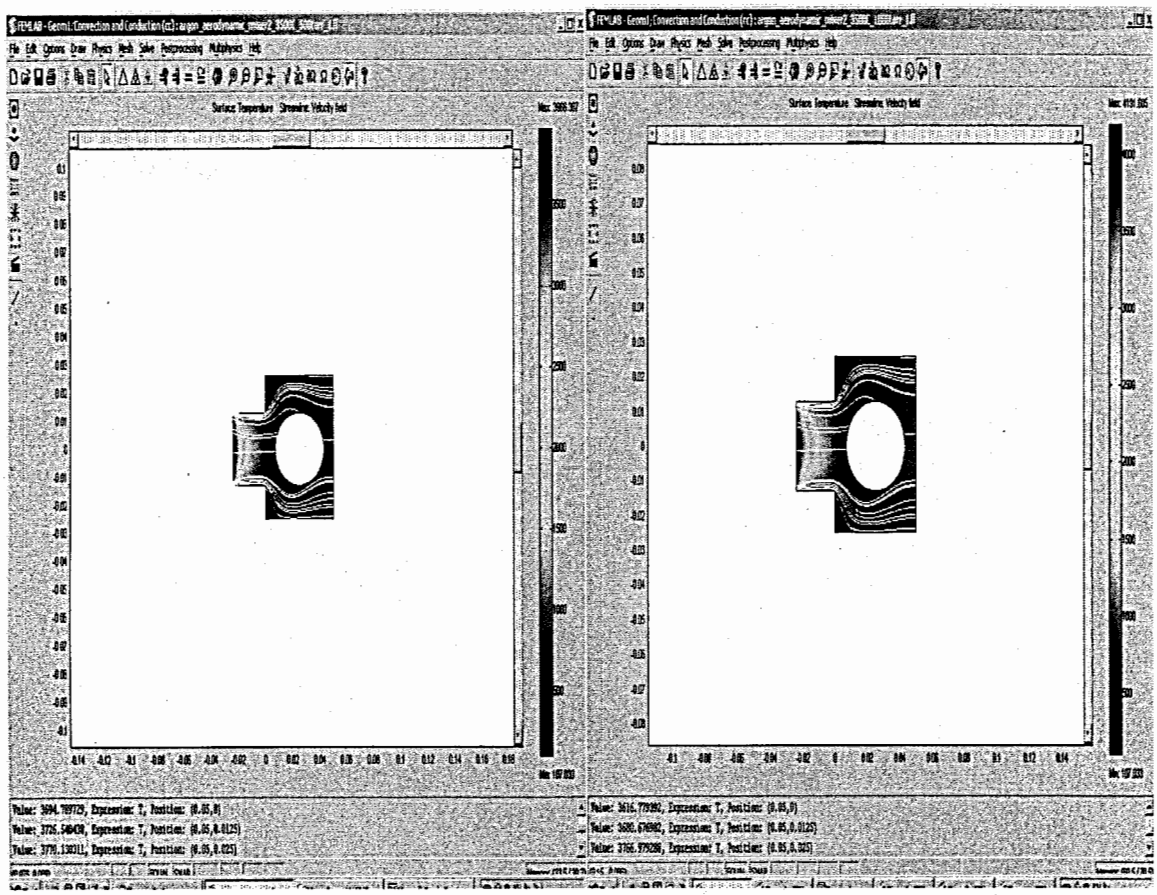

Figure K4. Streamlines in the model reactor due to argon flowing through the aerodynamic type static mixer at 3500 °C (3773.4 K). The left figure shows streamlines at pressure of 500 Torr (66650 Pa) and temperature of 3500 °C (3773.4 K). The right figure shows similar streamlines but at a pressure of 1000 Torr (133300 Pa).

APPENDIX L

STREAM LINES IN THE MODELED REACTOR MIXING ZONE BASED ON NITROGEN AND ARGON CARRIER GASES FLOWING THROUGH THE EXISTING REACTOR WITHOUT MIXER STATIC MIXER (CONCEPT 3)

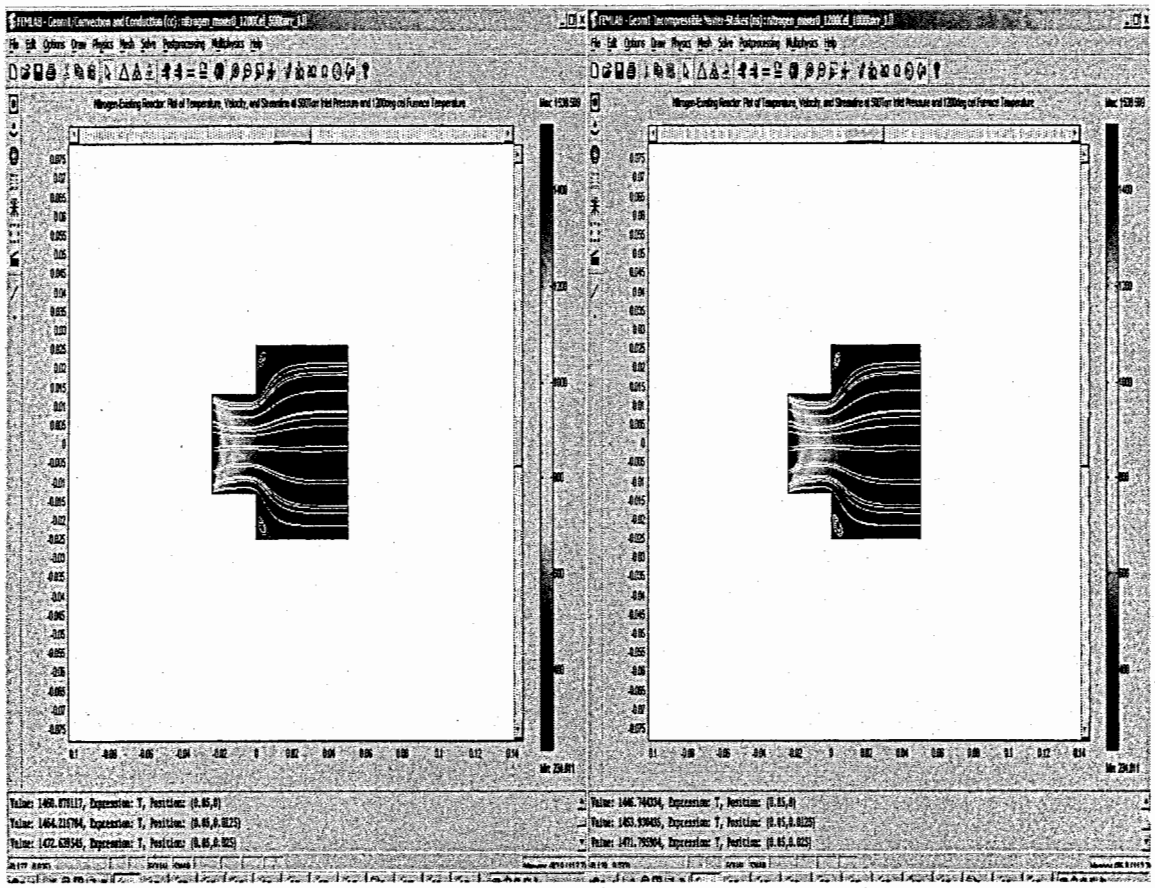

Figure L1. Streamlines in the model reactor due to nitrogen flowing through the existing reactor without static mixer at 1200 °C (1473.4 K). The left figure shows streamlines at pressure of 500 Torr (66650 Pa) and temperature of 1200 °C (1473.4 K). The right figure shows similar streamlines but at a pressure of 1000 Torr (133300 Pa).

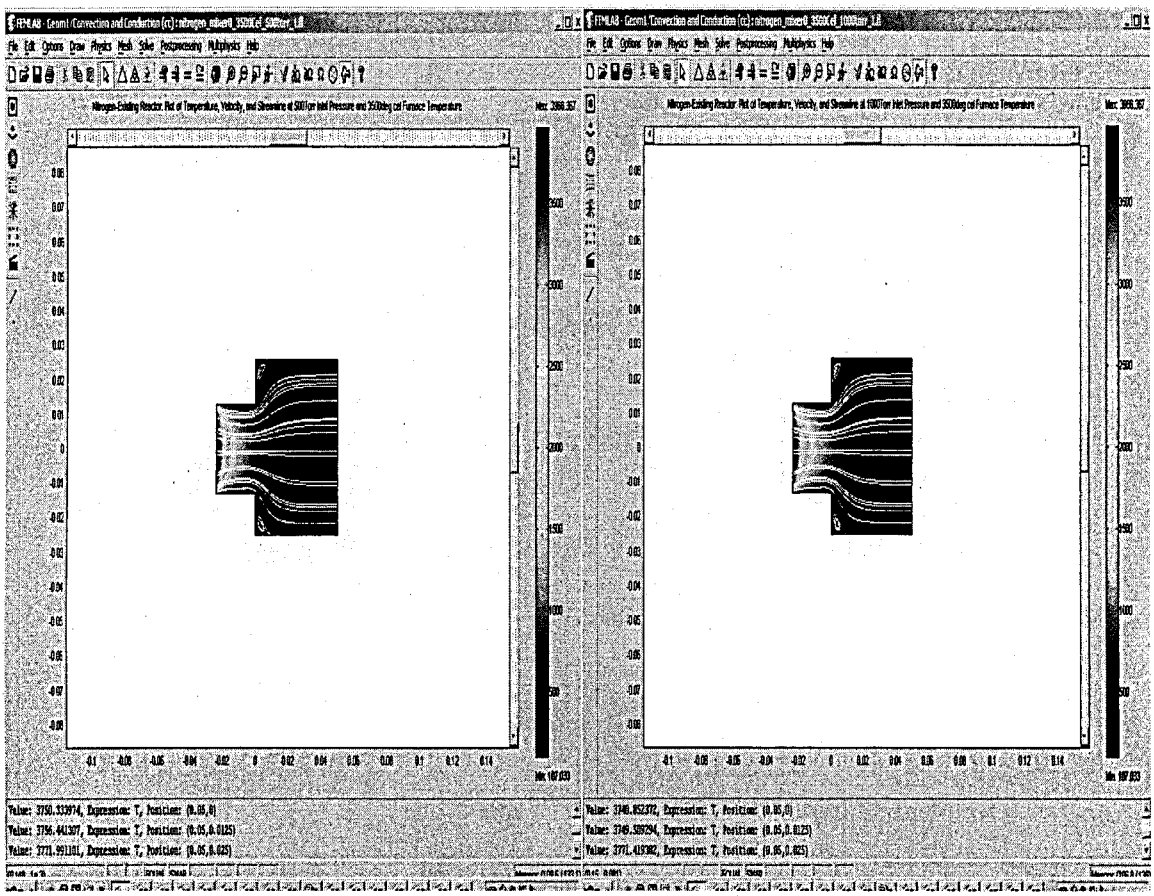

Figure L2. Streamlines in the model reactor due to nitrogen flowing through the existing reactor without static mixer at 3500 °C (3773.4 K). The left figure shows streamlines at pressure of 500 Torr (66650 Pa) and temperature of 3500 °C (3773.4 K). The right figure shows similar streamlines but at a pressure of 1000 Torr (133300 Pa).

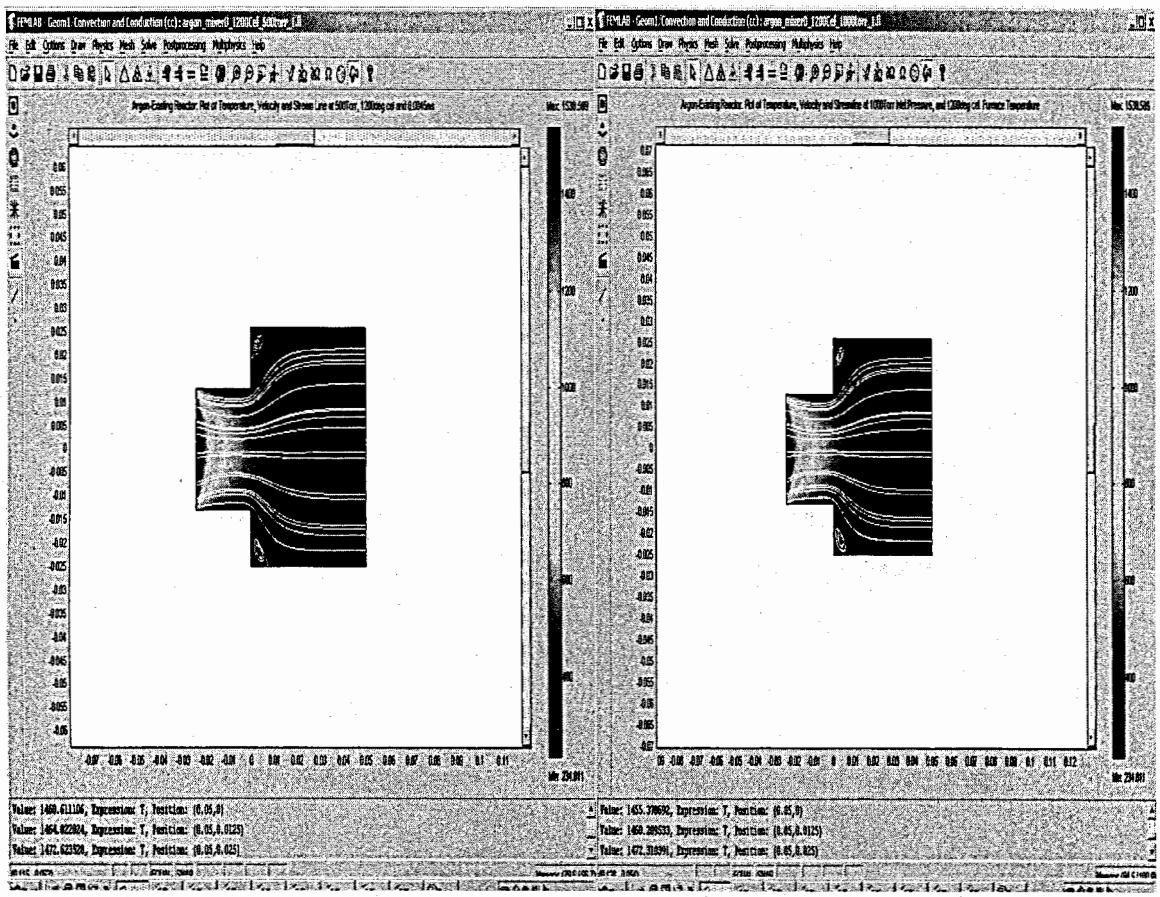

Figure L3. Streamlines in the model reactor due to argon flowing through the existing reactor without static mixer at 1200 °C (1473.4 K). The left figure shows streamlines at pressure of 500 Torr (66650 Pa) and temperature of 1200 °C (1473.4 K). The right figure shows similar streamlines but at a pressure of 1000 Torr (133300 Pa).

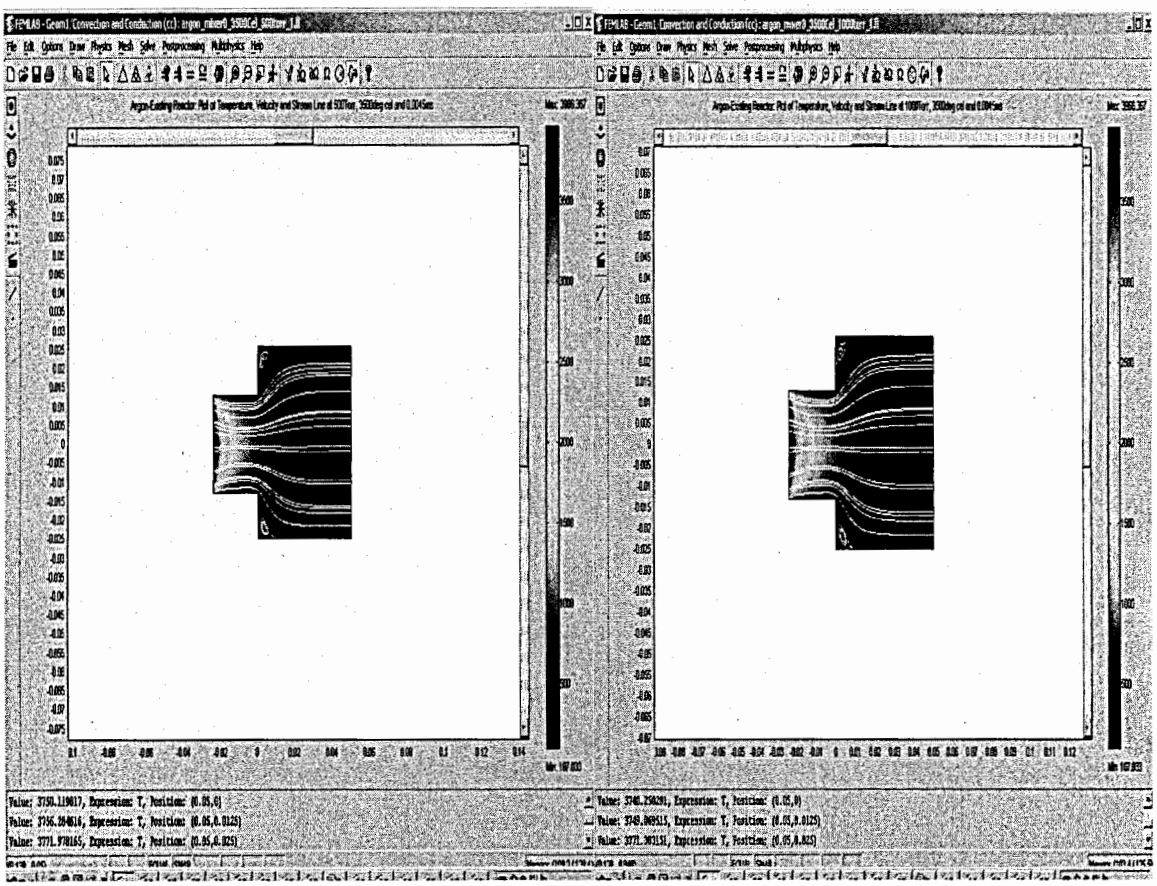

Figure L4. Streamlines in the model reactor due to argon flowing through the existing reactor without static mixer at 3500 °C (3773.4 K). The left figure shows streamlines at pressure of 500 Torr (66650 Pa) and temperature of 3500 °C (3773.4 K). The right figure shows similar streamlines but at a pressure of 1000 Torr (133300 Pa).

APPENDIX M

NUMENCLATURE

Nomenclature.

Mathematical Symbols

$\frac{\partial}{\partial t}$	convective acceleration term and it is an unsteady term which indicates change.
u_{max}	is the maximum velocity in the x-direction in *m/s*
s	is a variable at the boundary that varies from 0 to 1 (COMSOL AB., 2004f).
C_p	heat capacity at constant pressure in J/kgK
ρ	density of fluid in Kg/m^3
η	viscosity of fluid in kg/ms
T	temperature in K
p	pressure in Pa
V	velocity vector in m/s
B	body force defined as force per unit volume and it is assumed to be negligible
k	thermal conductivity in W/Km
$\nabla \cdot$	vector operator
M	molar mass of gas in Kg/mole
R	gas constant in J/mole.K
$T_{o,in}$	Constant inlet temperature of the carrier gas
$T_{w,furn}$	Variable temperature at the wall of the reactor or furnace or static mixer
ΔT	Temperature deviation obtained from temperatures obtained from the exit of the mixing zone of the reactor and the bulk temperature subtracted.

T_B Bulk temperature at the exit of the mixing zone of the reactor/static mixer

$p_{o,in}$ Variable inlet pressure of the carrier gas

MI Mixing index is the percentage of the mixing ratio obtained by dividing the temperature deviation by the bulk temperature and multiplied by 100%.

Chemical Symbols

Ar Argon

C Carbon

Co Cobalt

F_2 Fluorine

Kr Krypton

N_2 Nitrogen

Ne Neon

Ni Nickel